

NOVEL INSIGHTS INTO THE REGULATION OF AUTOPHAGY IN SACCHAROMYCES
CEREVISIAE

APPROVED BY SUPERVISORY COMMITTEE

Benjamin Tu, Ph.D.

Yi Liu, Ph.D.

Steven L. McKnight, Ph.D.

Ralph DeBerardinis, M.D., Ph.D.

DEDICATION

To my mother, Rong Wu, my father, Shifan Wu, and my boyfriend, Hui Jiang,
for their love and support

NOVEL INSIGHTS INTO THE REGULATION OF AUTOPHAGY IN SACCHAROMYCES
CEREVISIAE

By

XI WU

DISSERTATION

Presented to the Faculty of the Graduate School of Biomedical Sciences

The University of Texas Southwestern Medical Center at Dallas

In Partial Fulfillment of the Requirements

For the Degree of

DOCTOR OF PHILOSOPHY

The University of Texas Southwestern Medical Center at Dallas

Dallas, Texas

August, 2011

Copyright

by

Xi Wu, 2011

All Rights Reserved

NOVEL INSIGHTS INTO THE REGULATION OF AUTOPHAGY IN SACCHAROMYCES CEREVISIAE

XI WU

The University of Texas Southwestern Medical Center at Dallas, 2011

Supervising Professor: Benjamin Tu, Ph.D.

Autophagy is an evolutionarily conserved pathway for the degradation of intracellular contents. How autophagy is regulated, especially upon changes in metabolic and nutritional state, remains poorly understood. In *Saccharomyces cerevisiae*, autophagy is normally triggered by nutrient starvation. However, by using a prototrophic strain, I discovered that autophagy can be strongly induced upon switch from a rich medium (YPL) to a minimal medium (SL) without nutrient starvation. This new autophagy-inducing condition was termed SL-induced autophagy. Growth measurement confirmed that SL-induced autophagy was important for cellular homeostasis and growth following medium switch.

A genetic screen uncovered *IML1*, *NPR2*, *NPR3* and *PBPI*, which are all required for SL-induced autophagy, but not for nitrogen-starvation-induced autophagy. Iml1p, Npr2p and Npr3p function in the same complex and regulate autophagosome formation. During SL-induced autophagy, Iml1p can localize to the pre-autophagosomal structures, consistent with the role of the Iml1p complex in autophagosome formation. Moreover, a conserved domain in Iml1p was identified to be required for SL-induced autophagy as well as complex formation.

I discovered that sulfur containing amino acids, but not non-sulfur containing amino acids, can specifically inhibit SL-induced autophagy. I further demonstrated that cysteine is a key metabolite that inhibits SL-induced autophagy by regulating cellular processes related to cysteine metabolism. Cysteine does not suppress SL-induced autophagy by regulating oxidative stress, protein urmylation and thiolation of cytosolic tRNAs. Future studies will be required to reveal the exact mechanism through which cysteine inhibits SL-induced autophagy.

I also discovered that autophagy can be significantly induced upon depletion of a Fe-S cluster containing protein, Rli1p, and other factors that are also involved in rRNA processing and translation initiation. Interestingly, *IML1*, *NPR2*, *NPR3* and *PBPI* are also important for Rli1p-depletion-induced mitophagy. These results strongly suggest the mechanistic link between SL-induced autophagy and ribosome biogenesis or translation regulation.

Collectively, my studies have demonstrated the existence of additional mechanisms that regulate autophagy in response to relatively more subtle changes in metabolic and nutritional state.

TABLE OF CONTENTS

| | |
|---|-----------|
| I. INTRODUCTION..... | 1 |
| II. RESULTS..... | 6 |
| i. SELECTIVE REGULATION OF NON-NITROGEN- STARVATION-INDUCED AUTOPHAGY BY A NOVEL COMPLEX..... | 6 |
| Induction of Autophagy upon Switch from a Rich to a Minimal Medium, without Nitrogen Starvation..... | 6 |
| SL-Induced Autophagy Is Important for Cellular Homeostasis and Growth Following Medium Switch..... | 8 |
| Visual Screen to Identify Genes Required for SL-Induced Autophagy..... | 9 |
| Iml1p, Npr2p and Npr3p Function in One Complex..... | 11 |
| Iml1p Forms Punctate Structures that Occasionally Co-localize with Pre- Autophagosomal Structures | 13 |
| The Iml1p Complex Regulates Autophagosome Formation during SL-Induced Autophagy..... | 15 |
| Iml1p Contains a Conserved Domain Required for SL-Induced Autophagy..... | 16 |
| There Are No Significant Changes in the Iml1p-, Npr2p- and Npr3p-Interacting Proteins upon Switch from YPL to SL Medium..... | 17 |
| ii. SELECTIVE REGULATION OF SL-INDUCED AUTOPHAGY BY PBPI..... | 18 |
| <i>PBPI</i> Is Selectively Required for SL-Induced Autophagy..... | 18 |

| | |
|---|-----------|
| Stress Granule and P Body Are Not Involved in the Regulation of SL-Induced Autophagy..... | 18 |
| Pbp1-GFP Localization Does Not Change after Switch to SL Medium..... | 19 |
| <i>PBP1</i> Does Not Regulate Atg13p Phosphorylation..... | 19 |
| There Are No Significant Changes in the Pbp1-Interacting Proteins upon Switch from YPL to SL Medium..... | 20 |
| iii. SL-INDUCED AUTOPHAGY AND CYSTEINE | |
| METABOLISM..... | 20 |
| SL-Induced Autophagy Is Selectively Inhibited by Sulfur Amino Acids | 20 |
| Metabolic Flux from Cysteine to Methionine Is Not Required for the Inhibitory Effect of Cysteine on SL-Induced Autophagy..... | 22 |
| Addition of Cysteine to SL Medium Dose Not Affect Atg13p Phosphorylation..... | 22 |
| Cysteine Inhibits SL-Induced Autophagy through Regulating Cellular Processes that Are Related to Cysteine Metabolism..... | 23 |
| Cellular Processes that Are Related to Cysteine Metabolism..... | 24 |
| Cysteine Does Not Regulate SL-Induced Autophagy by Suppressing Oxidative Stress..... | 25 |
| Cysteine Does Not Inhibit SL-Induced Autophagy through Affecting Urmylation or Thiolation of Cytosolic tRNA..... | 26 |
| Autophagy Is Strongly Induced upon Depletion of Nfs1p, a Cysteine Desulfurase..... | 26 |
| Autophagy Is Strongly Induced upon Depletion of a Fe-S Cluster Containing Protein, Rli1p, and Its Functionally-Related Factors..... | 29 |

| | |
|--|------------|
| <i>IML1, NPR2, NPR3 and PBPI Are Also Required for Rli1p-Depletion-Induced</i> | |
| Autophagy..... | 30 |
| III. DISCUSSION..... | 32 |
| IV. EXPERIMENTAL PROCEDURES..... | 37 |
| V. FIGURES AND TABLES..... | 46 |
| VI. BIBLIOGRAPHY..... | 115 |

LIST OF FIGURES

| | |
|------------------|----|
| Figure I-1..... | 46 |
| Figure I-2..... | 47 |
| Figure I-3..... | 48 |
| Figure I-4..... | 49 |
| Figure I-5..... | 50 |
| Figure I-6..... | 51 |
| Figure I-7..... | 52 |
| Figure I-8..... | 53 |
| Figure i-1..... | 54 |
| Figure i-2..... | 56 |
| Figure i-3..... | 58 |
| Figure i-4..... | 59 |
| Figure i-5..... | 60 |
| Figure i-6..... | 61 |
| Figure i-7..... | 62 |
| Figure i-8..... | 64 |
| Figure i-9..... | 65 |
| Figure i-10..... | 66 |
| Figure i-11..... | 68 |
| Figure i-12..... | 69 |
| Figure i-13..... | 70 |

| | |
|--------------------|----|
| Figure i-14..... | 72 |
| Figure i-15..... | 73 |
| Figure i-16..... | 75 |
| Figure i-17..... | 76 |
| Figure i-18..... | 78 |
| Figure i-19..... | 79 |
| Figure ii-1..... | 80 |
| Figure ii-2..... | 81 |
| Figure ii-3..... | 82 |
| Figure ii-4..... | 83 |
| Figure ii-5..... | 84 |
| Figure ii-6..... | 85 |
| Figure iii-1..... | 86 |
| Figure iii-2..... | 88 |
| Figure iii-3..... | 89 |
| Figure iii-4..... | 90 |
| Figure iii-5..... | 91 |
| Figure iii-6..... | 92 |
| Figure iii-7..... | 93 |
| Figure iii-8..... | 94 |
| Figure iii-9..... | 95 |
| Figure iii-10..... | 96 |
| Figure iii-11..... | 97 |

| | |
|--------------------|-----|
| Figure iii-12..... | 99 |
| Figure iii-13..... | 100 |
| Figure iii-14..... | 101 |
| Figure iii-15..... | 103 |
| Figure iii-16..... | 104 |
| Figure iii-17..... | 105 |
| Figure iii-18..... | 106 |
| Figure iii-19..... | 108 |

LIST OF TABLES

| | |
|--------------|-----|
| Table 1..... | 109 |
| Table 2..... | 110 |
| Table 3..... | 111 |

LIST OF ABBREVIATIONS

| | |
|--------------|---|
| <i>ATG</i> | AuTophagy-related |
| TORC1 | Target Of Rapamycin Complex 1 |
| PAS | Pe-Autophagosomal Structures |
| PtdIns | Phosphatidylinositol |
| PtdIns3p | Phosphatidylinositol 3-phosphate |
| WT | Wild Type |
| YPL | Yeast extract and Peptone and Lactate |
| YPGL | Yeast extract and Peptone and Galactose and Lactate |
| SD | Synthetic medium and Glucose |
| SD-N | Synthetic medium and Glucose without Nitrogen sources |
| SL | Synthetic medium and Lactate |
| SL-N | Synthetic medium and Lactate without Nitrogen sources |
| ALP | Alkaline Phosphatase |
| GFP | Green Fluorescent Protein |
| <i>OM45</i> | mitochondrial Outer-Membrane protein 45 |
| <i>IDH1</i> | Isocitrate Dehydrogenase 1 |
| <i>PEX14</i> | Peroxisome related protein 14 |
| <i>IML1</i> | Increased Minichromosome Loss 1 |
| <i>NPR2</i> | Nitrogen Permease Regulator 2 |
| <i>NPR3</i> | Nitrogen Permease Regulator 3 |
| <i>PBP1</i> | Pab1p-Binding Protein 1 |

| | |
|-------------|---|
| TCA | trichloroacetic acid |
| <i>APE1</i> | leucine aminopeptidases 1 |
| AB | Autophagic Body |
| kDa | kilo Dalton |
| DUF3608 | Domain of Unknown Function 3608 |
| DEP | Dishevelled, Egl-10 and Pleckstrin |
| <i>PUB1</i> | PolyUridylate Binding 1 |
| <i>PAT1</i> | Protein Associated with Topoisomerase-II 1 |
| SAM | S-AdenosylMethionine |
| <i>STR2</i> | Sulfur TRansfer 2 |
| <i>MET6</i> | METHionine requiring 6 |
| LC-MS/MS | Liquid chromatography–mass spectrometry/mass spectrometry |
| GSH | glutathione |
| <i>GSH1</i> | Glutathione 1 |
| <i>NFS1</i> | NiFS-like 1 |
| <i>URM1</i> | Ubiquitin Related Modifier 1 |
| <i>UBA4</i> | UBiquitin-like protein Activating 4 |
| <i>GAL1</i> | GALactose metabolism 1 |
| <i>ACO1</i> | ACOnitase 1 |
| <i>RLI1</i> | RNase L Inhibitor |
| <i>LEU1</i> | LEUcine biosynthesis 1 |
| <i>BIO2</i> | BIOTin 2 |
| <i>NTG2</i> | eNdonuclease Three-like Glycosylase 2 |

| | |
|--------------|----------------------------------|
| <i>NHP2</i> | Non-Histone Protein 2 |
| <i>RRP3</i> | Ribosomal RNA Processing 3 |
| <i>RRP7</i> | Ribosomal RNA Processing 7 |
| <i>TIF11</i> | Translation Initiation Factor 11 |
| <i>TIF34</i> | Translation Initiation Factor 34 |
| <i>TIF35</i> | Translation Initiation Factor 35 |
| rRNA | ribosome RNA |
| tRNA | transfer RNA |
| LSM | Like-SM ribonucleoprotein |
| LSMAD | LSM-Associated Domain |
| Fe-S | Iron-Sulfur |

I. INTRODUCTION

Autophagy is a cellular pathway that enables delivery of cytoplasmic contents and organelles into the lysosomes or vacuole for degradation. Given its essential role in the maintenance of cellular homeostasis, autophagy has been closely associated with a variety of human diseases (Mizushima et al., 2008).

Roughly speaking, there are two routes for the intracellular contents to enter the lysosomes or vacuole (Klionsky and Ohsumi, 1999). One route is macroautophagy, which is characterized by the formation of a double-membrane structure, called autophagosome that contains the materials to be degraded (Figure I-1A). The outer-membrane of autophagosomes can fuse with the membrane of the lysosomes or vacuole, and the resulting structures are named autophagic bodies in yeast cells and autophagic vesicles in mammalian cells (Figure I-1). During the formation of autophagosomes, intracellular proteins or organelles can be sequestered either non-selectively or selectively. Cytoplasmic proteins are usually engulfed by the emerging autophagosome in a non-selectively manner. In contrast, subcellular organelles, like mitochondria and peroxisomes, are probably mainly selectively captured by autophagosomes (Figure I-2) (Kanki et al., 2009b; Klionsky and Ohsumi, 1999; Okamoto et al., 2009). The selective degradation of organelles requires specific interactions between the “receptor/tag” proteins on

the surface of the organelles and the Atg proteins that are engaged in selective autophagy.

Another route is microautophagy, which does not require the formation of autophagosomes, but instead, involves the direct interaction between the vacuole membrane and the target proteins or organelles. During microautophagy, there are dramatic changes in the vacuole membrane, which invaginate toward the lumen side of the vacuole until the formation of intraluminal vesicles containing cytoplasmic proteins or organelles (Figure I-3). Microautophagy is much less studied than macroautophagy and has only been described in yeast cells.

Macroautophagy will hereafter be referred to as autophagy since my study mainly focuses on macroautophagy.

Autophagy was first described in mammalian cells under different physiological conditions (Klionsky and Ohsumi, 1999). However, the physiological significance and the molecular mechanism of autophagy remained unclear without knowing the identity of the molecular machinery for autophagy. Later, autophagy was also observed in yeast cells with proteinase deficiency upon nutrient starvation (Figure I-4) (Klionsky and Ohsumi, 1999), which enabled the conduction of several yeast genetic screens to identify the *AuTophagy*-related genes or *ATG* genes (Harding et al., 1995; Thumm et al., 1994; Tsukada and Ohsumi, 1993). By far, forty-five *ATG* genes have been identified in yeast, including those that function in the

autophagy core machinery for autophagosome formation, and others that are involved in selective autophagy, including mitophagy, pexophagy and the cytoplasm-to-vacuole targeting (cvt) pathway that selectively delivers the preform of aminopeptidase I into the vacuole (Klionsky et al., 2003; Nakatogawa et al., 2009).

The autophagy core machinery consists of several subgroups: the initiation Atg1p/Atg13p complex, the Atg14p-containing PtdIns 3 kinase complex I, the Atg18p/Atg2p complex, the integral membrane protein Atg9p and the two ubiquitin-like conjugation systems: the Atg12p conjugation system and the Atg8p conjugation system (Nakatogawa et al., 2009).

The formation and activation of the initiation Atg1p/Atg13p complex can be regulated by changes in the nutritional and intracellular metabolic state (Nakatogawa et al., 2009; Suzuki and Ohsumi, 2010). Upon nitrogen starvation, the activity of the Target of Rapamycin Complex 1 (TORC1) is inhibited, which leads to the formation and activation of the Atg1p/Atg13p complex. The activated Atg1p/Atg13p complex can then recruit other core Atg proteins and organize the formation of the pre-autophagosomal structures (PAS) (Figure I-5 and Figure I-6). The formation and organization of PAS is thought to be important for autophagosome formation (Suzuki and Ohsumi, 2010).

The presence of Atg14p directs the PtdIns 3 kinase complex I to PAS, and the production of PtdIns3p by the complex is thought to be important for recruitment of the downstream core Atg proteins. The Atg18p/Atg2p complex is thought to be a good candidate for being the mediator of the PtdIns 3 kinase complex due to the capacity of Atg18p to bind to PtdIns3p. Atg9p is the only integral membrane protein in the autophagy core machinery. Since Atg9p is known to shuttle between PAS and non-PAS punctate structures, Atg9p is proposed to be involved in the delivery of membrane for autophagosome formation (Mari et al., 2010; Nakatogawa et al., 2009; Reggiori et al., 2004).

In the Atg12p conjugation system, Atg12p is processed by Atg7p, an E1-like enzyme and Atg10, an E2-like enzyme, and finally conjugated to Atg5p. The Atg12p/Atg5p conjugate then forms a complex with Atg16p (Figure I-7B). In the Atg8p conjugation system, in contrast, Atg8p is processed by Atg7p and another E2-like enzyme, Atg10p, and finally conjugated to phosphatidylethanolamine (PE), a major component of biological membranes. The C-terminal of newly-synthesized Atg8p is arginine but not glycine. Therefore, another core Atg protein, Atg4p, is required to carry out the cleavage of arginine and thus expose glycine at the new C-terminus of Atg8p (Figure I-7C) (Ohsumi, 2001).

One fundamental question in the autophagy field is how autophagy is regulated in coordination with cellular physiology and metabolism. In both yeast and

mammalian cells, deprivation of essential nutrients strongly induces autophagic degradation of proteins and organelles for survival (Levine and Klionsky, 2004). Therefore, nutrient starvation is a commonly-used model for the study of the metabolic regulation of autophagy. In *Saccharomyces cerevisiae*, it is known that nitrogen starvation induces autophagy primarily by inhibiting the activity of the TORC1, which leads to the dephosphorylation of Atg13p and the activation of the Atg1p-Atg13p initiation complex (Figure I-8) (Nakatogawa et al., 2009). However, the mechanism by which nitrogen availability regulates TORC1 activity remains poorly understood. Moreover, how other metabolic perturbations might regulate the autophagy pathway also remains unclear.

In this study, by using a prototrophic strain of *Saccharomyces cerevisiae*, CEN.PK (van Dijken et al., 2000), I discovered that yeast cells induce autophagy following switch from a rich to a minimal medium, in the absence of any severe nutrient starvation. Subsequently, I used this novel autophagy-inducing condition as a model to investigate the mechanisms by which autophagy is triggered in response to such fine changes in metabolic and nutritional state.

II. RESULTS

i. SELECTIVE REGULATION OF NON-NITROGEN-STARVATION-INDUCED AUTOPHAGY BY A NOVEL COMPLEX

Induction of Autophagy upon Switch from a Rich to a Minimal Medium, without Nitrogen Starvation

Instead of auxotrophic strains commonly used in previous studies of autophagy, I chose a prototrophic strain of *Saccharomyces cerevisiae*, CEN.PK (van Dijken et al., 2000), to study the regulation of autophagy. Since severe nutrient starvation is a well-known trigger for autophagy both in yeast and mammalian cells (Levine and Klionsky, 2004), I first asked whether autophagy could also be induced in the CEN.PK strain by nitrogen starvation. To address this question, wild type (WT) prototrophic cells were grown in a rich medium with lactate as the carbon source (YPL) to log phase and then switched into two kinds of nitrogen-starvation media (minimal medium with glucose but no nitrogen (SD-N), and minimal medium with lactate but no nitrogen (SL-N)). In contrast to glucose, lactate is a non-fermentable carbon source that requires mitochondria to be metabolized. Non-starvation media (SD and SL) were used as controls. As expected, both general autophagy and organelle autophagy were strongly induced by nitrogen starvation (Figure i-1A and i-1B).

However, surprisingly, the activity of the alkaline phosphatase (ALP) reporter for either general autophagy or mitophagy was also significantly elevated upon switch to SL medium, in the complete absence of nitrogen starvation (Figure i-1A). Two additional events that were previously shown to be associated with mitophagy, the translocation of mitochondria to the vacuole and the release of free GFP from Om45-GFP (Kanki et al., 2009b; Okamoto et al., 2009), were observed upon switch to SL medium as well (Figure i-1C and i-1D). Autophagic degradation of peroxisomes was also upregulated as assessed by the release of free GFP from Pex14-GFP (Figure i-1B). Furthermore, medium switch from YPL to SL led to dephosphorylation of Atg13p (Figure i-1E), which is thought to be one of the early steps during autophagy initiation (Nakatogawa et al., 2009). Consistently, all three reporters for autophagic activity were significantly reduced when previously characterized *ATG* genes were deleted (Nakatogawa et al., 2009) (Figure i-1D and Figure i-2). Taken together, these results demonstrate that autophagy is induced upon switch from the rich YPL medium to the minimal, non-starvation SL medium. This novel autophagy-inducing condition will henceforth be referred to as SL-induced autophagy. In subsequent experiments, I assessed the levels of SL-induced autophagy by measuring both general autophagy and mitophagy.

To better understand SL-induced autophagy, I measured autophagic activity at different time points after switching to SL medium (Figure i-3A and i-3B). The

time-course experiments showed that SL-induced autophagy became detectable after 2-4 hours following medium switch. The autophagic activity peaked after 6-8 hours, and started to decrease after 17-24 hours.

I then tested whether SL-induced autophagy could occur in the prototrophic versions of W303 and S288C, whose auxotrophic derivatives have been extensively used in yeast studies. Although autophagy was induced by nitrogen starvation in both strain backgrounds, SL-induced autophagy was observed in W303 cells but not in S288C cells (Figure i-4). Since SL-induced autophagy is very robust in both CEN.PK and W303, I propose that SL-induced autophagy is a fundamental phenomenon in *Saccharomyces cerevisiae*. The failure of S288C cells to trigger autophagy upon switch to SL medium might be due to genetic polymorphisms among the different yeast strains.

SL-Induced Autophagy Is Important for Cellular Homeostasis and Growth Following Medium Switch

What is the physiological role of SL-induced autophagy? To address this question, I disrupted the core machinery for autophagosome formation and tested whether a panel of *atg* mutants might exhibit growth phenotypes upon switch from YPL to SL medium. To ensure that potential growth phenotypes were caused by inhibition of autophagy and not due to gene-specific effects, I tested eight *ATG* genes, *ATG1*, *ATG5*, *ATG6*, *ATG7*, *ATG8*, *ATG9*, *ATG10* and *ATG13*, which each

encodes a core Atg protein (Nakatogawa et al., 2009). For all eight *atg* mutants, the growth rate in YPL was comparable to that of WT cells (Figure i-5A-B, left panel). However, upon switch to SL medium, cell growth was severely compromised in the *atg* mutants (Figure i-5A-B, right panel). These results clearly show that SL-induced autophagy is important for cell growth upon switch from YPL to SL medium and indicate that SL-induced autophagy is required for the maintenance of cellular homeostasis in response to changes in medium composition and cellular metabolic state.

Furthermore, since mitophagy is strongly induced upon switch to SL medium (Figure i-1A), I asked whether inhibition of mitophagy alone was sufficient to impair cell growth. However, selective disruption of mitophagy by deleting *ATG32* had no effect on cell growth upon switch to SL medium (Figure i-5B, right panel). Deletion of *ATG32* has been recently shown to cause near-complete inhibition of mitophagy (Kanki et al., 2009b; Okamoto et al., 2009).

Visual Screen to Identify Genes Required for SL-Induced Autophagy

To identify genes that are selectively required for SL-induced autophagy, I conducted a visual screen using a collection of insertion mutants (Figure i-6). Briefly, a prototrophic CEN.PK strain expressing a visual reporter for mitophagy was transformed with a transposon-based insertion library to randomly generate insertion mutants (Burns et al., 1994). In the primary screen, individual mutants

were grown in YPL in 96-well plates to log phase and then switched to SL medium to induce autophagy. Eight hours following medium switch, mitochondrial images were acquired using an automated imaging setup. Mutants with little or no vacuolar mitochondrial signal were saved for the secondary screen. The purpose of the secondary screen was to eliminate mutants in which the autophagy core machinery had been disrupted. The integrity of the autophagy core machinery was examined by monitoring the translocation of GFP-Atg8p from the cytoplasm to the vacuole during nitrogen-starvation-induced autophagy (Kirisako et al., 1999). After induction of autophagy by nitrogen starvation, the mutants in which GFP-Atg8p predominantly remained in the cytoplasm were discarded, while the mutants with strong vacuolar GFP-Atg8p signal were saved for further characterization.

Twenty-four mutants passed both the primary and the secondary screen. The insertion sites of these mutants were mapped and the genes identified proximal to the inserts are shown in Table 1. From this visual screen, I discovered four genes whose functional role in autophagy has not been clearly characterized before. This section mainly focuses on *IML1*, *NPR2* and *NPR3*, and the characterization of *PBP1* will be described in the next section.

Deletion of *IML1*, *NPR2* and *NPR3* led to significant inhibition of SL-induced autophagy, but strikingly, had minimal or no effect on nitrogen-starvation-

induced autophagy (Figure i-7). All three genes are essential for SL-induced autophagy in the W303 strain background as well (Figure i-8).

Since Npr2p and Npr3p have been linked to the negative regulation of TORC1 activity (Neklesa and Davis, 2009) and it is known that autophagy can be induced upon inhibition of TORC1 by rapamycin treatment (Noda and Ohsumi, 1998), I tested whether *IML1*, *NPR2* and *NPR3* are required for rapamycin-induced autophagy. Although $\Delta atg5$ cells failed to upregulate autophagic activity upon addition of rapamycin and became more sensitive to rapamycin-treatment, deletion of *IML1*, *NPR2* or *NPR3* had no effect on rapamycin-induced autophagy, and consistently did not affect sensitivity to rapamycin (Figure i-9). Recent studies reported that Npr2p and Npr3p might be important for nitrogen-starvation-induced autophagy (Dokudovskaya et al., 2011; Graef and Nunnari, 2011). However, I observed that Npr2p and Npr3p are selectively required for SL-induced autophagy (Figure i-7).

Iml1p, Npr2p and Npr3p Function in One Complex

Since *IML1*, *NPR2* and *NPR3* are all selectively involved in SL-induced autophagy and Npr2p and Npr3p are known to interact with each other (Neklesa and Davis, 2009), I hypothesized that the three proteins might function in one complex to regulate autophagy. To examine a potential interaction among Iml1p, Npr2p and Npr3p, I generated strains with N- or C-terminal epitope-tagged

versions of the three proteins. I confirmed that N- or C-terminal tagging of these proteins did not affect SL-induced autophagy (Figure i-10). Since the levels of Iml1p, Npr2p and Npr3p were too low to be detected in typical whole cell extracts (data not shown), I detected them using trichloroacetic acid (TCA)-precipitated whole cell extracts (Figure i-11E and i-12D).

I verified the interaction between Npr2p and Npr3p as assessed by co-immunoprecipitation (Figure i-11A). However, their interaction is independent of *IML1* (Figure i-11A). As reported previously (Spielewoy et al., 2010), I also observed the phosphorylation of Npr2p as assessed by phosphatase treatment of immunoprecipitated Npr2p (Figure i-11B). Npr3p bound to both phosphorylated and dephosphorylated Npr2p (Figure i-11A). In contrast, Iml1p primarily interacts with phosphorylated Npr2p, whose phosphorylation is dependent on both *NPR3* and *IML1* (Figure i-11A-C). I also detected an interaction between Iml1p and Npr3p and deletion of *NPR2* severely abolished the interaction (Figure i-11D). Collectively, I have shown that Iml1p indeed forms a complex with Npr2p and Npr3p, and loss of either *NPR2* or *NPR3* disrupts the binding between the other two components in the complex. In support of these data, a recent study reported that Iml1p, Npr2p, and Npr3p are present within a complex by mass spectrometry analysis (Dokudovskaya et al., 2011). The Iml1p-Npr2p-Npr3p complex will henceforth be termed the Iml1p complex for short.

Iml1p Forms Punctate Structures that Occasionally Co-localize with Pre-Autophagosomal Structures

I then monitored the localization of the Iml1p complex by tagging the proteins with GFP. I could not detect GFP signal for any of the three proteins when cells were cultured in YPL, which is probably due to their low expression (data not shown). However, upon switch from YPL to SL medium, I observed that Iml1-GFP formed punctate structures proximal to the vacuole in a small fraction of cells (Figure i-12A and i-12C). The failure to detect Iml1-GFP punctate structures in YPL is not due to a difference in Iml1-GFP expression because the expression of Iml1-GFP did not change at early time points following switch to SL medium (Figure i-12D).

I then asked whether the punctate structures could be detected under other autophagy-inducing conditions. However, similar structures were not observed upon switch to the nitrogen starvation medium (SD-N) (Figure i-12C). Therefore, Iml1-GFP forms punctate structures specifically during SL-induced autophagy, which is consistent with the autophagy phenotype of $\Delta iml1$.

In *Saccharomyces cerevisiae*, upon induction of autophagy by rapamycin, most of the Atg proteins identified thus far are recruited to pre-autophagosomal structures (PAS), whose organization and dynamics are important for autophagosome formation (Suzuki and Ohsumi, 2010). Since both PAS and Iml1-GFP punctate

structures are observed proximal to the vacuole and functionally related to autophagy, I suspected that Iml1-GFP might localize to PAS.

To address this possibility, I utilized Ape1p as a marker for PAS (Suzuki et al., 2007), and performed dual-color imaging for both Iml1-GFP and Ape1-mRFP1 after switch to SL medium for a few hours. Interestingly, I observed that Iml1-GFP punctate structures localized to both Ape1-positive PAS and Ape1-negative, non-PAS structures (Figure i-12B). The localization of Iml1p to PAS is consistent with the functional role of *IML1* in autophagy and suggests that Iml1p or the Iml1p complex might be involved in the regulation of autophagosome formation.

Similarly, Atg8p has been previously shown to form punctate foci that localize to both PAS and non-PAS structures, like isolation membranes (Kirisako et al., 1999; Suzuki et al., 2007). Therefore, I tested whether *ATG8* might regulate Iml1p localization. Deletion of *ATG8* partially blocked the formation of Iml1-GFP punctate structures at earlier time points upon switch to SL medium, without affecting the expression of Iml1-GFP (Figure i-13A and i-13C). In contrast, GFP-Atg8 dot formation is not affected in $\Delta iml1$, $\Delta npr2$ or $\Delta npr3$ cells (Figure i-13D-E). Based on these results, I hypothesize that Iml1p or the Iml1p complex functions at a step downstream of Atg8p during autophagosome formation. Consistent with this idea, loss of *IML1*, *NPR2* or *NPR3* did not reverse the dephosphorylation of Atg13p upon switch to SL medium (Figure i-14).

Although Npr2-GFP or Npr3-GFP signal was not detectable in SL medium either (data not shown), deletion of *NPR2* or *NPR3* led to complete loss of Iml1-GFP punctate structures without affecting the expression of Iml1-GFP (Figure i-13B and i-13C).

The Iml1p Complex Regulates Autophagosome Formation during SL-Induced Autophagy

To determine whether the Iml1p complex affects autophagosome formation or the fusion between autophagosomes and vacuole during SL-induced autophagy, I performed electron microscopy analysis of WT, $\Delta iml1$, $\Delta npr2$, $\Delta npr3$ and $\Delta atg5$ cells after switching medium from YPL to SL for 9 hours. The fusion between autophagosomes and the vacuole is not affected in $\Delta iml1$, $\Delta npr2$ and $\Delta npr3$ cells because I did not observe significant accumulation of autophagosomes outside the vacuole.

However, I observed that $\Delta iml1$, $\Delta npr2$ and $\Delta npr3$ cells contained fewer autophagic bodies (ABs) in the vacuole. To analyze autophagosome formation more quantitatively, I classified the cells into two groups based on the number of ABs observed in each cell. Cells with fewer than 8 ABs were counted as one group, while cells with 8 or more ABs were counted as the second group. Only 8.5% of WT cells contained fewer than 8 ABs, while in striking contrast, 56.3% of $\Delta iml1$ cells, 52.8% of $\Delta npr2$ cells, 43.5% of $\Delta npr3$ cells and 100% of $\Delta atg5$ in

cells contained fewer than 8 ABs (Figure i-15). Taken together, these results indicate that the Iml1p complex regulates autophagosome formation during SL-induced autophagy.

Iml1p Contains a Conserved Domain Required for SL-Induced Autophagy

IML1 encodes a ~182 kDa protein with two potential functional domains: a DUF3608 domain (henceforth referred to as DUF domain) at the N-terminus and a DEP domain at the C-terminus (Figure i-16A). The DUF (Domain of Unknown Function) domain is a previously uncharacterized domain. The DEP domain is named after Dishevelled, Egl-10 and Pleckstrin.

Similar to *NPR2* and *NPR3* (Neklesa and Davis, 2009), *IML1* is also predicted to have orthologs in higher eukaryotes, including *Homo sapiens*. All the orthologs are similar to *IML1* in terms of size and domain architecture but have not been characterized before either. The full-length alignment between Iml1p and its orthologs shows that the highly conserved residues are very dispersed throughout the whole protein (Figure i-17). Some regions are relatively more conserved, like the DUF domain, while other regions contain fewer or even no conserved residues, like the DEP domain (Figure 16B-C).

I tested whether the DUF and DEP domains were important for the function of Iml1p in autophagy by introducing Iml1 Δ dep or Iml1 Δ dof back into $\Delta iml1$ cells to

determine if they could rescue SL-induced autophagy. I observed that autophagy was significantly, but not fully rescued by plasmids that express full length Iml1p or Iml1 Δ dep (Figure i-18A-B). The expression of Iml1p or Iml1 Δ dep did not fully match the expression of Iml1p from the endogenous chromosomal locus, which could account for the partial rescue (Figure i-18C). In contrast, Iml1 Δ duf was not able to rescue SL-induced autophagy (Figure i-18A-B), which is very likely due to the near-complete loss of interaction with Npr2p and Npr3p (Figure i-18D).

Because the DUF domain is more evolutionarily conserved than the DEP domain and indeed plays an important role in SL-induced autophagy, I speculate that other orthologs in the *IML1* family might also be involved in the regulation of autophagy under particular conditions. In support of this idea, it has been shown that the human orthologs of Npr2p and Npr3p also interact with each other as observed in yeast cells (Neklesa and Davis, 2009). Since this is the first characterization of the function of the DUF3608 domain, I propose to rename it as RANS (Required for Autophagy induced under a Non-Starvation condition) domain to signify its functional role in autophagy.

There Are No Significant Changes in the Iml1p-, Npr2p- and Npr3p-Interacting Proteins upon Switch from YPL to SL Medium

I have tried to identify Iml1p-, Npr2p-, and Npr3p-interacting proteins by immunoprecipitation when cells were grown in YPL or after switched to SL

medium. However, I did not find anything significant from those experiments (Figure i-19 and data not shown). I have also tested for possible interactions between Iml1p and other Atg proteins that function in the autophagy core machinery, including Atg1p, Atg13p, Atg5p, Atg8p, Atg9p and Atg18p, using coimmunoprecipitation. However, I failed to detect an interaction between Iml1p and these Atg proteins (data not shown).

ii. SELECTIVE REGULATION OF SL-INDUCED

AUTOPHAGY BY *PBP1*

***PBP1* Is Selectively Required for SL-Induced Autophagy**

PBP1 is the fourth gene uncovered by the visual screen. Similar to *IML1*, *NPR2* and *NPR3*, deletion of *PBP1* selectively suppressed SL-induced autophagy, while in striking contrast, had no effect on nitrogen-starvation-induced autophagy.

(Figure ii-1)

Based on previous studies, the function of *PBP1* has been linked to translation regulation. Pbp1p is known to regulate mRNA polyadenylation and associate with ribosomes (Mangus et al., 1998; Tadauchi et al., 2004). Consistently, I have confirmed that Pbp1p interacts with ribosome proteins and translation elongation factors (Figure ii-2).

Stress Granules and P Bodies Are Not Involved in the Regulation of SL-Induced Autophagy

Furthermore, Pbp1p has been shown to be a component of stress granules induced by glucose deprivation and involved in the P-body-dependent formation of stress granules (Buchan et al., 2008). Therefore, I next tested whether stress granules and P bodies were required for SL-induced autophagy. *PUB1* and *PAT1* are involved in the assembly of stress granules and P bodies, respectively (Buchan et al., 2008; Pilkington and Parker, 2008). However, deletion of *PUB1* and *PAT1* had no effect on SL-induced autophagy (Figure ii-3). These results indicate that *PBP1* regulates SL-induced autophagy in a stress-granule- and P-body-independent manner.

Pbp1-GFP Localization Does Not Change after Switch to SL Medium

I then examined the localization of Pbp1p when cells were grown in YPL medium and after switched to SL medium by tagging the protein with GFP at the C-terminus. I observed that there were no significant changes in the localization of Pbp1p after medium switch from YPL to SL (Figure ii-4).

***PBP1* Does Not Regulate Atg13p Phosphorylation**

In section I, I have shown that deletion of *IML1*, *NPR2* or *NPR3* does not affect the phosphorylation status of Atg13p. Here, I also tested whether *PBP1* regulates Atg13p phosphorylation upon initiation of SL-induced autophagy. However, depletion of *PBP1* did not reverse the dephosphorylation of Atg13p upon switch to SL medium (Figure ii-5).

There Are No Significant Changes in the Pbp1-Interacting Proteins upon Switch from YPL to SL Medium

Similar to Iml1p, Npr2p and Npr3p, I have also performed immunoprecipitation experiments in order to identify any changes in the Pbp1-interacting proteins during SL-induced autophagy. However, there appears to be no significant changes in Pbp1-associated proteins upon switch from YPL to SL medium (Figure ii-6).

iii. SL-INDUCED AUTOPHAGY AND CYSTEINE METABOLISM

SL-Induced Autophagy Is Selectively Inhibited by Sulfur Amino Acids

What might represent the metabolic or nutritional cue during the regulation of SL-induced autophagy? Since SL medium contains all essential nutrients required for cell growth, I speculate SL-induced autophagy is induced by relatively more subtle changes in medium composition rather than severe nutrient starvation. One significant difference between YPL and SL medium is that YPL medium is rich in amino acids while SL contains no amino acids. I observed that addition of a mixture containing all twenty amino acids except for tyrosine (due to the poor solubility of tyrosine, it was tested separately) suppressed SL-induced autophagy (Figure iii-1). I next tested the effect of individual amino acids on SL-induced autophagy. Strikingly, SL-induced autophagy was significantly inhibited by the

sulfur-containing amino acids cysteine and methionine, even at concentrations as low as 0.2 mM (Figure iii-1). Non-sulfur-containing amino acids did not significantly inhibit SL-induced autophagy either singly or in combination, even at concentrations as high as 36 mM (Figure iii-2).

In contrast, nitrogen-starvation-induced autophagy was completely inhibited by a non-sulfur-containing amino acid mixture, but only slightly suppressed by 0.2 mM cysteine (Figure iii-3). The complete inhibition of nitrogen-starvation-induced autophagy by non-sulfur-containing amino acids is expected because amino acids can be utilized as a nitrogen source. The inclusion of 0.2 mM cysteine may not be sufficient to satisfy cellular nitrogen demands.

I then tested whether SL-induced autophagy would also be suppressed by other sulfur-containing metabolites that can be converted to both methionine and cysteine. In the de novo biosynthesis pathway of sulfur-containing amino acids (Figure iii-4A), S-adenosylmethionine (SAM) can be generated from methionine and converted back to homocysteine. Homocysteine can then be used as the substrate for methionine and cysteine synthesis (Thomas and Surdin-Kerjan, 1997). After adding SAM into the SL medium, I observed a significant suppression of SL-induced autophagy (Figure iii-4B). Collectively, these data reveal that SL-induced autophagy is selectively regulated by a novel mechanism which is linked to sulfur metabolism.

Metabolic Flux from Cysteine to Methionine Is Not Required for the Inhibitory Effect of Cysteine on SL-Induced Autophagy

Which might be the key metabolite at inhibiting SL-induced autophagy? Is it methionine, cysteine or SAM? To address this question, I blocked the metabolic flux from cysteine to methionine and SAM by knocking out *STR2* and *MET6* (Figure iii-4A) (Thomas and Surdin-Kerjan, 1997). As expected, the inhibitory effect of methionine on SL-induced autophagy was not affected in $\Delta str2$ and $\Delta met6$ cells (Figure iii-5), because the metabolic flow from methionine to other related metabolites remained unaffected in these mutants. Strikingly, cysteine inhibited SL-induced autophagy in $\Delta str2$ and $\Delta met6$ cells as effectively as in WT cells (Figure iii-5). These results clearly show that the conversion of cysteine to methionine and SAM is not required for the inhibition of SL-induced autophagy by cysteine, and indicate that cysteine is the key metabolite at inhibiting SL-induced autophagy.

After confirming the critical role of cysteine at inhibiting SL-induced autophagy, I tested whether cysteine also affects SL-induced autophagy in the W303 strain background. As expected, cysteine potently suppressed SL-induced autophagy in W303 cells, while in striking contrast, a non-sulfur-containing amino acid mixture had minimal to no effect (Figure iii-6).

Addition of Cysteine to SL Medium Dose Not Affect Atg13p Phosphorylation

Then, I asked whether inclusion of cysteine would affect the initiation of SL-induced autophagy. I addressed this question by examining the effect of cysteine on Atg13p phosphorylation. However, dephosphorylation of Atg13p induced by medium switch was not reversed by addition of cysteine (Figure iii-7). Since dephosphorylation of Atg13p is thought to be one of the early steps during initiation of autophagy (Nakatogawa et al., 2009), the failure of cysteine to promote Atg13p phosphorylation indicates that SL-induced autophagy is not due to cysteine starvation.

Cysteine Inhibits SL-Induced Autophagy through Regulating Cellular Processes that Are Related to Cysteine Metabolism

I measured the concentration of cysteine and cystine, the oxidized form of cysteine, in YP medium. Assuming intracellular cystine can be easily converted to cysteine, the concentration of “available” cysteine in YP medium is no more than 10 μ M (Table 2). However, cysteine had no inhibitory effect on SL-induced autophagy even when added at concentrations as high as 15 μ M (Figure iii-8). These results suggest that SL-induced autophagy is not regulated by directly sensing the level of cysteine in the medium or environment. Alternatively, I hypothesize that cysteine inhibits SL-induced autophagy by regulating the cellular processes that are related to cysteine metabolism.

Although the cysteine in the YP medium was detectable, the amount of intracellular cysteine when cells were grown in YPL or SL was beyond the detection limit of LC-MS/MS (data not shown). However, a nice and sharp peak corresponding to cysteine was detected shortly after addition of cysteine into SL medium, which then quickly decreased over time (Figure iii-9). These data indicate that intracellular cysteine is quickly consumed and might be limiting for processes that has high demand of cysteine.

Cellular Processes that Are Related to Cysteine Metabolism

Cysteine is the substrate for glutathione (GSH) biosynthesis (Figure iii-10). Cells will become very sick upon deletion of *GSH1*, which catalyzes the first reaction during GSH biosynthesis that utilizes cysteine and glutamate as the substrates (Ohtake and Yabuuchi, 1991).

Cysteine can also donate its sulfur atom to many cellular pathways (Figure iii-10). One pathway is the assembly of Fe-S cluster, in which the sulfur atom is derived from cysteine by Nfs1p, a cysteine desulfurase (Kispal et al., 1999). The cysteine desulfurase activity of Nfs1p is also important for thiolation of cytosolic and mitochondrial tRNAs (Nakai et al., 2004). In addition, the sulfur atom from cysteine can be transferred to Urm1p by the formation of a thiocarboxylate at its C-terminal glycine (Noma et al., 2009). Urm1p is an ubiquitin-like small protein and functions as either a protein modifier (urmylation) (Goehring et al., 2003) or a

sulfur carrier during cytosolic tRNA thiolation (Leidel et al., 2009; Noma et al., 2009). Uba4p, an E1-like enzyme, activates Urm1p by transferring the sulfur atom to the C-terminal glycine of Urm1p (thiocarboxylation) (Furukawa et al., 2000; Van der Veen et al., 2011).

Cysteine Does Not Regulate SL-Induced Autophagy by Suppressing Oxidative Stress

Since addition of cysteine into the SL medium significantly increased the level of intracellular GSH (Figure iii-11A), I hypothesize that cysteine inhibits SL-induced autophagy by suppressing oxidative stress through promoting the biosynthesis of GSH. Consistent with the hypothesis, inclusion of GSH also strongly inhibited SL-induced autophagy, although only when added at very high concentrations (Figure iii-11B).

However, addition of other antioxidants that are not linked to cysteine metabolism, including dithiothreitol (DTT), beta mercaptoethanol (BME) and sodium ascorbate, had no effect on SL-induced autophagy (Figure iii-11B and iii-11C). The failure of DTT, BEM and sodium ascorbate to suppress SL-induced autophagy suggests that cysteine or GSH does not affect autophagy through inhibiting oxidative stress. Consistently, I confirmed that oxidative stress is not induced as assessed by the measurement of intracellular GSH and GSSG, the oxidized form of GSH (Figure iii-11D and iii-11E). Collectively, these results indicate that cysteine does not

regulate SL-induced autophagy by suppressing oxidative stress. The inhibition of SL-induced autophagy by GSH could probably be due to peptidase-mediated conversion of GSH to cysteine.

Cysteine Does Not Inhibit SL-Induced Autophagy through Affecting Protein Urmylation or Thiolation of Cytosolic tRNA

Since *UBA4* is not an essential gene and critical for Urm1p activation (Furukawa et al., 2000), I tested whether protein urmylation or thiolation of cytosolic tRNA is important for the inhibitory effect of cysteine on SL-induced autophagy by knocking-out *UBA4*. Preliminary data showed that cysteine still strongly suppressed SL-induced autophagy in $\Delta uba4$ cells (Figure iii-12), which indicate that cysteine does not inhibit SL-induced autophagy through affecting protein urmylation or thiolation of cytosolic tRNA. The potential role of thiolation of mitochondrial tRNA in SL-induced autophagy is difficult to be determined because the proteins those are specifically required for such modifications have not been identified yet.

Autophagy Is Strongly Induced upon Depletion of Nfs1p, a Cysteine Desulfurase

Then, I tested the potential role of the Fe-S cluster biosynthesis pathway in the regulation of SL-induced autophagy. Since all the genes involved in Fe-S cluster

biosynthesis, like *NFS1*, are essential for cell growth and survival, I could not test the Fe-S cluster possibility simply by knocking out those genes. Instead, I used an inducible system to control the activity of the Fe-S cluster biosynthesis pathway by manipulating the expression of *NFS1*, and tested whether autophagy could be induced upon disruption of Fe-S cluster biosynthesis. To control the expression of *NFS1*, the *GALI* promoter was integrated into the genomic loci right before the open reading frame of *NFS1*. The activity of the *GALI* promoter is induced by addition of galactose into the medium, while suppressed by glucose. Lactate has no inducing or suppressing effect on the *GALI* promoter (Lohr et al., 1995). Since SL-induced autophagy is subject to glucose suppression (Figure i-1A and Figure iii-13), lactate is used, instead of glucose, to induce the down-regulation of *NFS1* expression.

As expected, cells had very low autophagic activity when cells were grown in the inducing medium containing galactose and lactate as the carbon source (YPGL) (Figure iii-14). However, in striking contrast, the autophagic activity was highly upregulated after 2-3 days following switch to the non-inducing medium (YPL), which led to depletion of Nfs1p and thus inhibition of Fe-S cluster biosynthesis (Figure iii-14). These results demonstrate that autophagy can be induced upon disruption of Fe-S cluster assembly.

Is the Fe-S cluster biosynthesis pathway compromised upon switch from YPL to SL medium? It is very difficult to address this question for various technical issues. For example, the only way to directly examine the functionality of the biosynthesis pathway is to measure heavy Fe incorporation into the Fe-S cluster containing proteins. However, the measurement is only doable when cells are grown in synthetic media (Pierik et al., 2009).

Alternatively, the activity of the biosynthesis pathway can be examined in an indirect way by measuring the activity of the Fe-S cluster containing proteins (Pierik et al., 2009). Functioning as a cofactor, incorporation of Fe-S cluster into the apo-proteins is thought to be important for the function of the holo-proteins (Lill and Muhlenhoff, 2008). Therefore, the activity of the Fe-S cluster containing proteins will be severely affected upon disruption of Fe-S cluster biosynthesis. More than a dozen of Fe-S cluster containing proteins have been identified in fungi (Figure iii-15A) (Lill and Muhlenhoff, 2008). Some of them, like Aco1p, exhibit enzymatic activities, which would be severely compromised upon disruption of Fe-S cluster biosynthesis (Kispal et al., 1999). I examined the activity of Aco1p when cells were grown in YPL and at different time points after switched to SL medium. However, I did not observed any significant changes in the activity of Aco1p (Figure iii-15B). These data suggest that the Fe-S cluster biosynthesis is not severely affected by medium switch. However, I cannot rule out the possibility that the Fe-S cluster biosynthesis pathway has been modestly or

slightly inhibited upon switch to SL medium. Such changes might not be detectable by measuring the enzymatic activities of specific Fe-S cluster proteins, especially those localized in the mitochondria, like Aco1p, which have more access to newly-synthesized Fe-S clusters.

Autophagy Is Strongly Induced upon Depletion of a Fe-S Cluster Containing Protein, Rli1p, and Its Functionally-Related Factors

Then, I tested whether depletion of individual Fe-S cluster containing proteins is sufficient to induce autophagy using the *GALI* promoter. I have tested four Fe-S cluster containing proteins, which are Bio2p localized in the mitochondria, Leu1p localized in the cytosol, Ntg2p localized in the nucleus and Rli1p found both in the cytosol and nucleus (Lill and Muhlenhoff, 2008). Interestingly, autophagy is only strongly induced upon depletion of Rli1p (Figure iii-16 and Figure iii-17).

Similar to Nfs1p, Rli1p is also essential for cell growth and survival. The protein sequence of Rli1p, especially the cysteine residues that are predicted to coordinate the Fe-S clusters, is a highly conserved through evolution (Kispal et al., 2005).

Rli1p has been implicated in the regulation of many translation-related processes, including rRNA processing, ribosome assembly and translation initiation, although its biochemical functions still remain unknown (Dong et al., 2004; Kispal et al., 2005; Yarunin et al., 2005).

To determine whether the induction of autophagy by depletion of Rli1p is caused by gene-specific effects or due to disruption of rRNA processing or translation initiation, I measured the changes in the autophagic activity upon depletion of other factors whose functions are similar to that of Rli1p. I chose three factors involved in either rRNA processing or translation initiation, respectively, and tested whether autophagy would be induced by knocking-down their expression. Again, autophagy was strongly induced after 2-3 days following switch to the non-inducing medium (YPL) (Figure iii-18), which, together with the results of Rli1p depletion, demonstrate that disruption of rRNA processing or translation initiation can significantly upregulate autophagic activity.

IML1, NPR2, NPR3 and PBPI Are Also Required for Rli1p-Depletion-Induced Mitophagy

Since SL-induced autophagy is selectively regulated by *PBPI*, whose function is linked to ribosome or translation regulation (Mangus et al., 1998; Tadauchi et al., 2004), I asked whether *IML1*, *NPR2*, *NPR3* and *PBPI* are also required for autophagy induced by depletion of Rli1p and its functionally related factors. The preliminary data showed that, strikingly, Rli1p-depletion-induced mitophagy was significantly blocked upon deletion of *IML1*, *NPR2*, *NPR3* and *PBPI* (Figure iii-19).

These results implicate that SL-induced autophagy and Rli1p-depletion-induced autophagy might share the same or similar mechanisms and SL-induced autophagy might have something to do with rRNA processing or translation initiation. It will be interesting to test whether medium switch from YPL to SL affects the generation of mature or intermediate rRNA products or the translation of global or a specific subset of mRNA. Since both Pbp1p and its human homolog, ATX2, are predicted to contain a putative RNA-binding LSM domain and a LSM-associated domain (LSMAD) (Ralser et al., 2005), fishing for Pbp1p-associated RNAs (mRNA or rRNA) when cells are cultured in YPL or after switched to SL medium might illustrate the mechanisms underlying the regulation of SL-induced autophagy and provide novel insights into the link between SL-induced autophagy and autophagy induced by depletion of RLi1p and its functional-related factors.

III. DISCUSSION

I have discovered a previously unrecognized autophagy-inducing condition, which is referred to as SL-induced autophagy. The observation of SL-induced autophagy implies that besides severe nutrient starvation, autophagy can also be regulated by relatively more subtle changes in medium composition and cellular metabolic state. Importantly, SL-induced autophagy plays a critical role in maintaining cellular homeostasis upon changes in medium composition and metabolic state, because blocking SL-induced autophagy by disruption of the autophagy core machinery leads to a moderate to severe growth phenotype upon switch to SL medium. Thus, SL-induced autophagy might be important for enabling cells to rapidly adapt to changing growth environments.

Another interesting feature of SL-induced autophagy is that such autophagy is carbon source-dependent, unlike starvation-induced autophagy. Autophagy is not induced upon switch to SD medium, in which glucose is the carbon source (Figure i-1A). Consistently, glucose addition to SL medium completely blocked the induction of autophagy upon switch to SL (Figure iii-13). These results imply that SL-induced autophagy is very strictly controlled by cellular metabolic state and may be subject to glucose-repression. For example, the upregulation of mitochondrial respiratory function triggered by lactate, a non-fermentable carbon source, might be essential for SL-induced autophagy. Alternatively, the

abundance of a rich, fermentable carbon source such as glucose may repress the pathways that regulate SL-induced autophagy. Based on these observations, I predict that studies of SL-induced autophagy will improve our understanding of how the induction of autophagy is intimately coordinated with metabolism.

In addition, I propose that prototrophic strains of *Saccharomyces cerevisiae*, such as CEN.PK, will be valuable for the study of the metabolic regulation of autophagy. Such prototrophic strains do not have genomic lesions that disrupt the biosynthetic pathways for certain essential metabolites, like amino acids and nucleotides, which could impact the regulation of autophagy and other metabolic processes (Tu, 2010; Tu et al., 2005). Therefore, the metabolic behavior of prototrophic cells is presumably more realistic and representative of wild yeast cells.

By conducting a visual screen designed based on these considerations, I identified four novel regulators of autophagy. Three of them, *IML1*, *NPR2* and *NPR3* have been carefully characterized. I found that Iml1p, Npr2p and Npr3p form a protein complex, termed the Iml1p complex. The Iml1p complex is selectively required for SL-induced autophagy and regulates autophagosome formation. I propose that the Iml1p complex might be evolutionarily conserved for three reasons. First, all three components of the complex, Iml1p, Npr2p and Npr3p, are predicted to have orthologs in higher eukaryotes. Secondly, the Npr2p-Npr3p interaction has

previously been shown to be conserved in human cells (Neklesa and Davis, 2009).

Finally, I have demonstrated that Iml1p contains an evolutionarily conserved domain (RANS domain), which is not only important for the formation of the Iml1p complex but also critical for SL-induced autophagy. Therefore, it will be of great interest and importance to decipher the exact role of the Iml1p complex in autophagy in future studies.

PBPI is the fourth novel regulator of autophagy uncovered from the visual screen and specifically regulates SL-induced autophagy but not nitrogen-starvation-induced autophagy. Unfortunately, I have very little clues about the mechanisms underlying the functional role of *PBPI* in SL-induced autophagy. I have confirmed that the formation of stress granules and P bodies are not involved in the regulation of autophagy based on two pieces of evidence. First, medium switch from YPL to SL does not lead to formation of Pbp1p-containing stress granules or any other significant changes in the localization of Pbp1p. Secondly, blocking the formation of stress granules or P bodies by deleting *PUB1* or *PAT1*, respectively, has no effect on SL-induced autophagy.

The selective inhibition of SL-induced autophagy by sulfur-containing amino acids, but not other amino acids, is unexpected and suggests a potential link between SL-induced autophagy and sulfur metabolism in the cell. Further characterization led to discoveries that cysteine is the key metabolite at inhibiting

SL-induced autophagy and cysteine inhibits SL-induced autophagy by regulating cellular pathways that are related to cysteine metabolism. I have ruled out three cysteine-related pathways: GSH biogenesis, protein urmylation and thiolation of cytosolic tRNAs (Nakai et al., 2004; Noma et al., 2009). However, I still have not figured out the exact pathway through which cysteine regulates SL-induced autophagy.

Fe-S cluster biosynthesis is another pathway that utilizes the sulfur atoms donated from cysteine (Kispal et al., 1999). Although autophagy could be strongly induced upon disruption of Fe-S cluster biosynthesis pathway, additional evidence is needed to demonstrate the involvement of Fe-S cluster biogenesis in the regulation of SL-induced autophagy by cysteine. For example, I need to determine whether addition of cysteine into SL medium is able to promote Fe-S cluster biosynthesis. Also, I need to test whether SL-induced autophagy could be suppressed by enhancing Fe-S cluster biosynthesis. These experiments have not been done due to various technical issues. Future studies will be required to understand precisely how cysteine inhibits SL-induced autophagy.

I speculate that SL-induced autophagy is mechanistically linked to rRNA processing or translational regulation based on three observations. First, Pbp1p is functionally linked to translation regulation and contains a putative RNA-binding LSM domain (Mangus et al., 1998; Ralser et al., 2005; Tadauchi et al., 2004).

Secondly, autophagy could be strongly induced upon depletion of Rli1p and other factors, which are critical for rRNA processing and/or translation initiation.

Thirdly, all the four genes, *IML1*, *NPR2*, *NPR3* and *PBP1*, which are specifically involved in the regulation of SL-induced autophagy, are also important for Rli1p-depletion-induced mitophagy. Future studies will be needed to confirm that all the four genes are required for autophagy induced by depletion of Rli1p and its functionally-related factors.

Given the potential capacity of Pbp1p to bind to RNA (Ralser et al., 2005), the future studies could focus on the identification of Pbp1p-associated RNAs under different growth conditions, which might lead to novel insights into the regulation of autophagy by *PBP1* and the link between SL-induced autophagy and autophagy induced by depletion of RLi1p and its functional-related factors.

IV. EXPERIMENTAL PROCEDURES

Yeast Strains and Media

Strains used in this study are listed in Table 3.

Media used in this study (Sherman, 2002): YPL (1% yeast extract, 2% peptone and 2% lactate); YPGL (% yeast extract, 2% peptone, 2% lactate and 1% galactose); SL (0.17% yeast nitrogen base without amino acids and ammonium sulfate, 0.5% ammonium sulfate, 2% lactate); SD (0.17% yeast nitrogen base without amino acids and ammonium sulfate, 0.5% ammonium sulfate, 2% glucose); SD-N (0.17% yeast nitrogen base without amino acids and ammonium sulfate, 2% glucose); SL-N (0.17% yeast nitrogen base without amino acids and ammonium sulfate, 2% lactate).

Plasmids

Plasmid pFA6a-OM-KanMX6 was created for making ALP reporters (Pho8 Δ 60 and Om-pho8 Δ 60). OM stands for mitochondria outer-membrane targeting. To generate plasmid pFA6a-OM-KanMX6, I first made p417-TEF1 by replacing the *CYC1* promoter in p417-CYC1 (Dualsystems Biotech) with ~411 bp-long *TEF1* promoter at SacI and XbaI sites. Primers used to amplify *TEF1* promoter are 5'-ATTGCGAGCTCATAGCTTCAAAATGTTTCTACTCCTTT-3' (forward primer) and 5'-ATTGCTCTAGAAACTTAGATTAGATTGCTATGCTTTC-3'

(reverse primer). Base pairs 1-96 of *TOM20* that encodes the mitochondria outermembrane targeting sequence was inserted into p417-TEF1 at XbaI and EcoRV sites. Primers used to amplify the targeting sequence are 5'-GACTTCTAGAATGTCCCAGTCGAACCCTATCTTAC -3' (forward primer) and 5'-CAGTGATATCTTGATAGTCAAAGTAGATAGCATAAC-3' (reverse primer). Then, the *TEF1* promoter together with the outer membrane targeting sequence was digested at SacI and EcoRV sites and inserted into pFA6a-KanMX6 (Longtine et al., 1998) to make pFA6a-OM-KanMX6.

The plasmid HO-poly-MtRFP-KanMX4-HO for generating the mitophagy imaging reporter was created as described below. Plasmid vt100-DsRed, a generous gift from the Nunnari lab (Westermann and Neupert, 2000), was cut with SphI and the resulting fragment containing the mitochondria-targeting sequence and the coding sequence for DsRed was blunted with Klenow and cloned into the SmaI site of plasmid HO-poly-KanMX4-HO (Voth et al., 2001).

The GFP-Atg8p expressing plasmid p417-GFP-ATG8 was generated as described below. The 500 bp-long *ATG8* promoter was inserted into plasmid p417-TEF1 at SacI/BamHI sites. Then, the *GFP* coding sequence was inserted into the resulting plasmid at BamHI/EcoRI sites. Finally, *ATG8* coding sequence was cloned into the plasmid at EcoRI/SalI sites. To make plasmid pRS41N/H-GFP-ATG8, the

coding sequence for GFP-ATG8 was cut from p417-GFP-ATG8 and cloned into the vector pRS41N/H (Taxis and Knop, 2006) at SacI/SpeI sites.

Using plasmid p417-CYC1 as the backbone, I created plasmid p417-CYC1-IML1-FLAG, p417-CYC1-*iml1* Δ dep-FLAG and p417-CYC1-*iml1* Δ dof-FLAG for the rescue experiments in Figure 7. Genomic DNA prepared from cells that express *Iml1*-FLAG was used as the template to amplify the coding sequence for *Iml1*-FLAG. Since it was difficult for us to amplify the whole coding sequence in one PCR reaction, I split the gene into two pieces by introducing an EcoRI site right before the DEP domain and cloned the N- or C-terminal fragments into the p417-CYC1 at SpeI/EcoRI sites or EcoRI/SalI sites, respectively. Similar procedures were performed to clone plasmids that express *Iml1* Δ dep-FLAG or *Iml1* Δ dof-FLAG except that the sequences encoding the DEP domain or the DUF domain were skipped in the PCR reactions.

Assays to Monitor Autophagy

Imaging

A dual-color reporter strain expressing mitochondria-localized DsRed (MtRFP) and GFP-tagged vacuole membrane protein Vph1p (Vph1-GFP) was constructed to visualize mitophagy. An increase in the signal of MtRFP in the vacuole indicates the induction of mitophagy.

Western blot

The release of free GFP from Om45-GFP, Idh1-GFP and Pex14-GFP was examined to assay mitophagy or pexophagy based on a previously described method (Kanki et al., 2009a). Om45p is a mitochondrial outer-membrane protein. Idh1p is a mitochondrial matrix protein. Pex14p is a peroxisomal membrane protein.

ALP (alkaline phosphatase) activity assay

Cells that express cytosolic Pho8 Δ 60p or mitochondria-outermembrane-targeted Om-pho8 Δ 60p were subject to ALP activity assay to measure the level of general autophagy or mitophagy, respectively.

The protocol for ALP assay essentially followed previously described methods (Noda et al., 1995) with some modifications. Briefly, cell pellets were resuspended with 400 μ L lysis buffer (250 mM Tris-HCl pH 9, 25 mM MgSO₄, 1% Triton, 1X EDTA-free protease inhibitor cocktail (Roche)). After adding \sim 100 μ L glass beads (Sigma), cells were lysed by three rounds of bead-beating: 1 min beating with 1 min cooling on ice. Cell debris and glass beads were separated from the cell extracts by centrifugation at max speed for 10 min at 4 C. For each sample, 70 μ L cell extracts were added to triplicate wells in 96-well flat bottom plates. Plates were kept on ice before the substrate was added. 70 μ L lysis buffer

were added to the blank well. 70 μ L substrate solution (250 mM Tris-HCl pH 9, 25 mM MgSO₄, 1% Triton, 2.7 mM p-nitrophenyl phosphate (MP Biomedicals)) were then added to each well. Then, the plate was incubated at room temperature for 5 min before the reaction was stopped with 140 μ L stop buffer (1 M glycine pH 11). The plates were read at 400 nm to measure the production of p-nitrophenol.

Visual Screen

The founder strain *MtRFP*, Δ *leu2* was transformed with the yeast genomic mini-Tn3:: lacZ::LEU2 transposon insertion library to randomly generate insertion mutants by homologous recombination (Burns et al., 1994). Approximately 5,000 mutants were made and tested in the primary screen. In the primary screen, individual mutants were grown in YPL in 96-well plates to log phase and then switched to SL medium for 8 h. Then the cells were transferred to 384-well glass-bottom plates for imaging. The MtRFP signal was automatically captured at 40X magnification using a BD Pathway 855 microscope. Approximately 60 mutants were found to have little or no vacuolar MtRFP signal and saved for the secondary screen. The purpose of the secondary screen was to eliminate the mutants in which the autophagy core machinery had been disrupted by random insertion. To do this, a centromeric plasmid expressing GFP-Atg8p was transformed into the mutants isolated from the primary screen. The mutants were

then grown in YPL to log phase and then switched to the nitrogen starvation medium (SD-N). About 6 h following medium switch, cells were imaged at 100X magnification to visualize both GFP-Atg8p and MtRFP. Twenty-four mutants with vacuolar Atg8p signal but little or no vacuolar MtRFP signal were found and saved for further characterization. The sites of insertion in these mutants were then mapped using the Vectorette PCR method (Riley et al., 1990).

Western Blot

Whole Cell Extracts Preparation: cell pellets were resuspended with 300 μ L yeast lysis buffer (50 mM NaCl, 50 mM NaF, 100 mM Tris-HCl (pH 7.5), 1 mM EDTA, 1 mM EGTA, 1% Triton X-100, 10% Glycerol, 14 mM 2-mercaptoethanol, 1X EDTA-free protease inhibitor cocktail (Roche), 2 mM PMSF, 5 μ M Pepstatin A, 10 μ M Leupeptin). After adding \sim 80 μ L glass beads, cells were lysed by three rounds of bead-beating: 1 min beating with 1 min cooling on ice.

Antibodies: mouse anti-GFP monoclonal antibody (Roche, clone 7.1 and 13.1), mouse anti-Pgk1 monoclonal antibody (Invitrogen), mouse anti-FLAG M2 antibody (Sigma), mouse anti-HA monoclonal antibody (Roche, clone 12CA5).

Microscopy

Cells were imaged using a Yokogawa CSU-22 spinning disc confocal on a Nikon ECLIPSE Ti microscope. GFP was excited with the 488 nm SDSS laser line and RFP with the 568 nm SDSS laser line. Images were recorded with a 100x/1.45 NA CFI Apochromat objective with an Andor ix897 EMCCD.

Immunoprecipitation

At the indicated time points, 80-150 OD cells were harvested, flash frozen with liquid nitrogen and stored at -80°C until cell lysis. Then, the cell pellet was thawed on ice and resuspended with 500 μ L yeast lysis buffer. After adding ~500 μ L glass beads, cells were lysed by bead-beating for 9-10 times: 20 s beating followed by 3 min cooling on ice. The crude cell extracts were subjected to centrifugation (13,200 *rpm*) for 5 min at 4 °C. The supernatant was transferred to a new tube and 500 μ L lysis buffer was added to the tubes with glass beads. The beads were washed twice. The supernatant was collected by centrifugation and combined with that obtained from the first round of bead beating. The combined supernatant was subject to centrifugation to eliminate cell debris and glass beads. The cleared supernatant was then mixed with 15 μ L magnetic beads (Invitrogen) that had been conjugated with 2 μ g FLAG or HA antibody, and incubated at 4 °C for 4 h for FLAG immunoprecipitation or 8 h for HA immunoprecipitation.

Preparation of TCA-Precipitated Whole Cell Extracts

The TCA precipitated whole cell extracts were prepared following a previously described protocol (Keogh et al., 2006) with slight modifications. Briefly, at the indicated time points, 5 OD cells were pelleted, washed with 20% TCA, flash frozen with liquid nitrogen and then stored at -80°C until cell lysis. Then the cell pellet was thawed on ice and resuspended with 250 μ L 20% TCA. After adding ~250 μ L glass beads, cells were lysed by bead-beating for 3 times: 1 min beating with 1 min cooling on ice. The precipitates were collected by centrifugation and washed once with 5% TCA and once with 100% ethanol. The washed pellet was then solubilized in 120 μ L buffer (40 μ L 1 M Tris-HCl pH 8.0+80 μ L 2X SDS sample buffer) and boiled for 5-10 min.

Electron Microscopy

Electron microscopy analysis was performed by the UTSW electron microscopy core facility using the rapid freezing and freezing-substitution method. Sample preparation was done according to the protocol described in (Baba, 2008) except that yeast cells were subject to high-pressure freezing instead of plunge freezing. Ultra-structural images were captured using a FEI Tecnai G2 Spirit transmission electron microscope.

Metabolite Measurement

Intracellular metabolites were extracted and analyzed as described in (Tu et al., 2007).

Enzymatic Activity Measurement

Measurement of Aco1p and Zwflp activity was based on the protocol described in (Kispal et al., 1999).

Protein Sequence Alignment for *IML1* Family Members

Sequence alignment was performed using ClustalW. The alignment results were analyzed by Genedoc.

Accession number for protein sequences:

Saccharomyces cerevisiae NP_012672.1

Schizosaccharomyces pombe NP_596645.1

Drosophila melanogaster NP_728621.1

Gallus gallus XP_415249.2

Mus musculus NP_001020597.1

Rattus norvegicus NP_001100699.1

Homo sapiens NP_055477.1

V. FIGURES AND TABLES

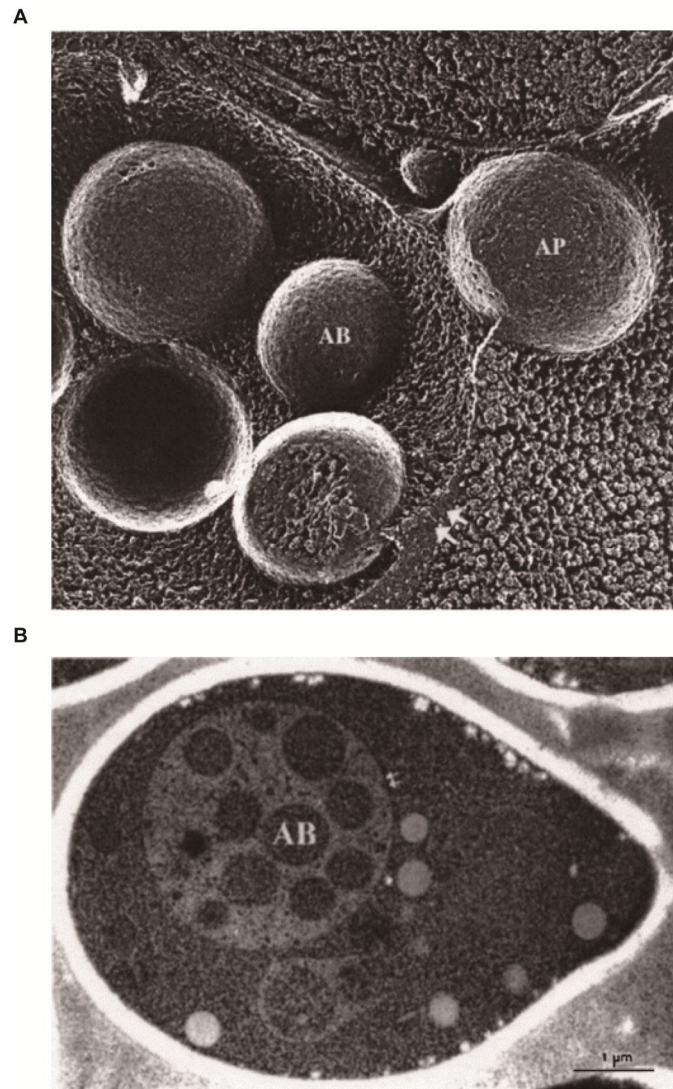


Figure I-1. (A) Freeze-fracture image of an autophagosome (AP) fusing with the vacuole (double arrow). Autophagic bodies (ABs) can be seen inside the vacuole lumen. (B) Yeast cells deficient in vacuolar proteases accumulate ABs within the vacuole (double arrows) lumen under conditions of nitrogen starvation. The figures and legend were modified from (Klionsky and Ohsumi, 1999).

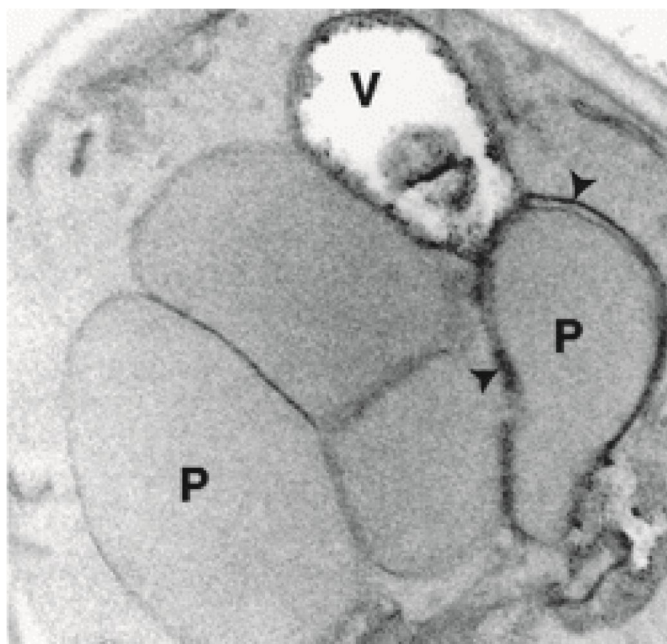


Figure I-2. During ethanol adaptation in *P. pastoris*, peroxisomes are sequestered within an autophagosome-like membrane (arrowheads). The figures and legend were modified from (Klionsky and Ohsumi, 1999).

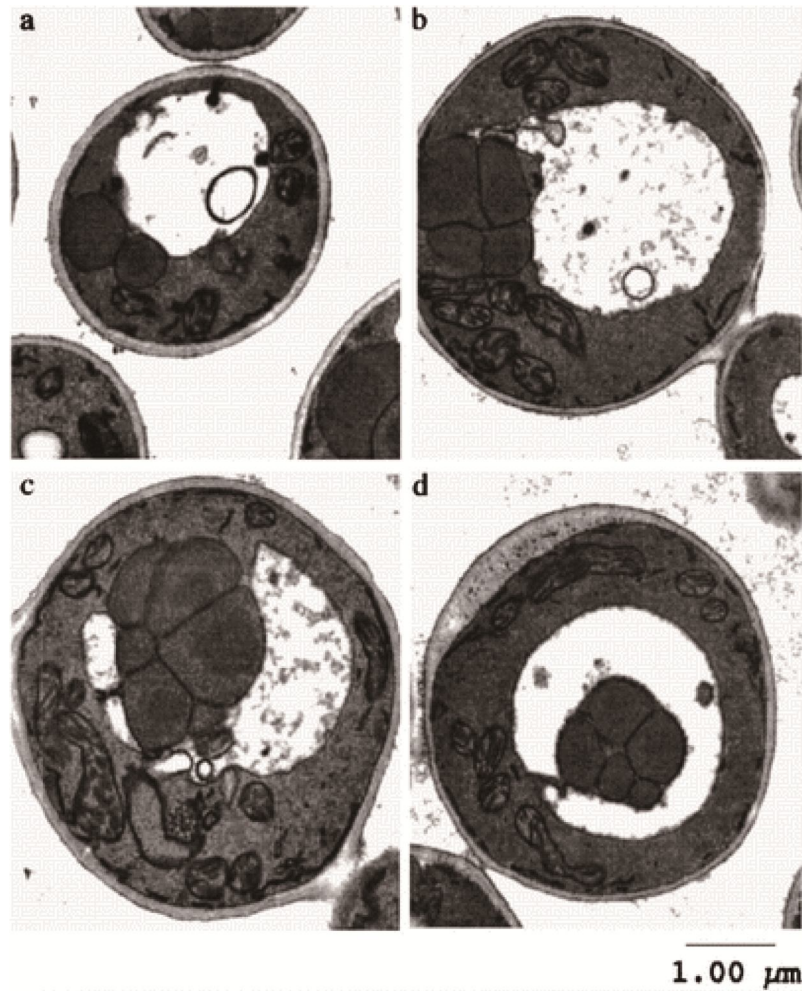


Figure I-3. Electron microscopic images showing glucose-induced peroxisomal degradation in *P. pastoris*. The panels correspond to the following stages: (a) 0, (b) early 1, (c) late 1, and (d). The figures and legend were modified from (Klionsky and Ohsumi, 1999).

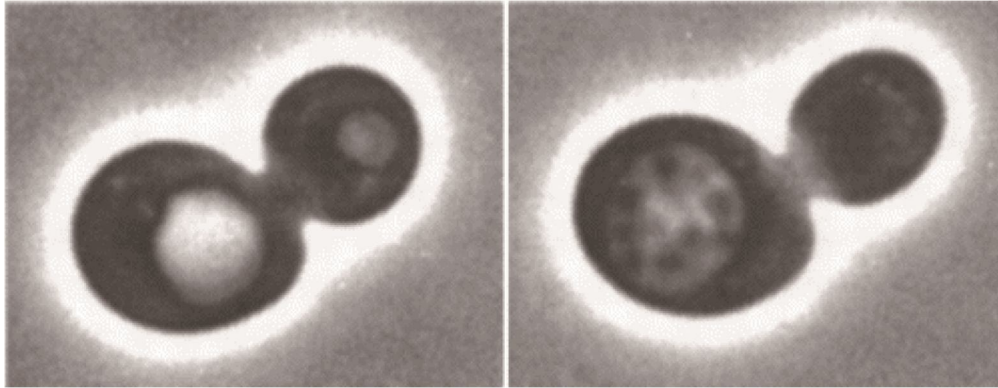


Figure I-4. Phase contrast image of wild-type (*left*) and protease-deficient (*right*) yeast cells under starvation conditions. Autophagic bodies can be seen to accumulate in the vacuole lumen in cells lacking vacuolar hydrolase activity. The figures and legend were modified from (Klionsky and Ohsumi, 1999).

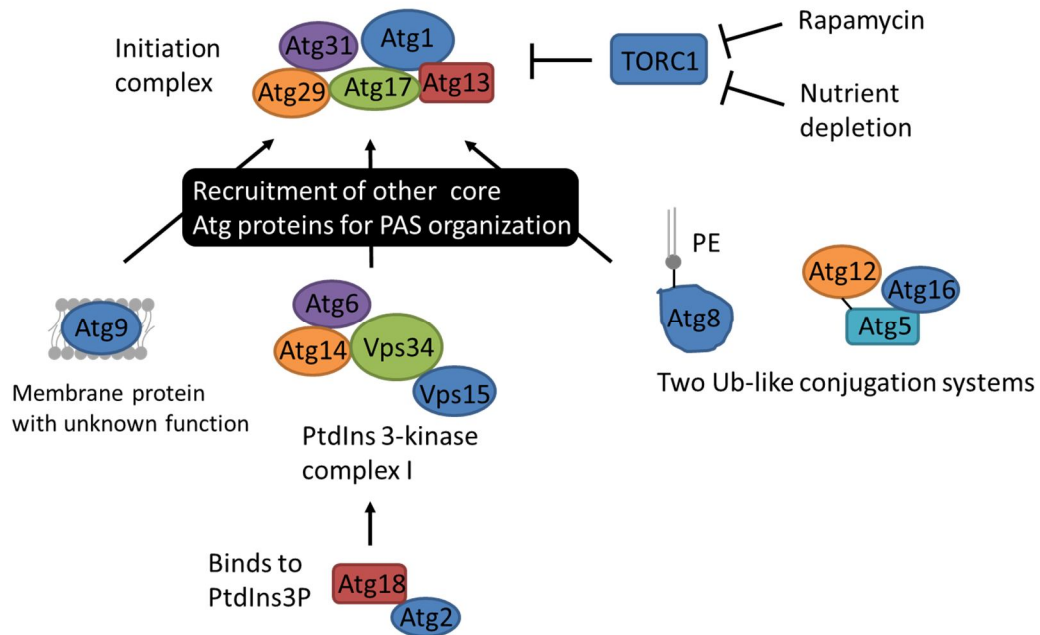


Figure I-5. Autophagy Core Machinery for Autophagosome Formation.

Please see the text for more details.

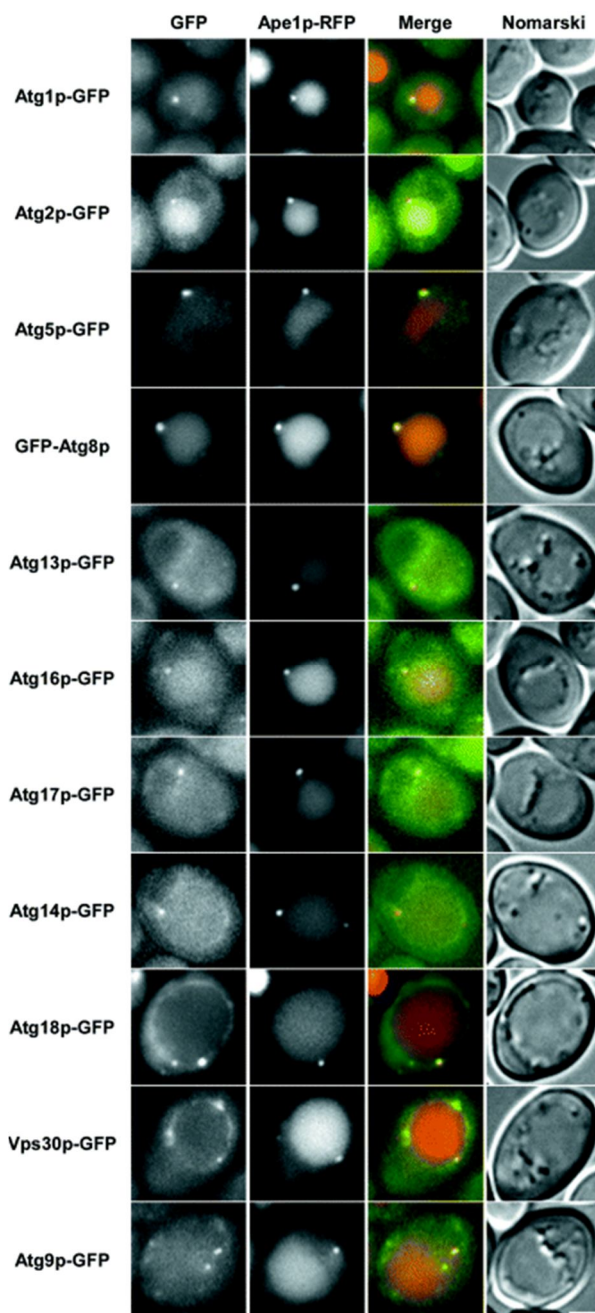
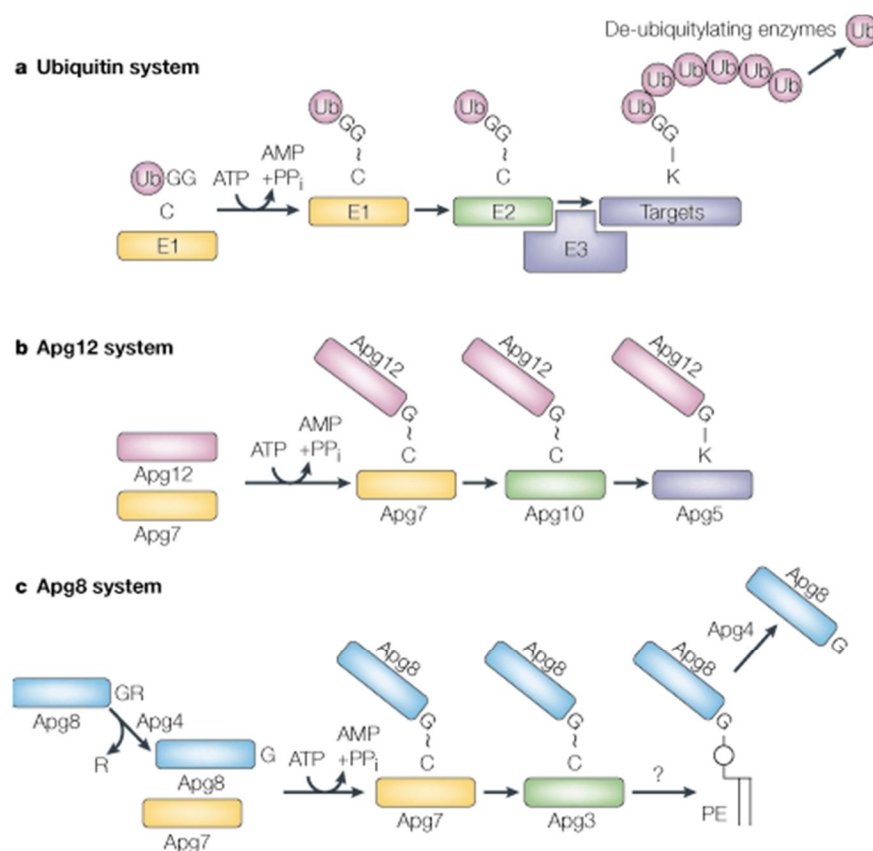


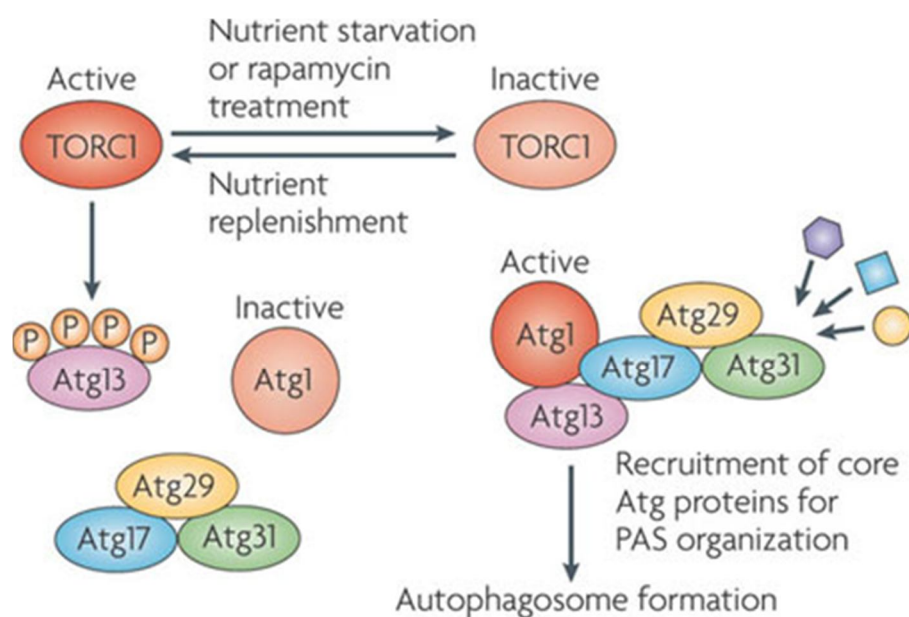
Figure I-6. Localization of Atg proteins to the PAS Each Atg-GFP strain was mated with an Ape1p-RFP strain of the opposite mating type. The resulting diploids were grown in SD + CA medium, incubated with rapamycin for 3 h, and then analyzed. Bar represents 2 μ m. The figures and legend were modified from (Suzuki et al., 2007). CA, casamino acid.



Nature Reviews | Molecular Cell Biology

Figure I-7. Two Ubiquitin-Like Conjugation Systems Required for Autophagosome Formation

(A) The ubiquitin system. (B) The autophagy-defective 12 (Apg12) system. The carboxy-terminal glycine of Apg12 is activated by Apg7, an E1-like enzyme of the ubiquitin (Ub) system. Subsequently, Apg12 is transferred to Apg10, an E2-like conjugating enzyme. Finally, Apg12 forms a conjugate with Apg5 through an isopeptide bond. The Apg12-Apg5 conjugate forms a large protein complex with Apg16. Apg12 is synthesized as an active precursor and immediately forms a conjugate with Apg5. No deconjugation of Apg12-Apg5 has been observed. (C) The Apg8 system. Nascent Apg8 is first processed to a glycine-exposed form by a protease, Apg4. Apg8 is also activated by Apg7 (an E1) then transferred to Apg3 (an E2). Finally, Apg8 forms a conjugate with phosphatidylethanolamine (PE). Apg8-PE is deconjugated by Apg4. Apg12 equals to Atg12; Apg7 equals to Atg7; Apg10 equals to Atg10; Apg5 equals to Atg5; Apg8 equals to Atg8; Apg3 equals to Atg3; Apg4 equals to Atg4. The figures and legend were modified from (Ohsumi, 2001).



Nature Reviews | Molecular Cell Biology

Figure I-8. Regulation of the Activation of the initiation Atg1p/Atg13p complex by TORC1

When target of rapamycin complex 1 (TORC1) is inactivated following nutrient depletion or rapamycin treatment, autophagy-related 13 (Atg13) is dephosphorylated. This allows the association of Atg1 subfamily proteins with Atg13, followed by the upregulation of the Atg1 kinase activity and recruitment of other core Atg proteins to the pre-autophagosomal structure (PAS) to initiate autophagosome formation. These events are immediately reversed on the addition of nutrients. The figures and legend were modified from (Nakatogawa et al., 2009).

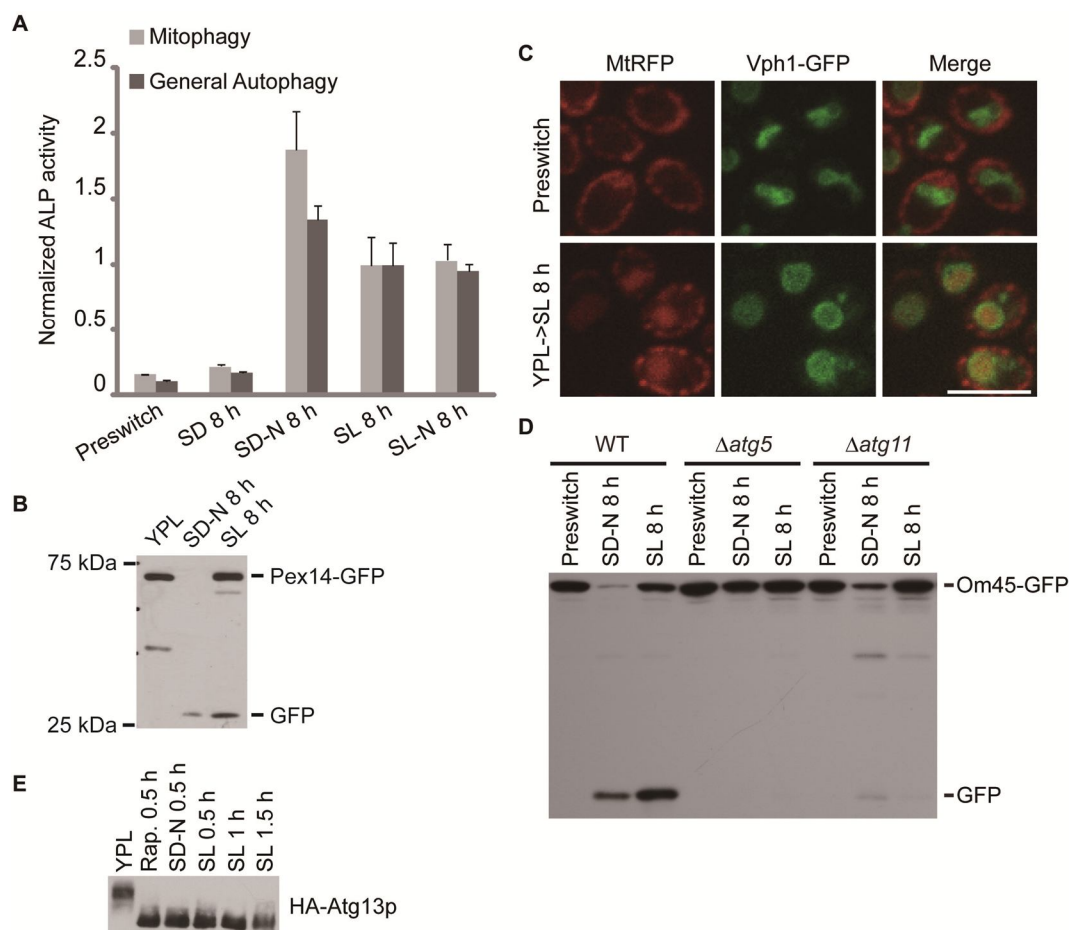


Figure i-1. Induction of Autophagy upon Switch from a Rich Medium to a Minimal, Non-Starvation Medium

Cells were grown in rich medium (YPL) to log phase before switch to nitrogen-starvation media (SD-N or SL-N). Non-starvation media (SD and SL) were used as controls. General autophagy, mitophagy and pexophagy were examined at the indicated time points.

(A) As expected, autophagy was induced in starvation media (SD-N and SL-N) but not in the control medium SD. Surprisingly, autophagy was also significantly induced upon switch to SL medium. Data represent averages of 3-5 samples with error bars for standard deviations.

(B) The release of free GFP from Pex14-GFP increased upon switch to autophagy-inducing media (SD-N and SL). Pex14p is a peroxisomal membrane protein.

C) Mitochondria reporter was detected in the vacuole after switch to SL medium for 8 h. MtRFP is a reporter targeted to the mitochondrial matrix. Vph1p is a vacuole-resident protein. Scale bar, 10 μ m.

(D) The release of free GFP from Om45-GFP increased upon switch to autophagy-inducing media (SD-N and SL) and was blocked in $\Delta atg5$ and $\Delta atg11$ cells. Om45p is a mitochondrial outer-membrane protein.

(E) Dephosphorylation of Atg13p triggered by autophagy-inducing conditions. Rapamycin treatment and nitrogen starvation led to dephosphorylation of Atg13p as reported previously (Kamada et al., 2000). Atg13p was also dephosphorylated upon switch to SL medium. Cells were grown in YPL to log phase before switch to rapamycin-containing (0.2 μ g/mL) YPL medium, nitrogen-starvation medium (SD-N) or SL medium. At the indicated time points, 5 OD cells were quenched by mixing with TCA to a final concentration of 5-6% and incubated on ice for at least 5 min before centrifugation. Cell pellets were then subject to whole cell TCA extraction and analyzed by immunoblotting. Rap., rapamycin.

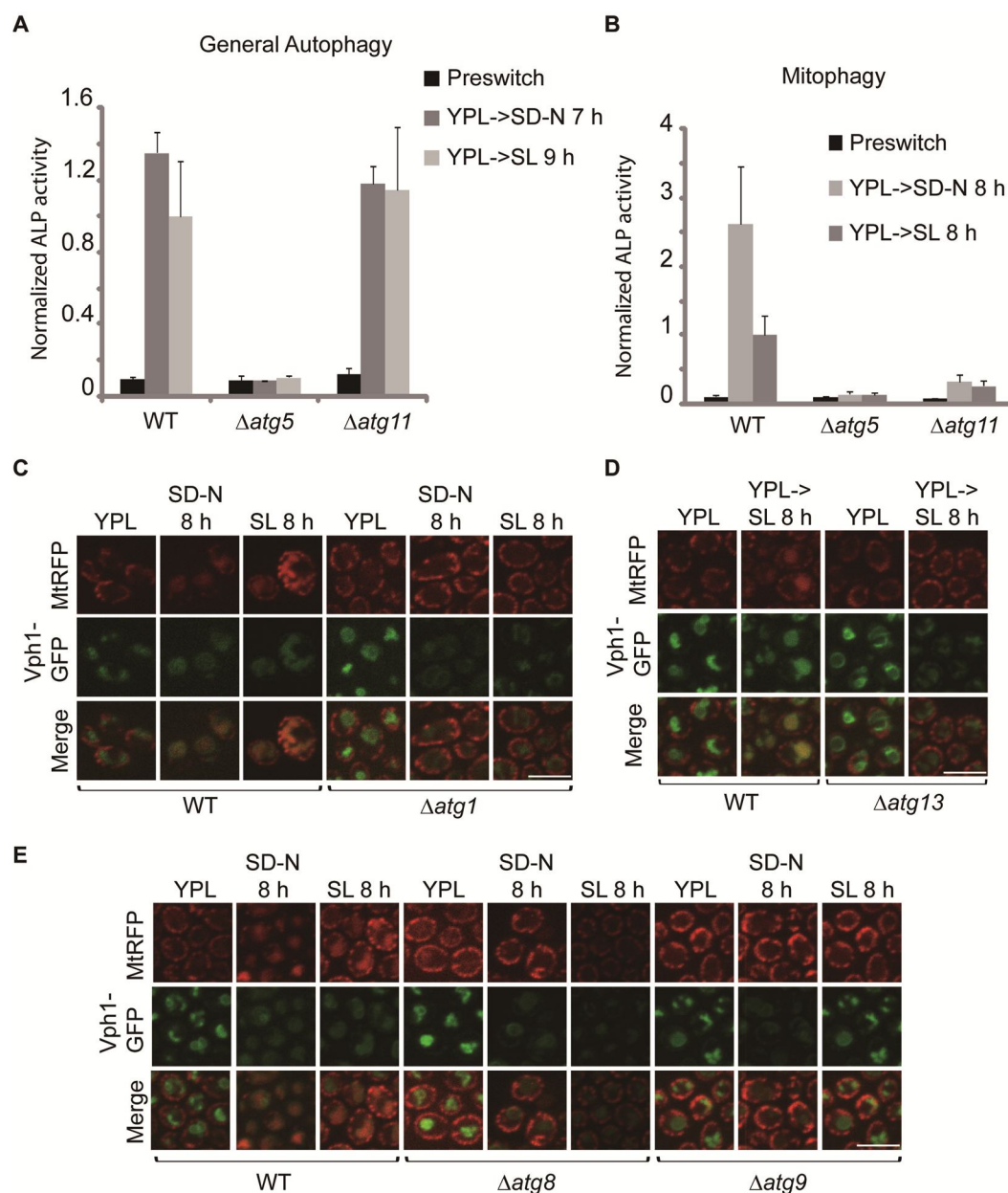


Figure i-2. SL-Induced Autophagy Is Inhibited upon Deletion of Previously Characterized *ATG* Genes

Cells were cultured as described in Figure i-1. General autophagy and mitophagy were examined at the indicated time points.

(A) SL-induced general autophagy and nitrogen-starvation-induced general autophagy were inhibited in $\Delta atg5$ cells, and not affected in $\Delta atg11$ cells. Data represent averages of 3-5 samples with error bars for standard deviations.

(B) SL-induced mitophagy and nitrogen-starvation-induced mitophagy were inhibited in both $\Delta atg5$ and $\Delta atg11$ cells. Data represent averages of 3-5 samples with error bars for standard deviations.

(C-E) In contrast to WT cells, the vacuolar mitochondrial signal was undetectable in $\Delta atg1$, $\Delta atg13$, $\Delta atg8$ and $\Delta atg9$ cells following switch to the autophagy-inducing media (SD-N and/or SL). Scale bar, 10 μm .

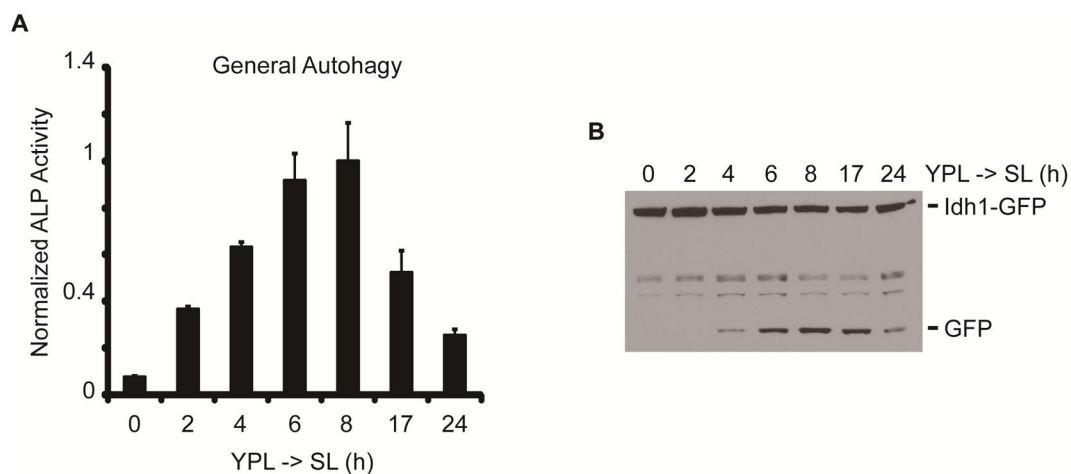


Figure i-3. Time Course for SL-Induced Autophagy

Cells were cultured as described in Figure i-1. General autophagy and mitophagy were examined at the indicated time points. Idh1p is a mitochondrial matrix protein.

(A and B) Time course experiments revealed that autophagic activity became detectable after 2-4 hours, peaked around 6-8 hours and started to decrease after 17-24 hours following switch to SL medium. In (A), data represent averages of 3-5 samples with error bars for standard deviations.

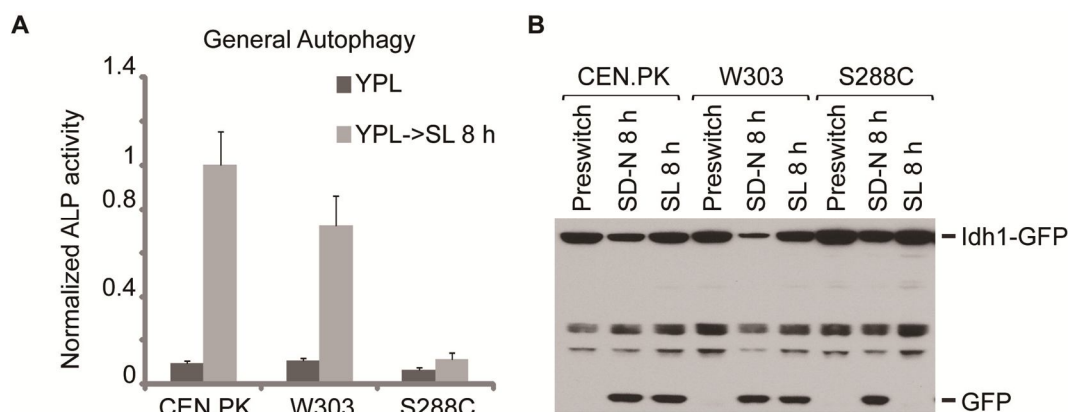


Figure i-4. SL-Induced Autophagy in the W303 Strain Background

The prototrophic versions of CEN.PK, W303 and S288C were cultured as described in Figure i-1. General autophagy and mitophagy were examined at the indicated time points.

(A) Medium switch from YPL to SL led to robust induction of general autophagy in CEN.PK and W303 cells, but not in S288C cells. Data represent the averages of 3-5 samples with error bars for standard deviations.

(B) Medium switch from YPL to SL led to robust induction of mitophagy in CEN.PK and W303 cells, but not in S288C cells. Another autophagy-inducing condition, nitrogen starvation, served as the positive control.

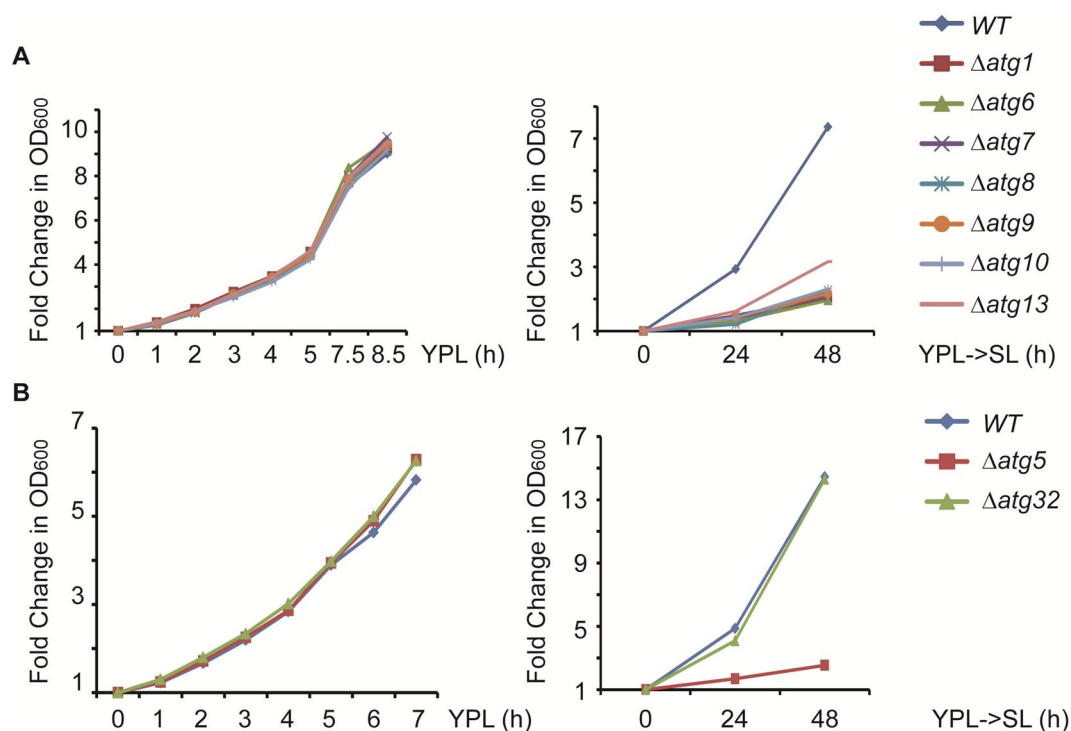


Figure i-5. SL-Induced Autophagy Is Important for Cell Growth upon Switch from YPL to SL Medium

(A) Growth curve of WT and *atg* mutant cells in YPL medium and after switch to SL medium. For growth measurements in YPL, cells of the indicated genotypes were cultured in YPL to log phase and then diluted to OD₆₀₀ 0.05-0.1. OD₆₀₀ was measured every 1-3 hours after dilution and normalized against the first time point. For growth measurements after switch from YPL to SL medium, cells of the indicated genotypes were grown in YPL to log phase (OD₆₀₀ 0.1-0.15) and then switched to SL medium. OD₆₀₀ was measured every 24 hours after medium switch and normalized against the first time point.

(B) Growth curve of WT, $\Delta atg5$ and $\Delta atg32$ cells in YPL medium and after switch to SL medium. Growth measurements were performed as described in (A).

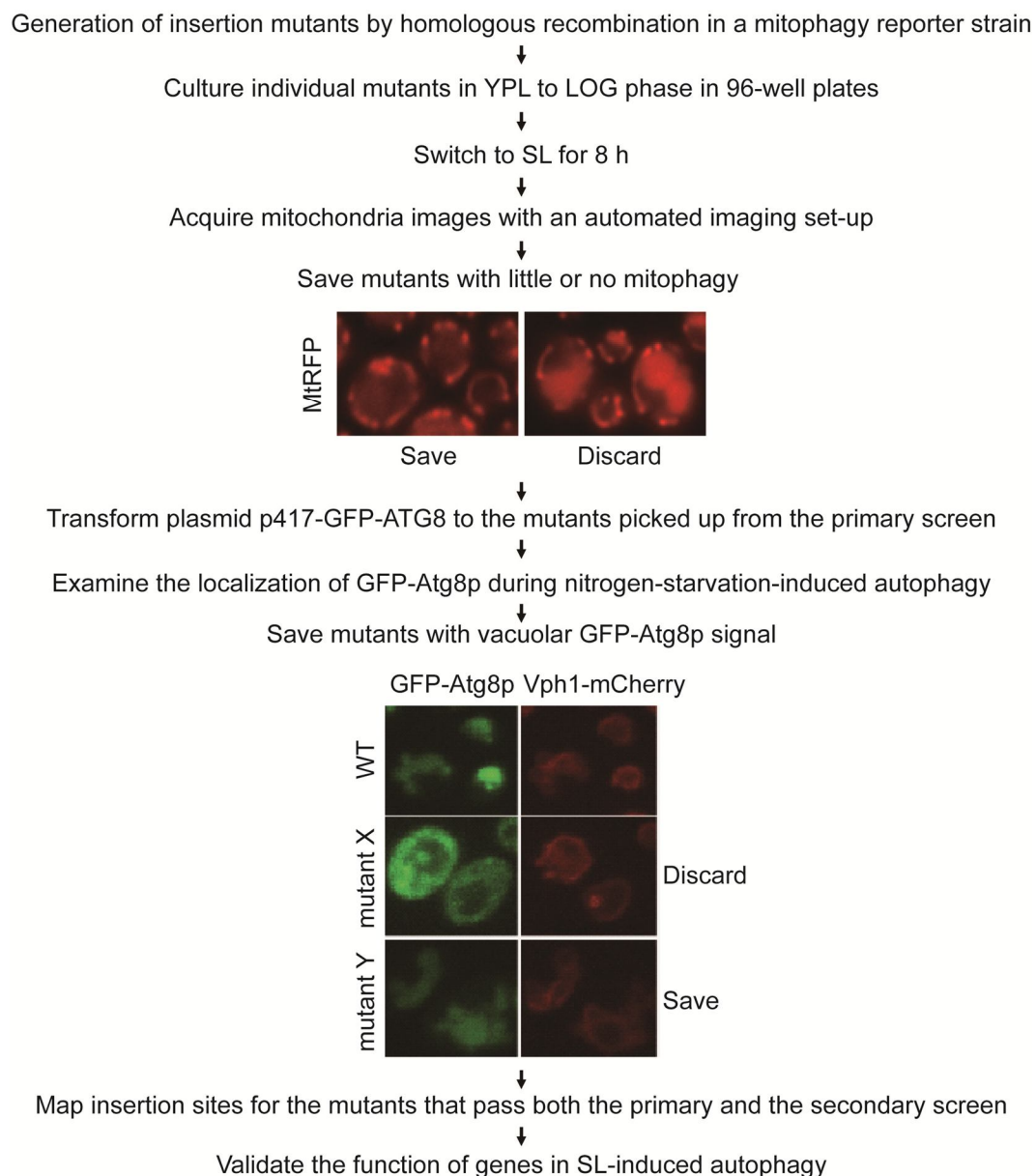


Figure i-6. Flow Chart for the Visual Screen

Please see the text for more details.

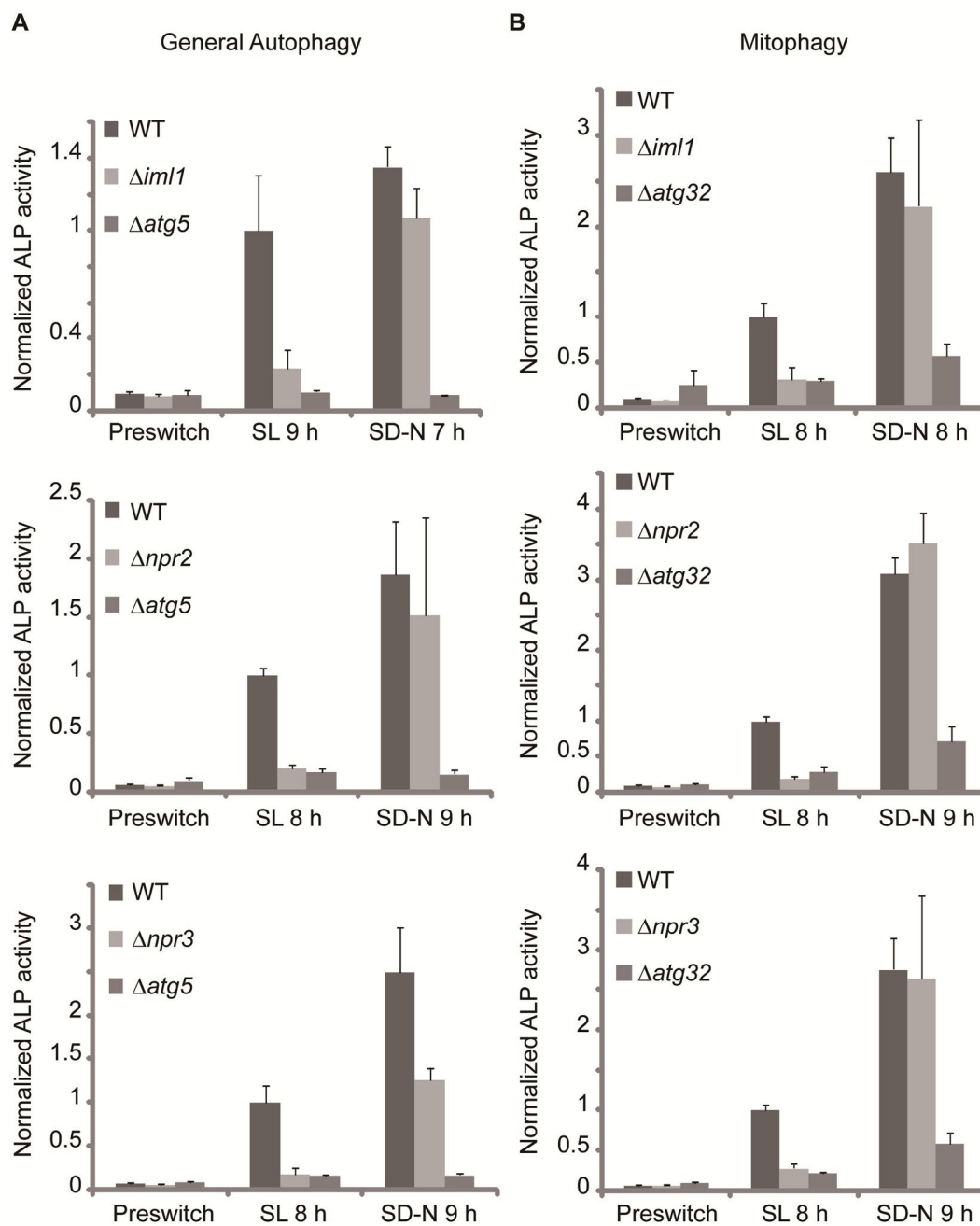


Figure i-7. Visual Screen Uncovers Three Genes that Are Selectively Required for SL-Induced Autophagy

Cells were cultured in YPL to log phase before switch to nitrogen-starvation medium (SD-N) or non-starvation medium (SL). Seven to nine hours following medium switch,

general autophagy or mitophagy was measured by the ALP activity assay. Data represent averages of 3-5 samples with error bars for standard deviations.

(A and B) SL-induced general autophagy and mitophagy were strongly inhibited in $\Delta iml1$, $\Delta npr2$ and $\Delta npr3$ cells. However, deletion of *IML1*, *NPR2* or *NPR3* had minimal to no effect on nitrogen-starvation-induced autophagy. $\Delta atg5$ and $\Delta atg32$ mutants were used as positive controls.

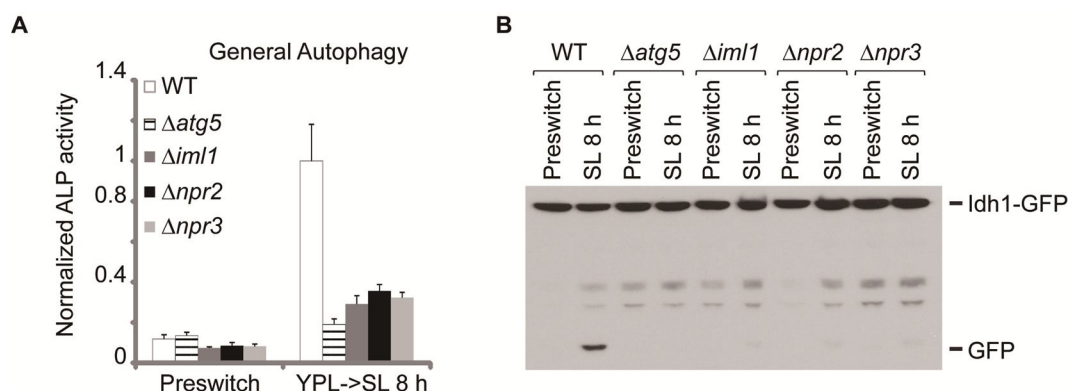


Figure i-8. *IML1*, *NPR2* and *NPR3* Are Essential for SL-Induced Autophagy in the W303 Strain Background

Cells were grown in YPL to log phase before switch to SL medium. General autophagy and mitophagy were examined after eight hours following medium switch.

(A) Loss of *IML1*, *NPR2* or *NPR3* in W303 cells strongly inhibited SL-induced general autophagy. $\Delta atg5$ cells were used as the positive control. Data represent averages of 3-5 samples with error bars for standard deviations.

(B) Loss of *IML1*, *NPR2* or *NPR3* in W303 cells strongly inhibited SL-induced mitophagy. $\Delta atg5$ cells were used as the positive control.

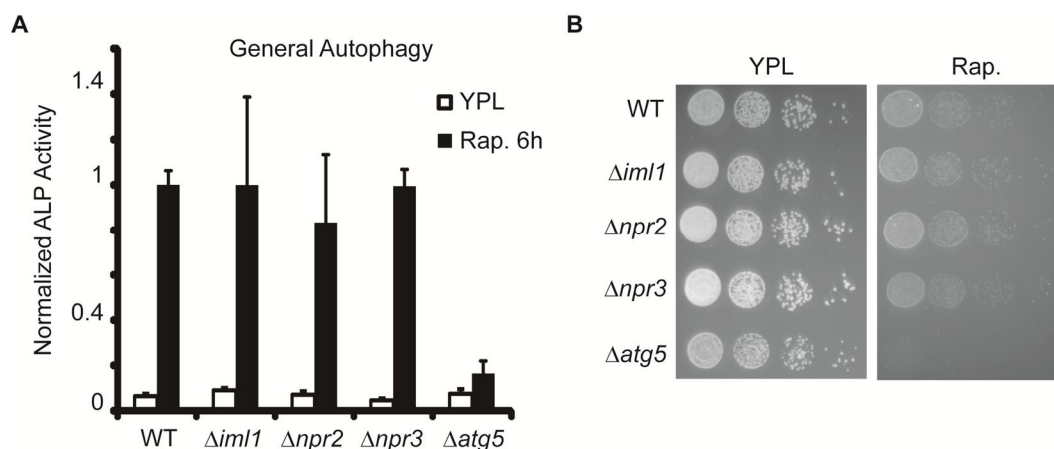


Figure i-9. *IML1*, *NPR2* and *NPR3* Are Not Required for Rapamycin-Induced Autophagy

(A) Cells were grown in YPL to log phase (OD 0.5-0.8) and then continued to be grown in YPL in the presence or absence of rapamycin (0.2 $\mu\text{g}/\text{mL}$) for 6 hours. After rapamycin treatment, general autophagy was measured by ALP activity assay. Data represent the averages of 3-5 samples with error bars for standard deviations. Rap., rapamycin.

(B) Deletion of *IML1*, *NPR2* or *NPR3* did not affect rapamycin sensitivity. Cells of the indicated genotypes were grown in YPL to log phase and then serial 10-fold dilutions of cells were stamped onto YPL plates supplemented with or without rapamycin (0.2 $\mu\text{g}/\text{mL}$). Images were captured after cells had been incubated at 30 $^{\circ}\text{C}$ for 2-4 days.

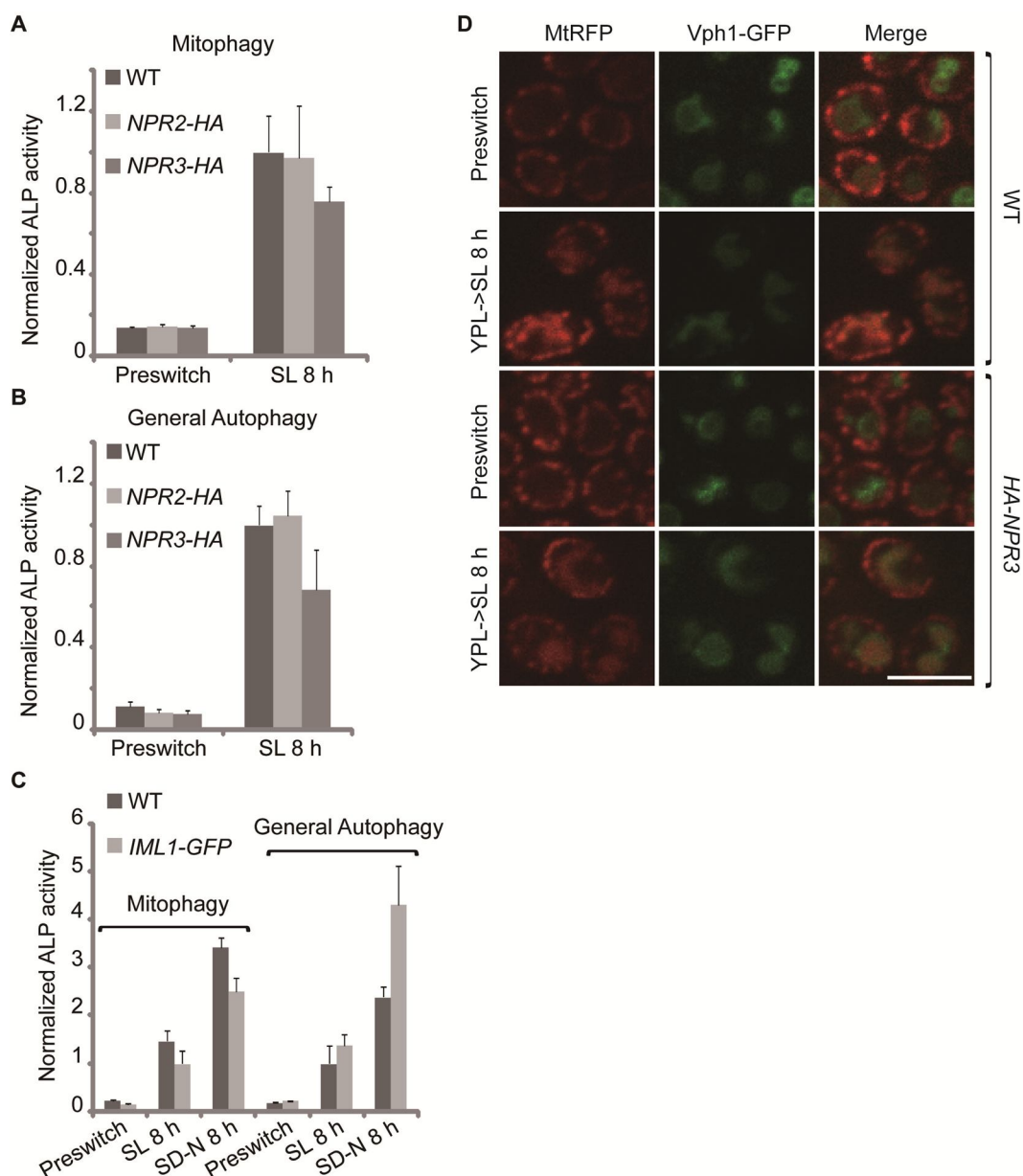


Figure i-10. N- or C-Terminal Epitope-Tagging of Iml1p, Npr2p or Npr3p Does Not Affect SL-Induced Autophagy

Cells of the indicated genotypes were grown in YPL to log phase before switch to autophagy-inducing media (SL and SD-N). General autophagy and mitophagy were examined after eight hours following medium switch.

(A and B) C-terminal HA-tagging of Npr2p or Npr3p did not affect SL-induced autophagy.

(C) C-terminal GFP tagging of Iml1p did not affect SL-induced autophagy. In (A-C), data represent the averages of 3-5 samples with error bars for standard deviations.

(D) N-terminal HA-tagging of Npr3p had no effect on SL-induced mitophagy. Scale bar, 10 μ m.

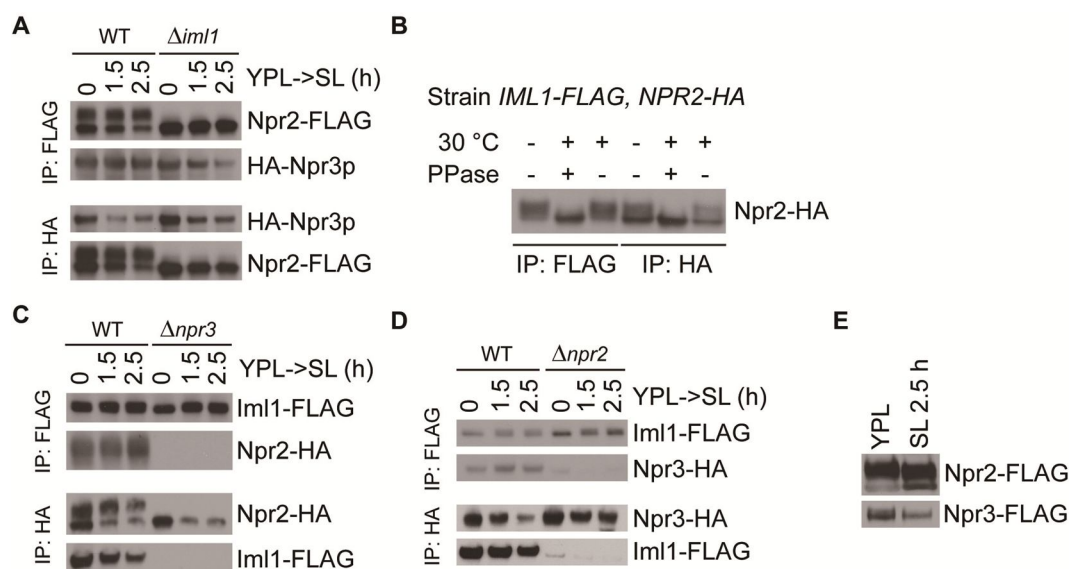


Figure i-11. Iml1p, Npr2p and Npr3p Function in One Complex

Cells were grown in YPL to log phase and then switched to SL medium. At the indicated time points, 80-150 OD cells of the specified double-tagged strains were collected and subject to FLAG or HA immunoprecipitation.

(A) Npr2-FLAG and HA-Npr3p interact with each other. Two forms of Npr2p were observed on the immunoblot. Npr3p associates with both forms of Npr2p. Deletion of *IML1* led to loss of the slower migrating band of Npr2p, but did not affect the interaction between Npr2p and Npr3p.

(B) Iml1p primarily interacts with the phosphorylated form of Npr2p. Cells grown in YPL to log phase were collected and subject to FLAG or HA immunoprecipitation followed by phosphatase treatment. The slower migrating band of Npr2p was eliminated by phosphatase treatment, which indicates that Npr2p is a phosphorylated protein. Iml1p primarily pulled down the phosphorylated form of Npr2p, which collapsed into a signal band after phosphatase treatment.

(C) *NPR3* is required for both Npr2p phosphorylation and the Iml1p-Npr2p interaction. In the absence of Npr3p, dephosphorylated Npr2p was unable to pull down Iml1p.

(D) Iml1p also associates with Npr3p. The Iml1p-Npr3p interaction was disrupted in the absence of *NPR2*. There appeared to be no significant changes in the degree of Iml1p-Npr2p-Npr3p interaction or the phosphorylation status of Npr2p upon switch to SL medium.

(E) Detection of Npr2p and Npr3p expression using TCA precipitated whole cell extracts.

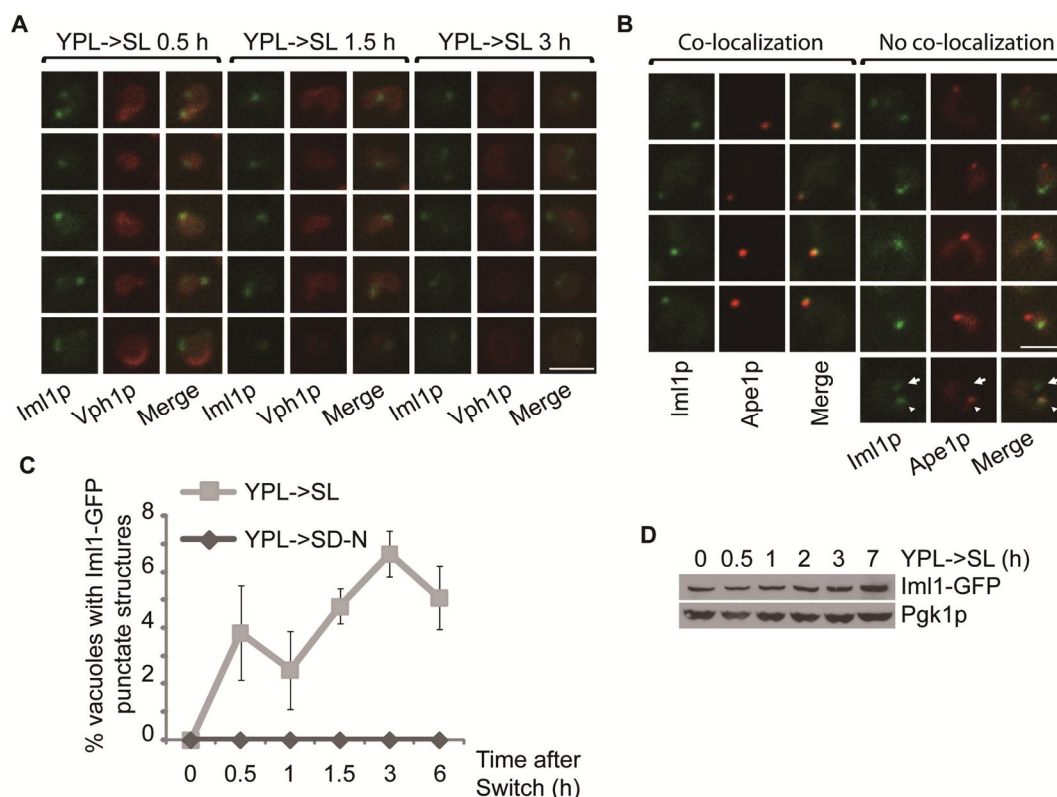


Figure i-12. Iml1-GFP Localizes to Both PAS and Non-PAS Punctate Structures during SL-Induced Autophagy

(A) Upon switch to SL medium, Iml1-GFP formed punctate structures proximal to the vacuole marked by Vph1-mCherry. Vph1p is a vacuole-resident protein. Representative images from different time points are shown. Scale bar, 5 μ m.

(B) Upon switch to SL medium, Iml1-GFP localized to both PAS (arrowhead) and non-PAS punctate foci (arrow). PAS is marked by Ape1-mRFP1 (Suzuki et al., 2007). Representative images from different time points (YPL->SL 1.5-3 h) are shown. Scale bar, 5 μ m.

(C) Iml1-GFP punctate structures were detected in a small fraction of cells upon switch to SL medium. However, medium switch from YPL to nitrogen-starvation medium (SD-N) did not induce the formation of Iml1-GFP punctate structures. At least 200 cells were counted for each time point. Data represent averages from three independent experiments with error bars for standard deviations.

(D) The abundance of Iml1-GFP did not change at the early time points following switch to SL medium, while modestly increased at the later time points. At the indicated time points, 5 OD cells were collected for whole cell TCA extraction and then analyzed by immunoblotting. Pgk1p was used as the loading control.

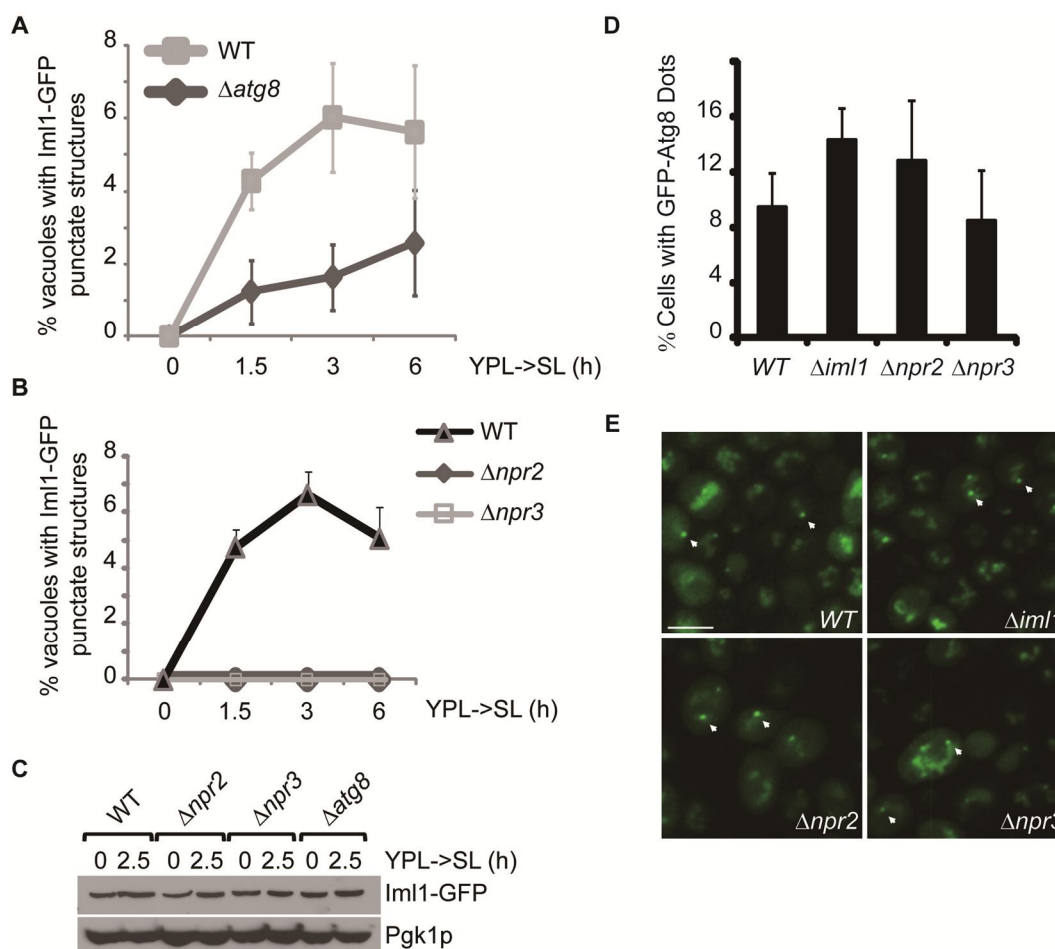


Figure i-13. *NPR2*, *NPR3* and *ATG8* Are Required for the Formation of Iml1-GFP Punctate Structures

(A) The formation of Iml1-GFP punctate structures was partially inhibited in $\Delta atg8$ cells at early time points following switch to SL medium. At least 200 cells were counted for each genotype. Data represent averages from three independent experiments with error bars for standard deviations.

(B) Iml1-GFP punctate structures were not detectable in $\Delta npr2$ and $\Delta npr3$ cells after switch to SL medium. At least 200 cells were counted for each genotype. Data represent averages from three independent experiments with error bars for standard deviations.

(C) The expression of Iml1-GFP is not affected in $\Delta npr2$, $\Delta npr3$ and $\Delta atg8$ cells. TCA-precipitated whole cell extracts from either control or mutant cells were analyzed by immunoblotting.

(D) WT or mutant cells that express GFP-Atg8 were grown in YPL to log phase and then switched to SL medium. Thirty minutes after medium switch, cells were collected for GFP imaging. At least 200 cells were counted for each genotype. Data represent averages from three independent experiments with error bars for standard deviations.

(E) Representative images showing the formation of Atg8p dots in SL as indicated by the arrows. Scale bar, 5 μ m.

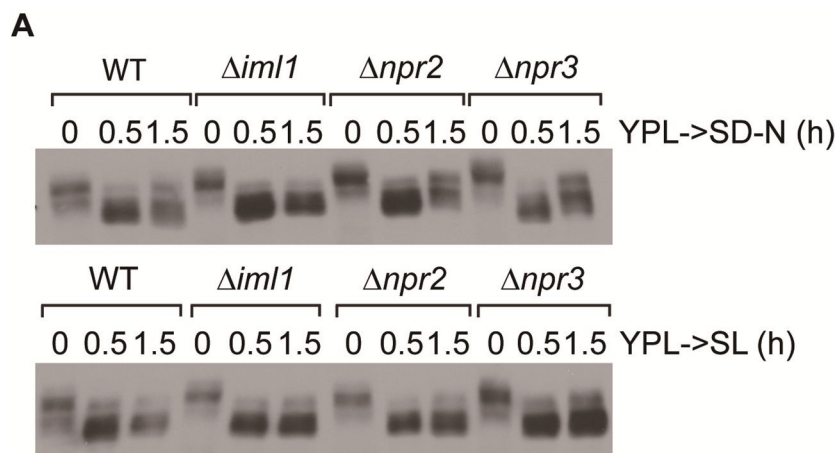


Figure i-14. *IML1*, *NPR2* and *NPR3* Do Not Regulate Atg13p Phosphorylation

Cells were grown in YPL to log phase before switch to nitrogen-starvation medium (SD-N) or SL medium. At the indicated time points, cells were collected and processed as described in Figure i-1E.

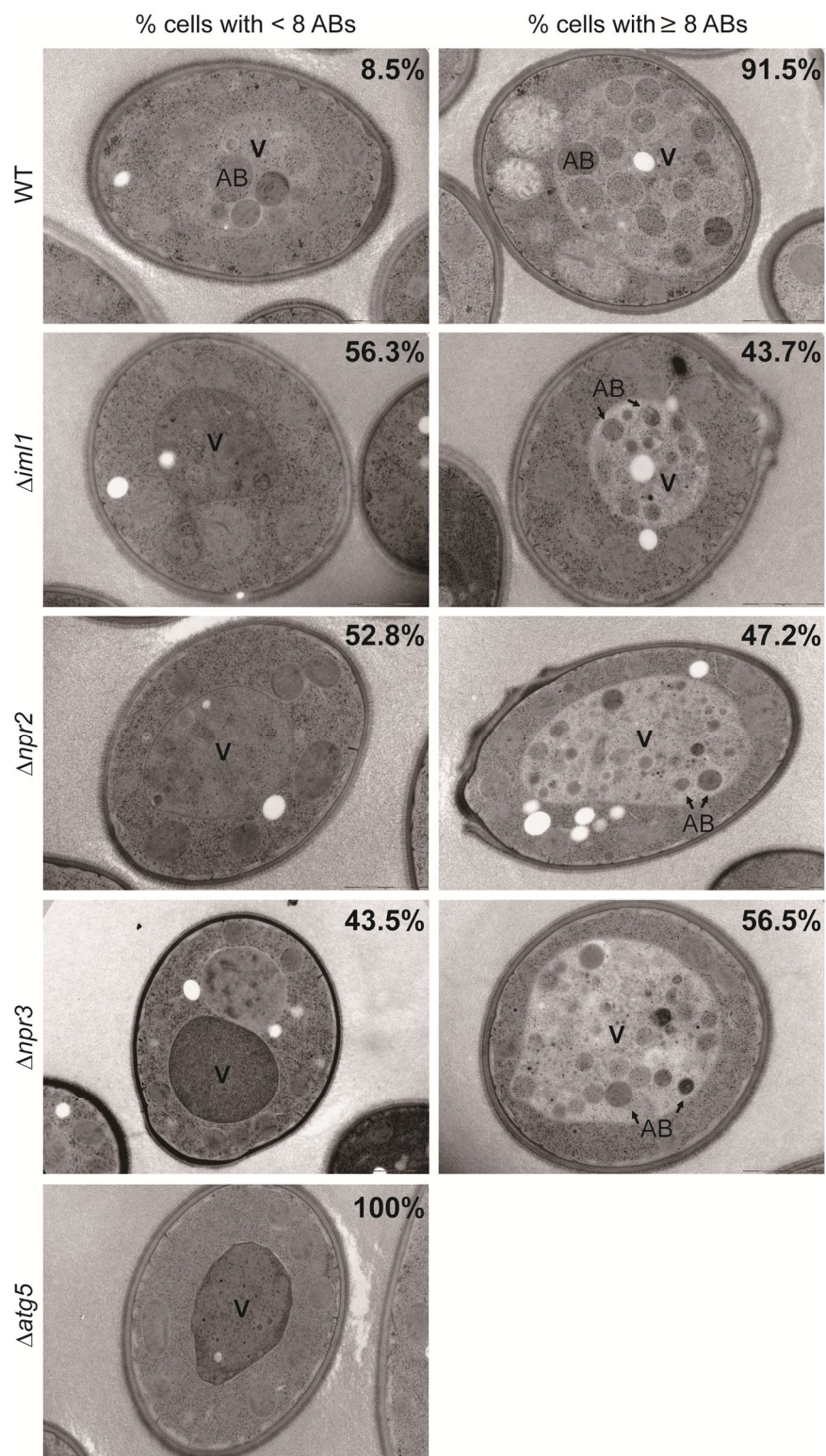


Figure i-15. Iml1p-Npr2p-Npr3p Complex Regulates Autophagosome Formation during SL-Induced Autophagy

After 9 hours following medium switch from YPL to SL, cells of the indicated genotypes were collected and processed for ultra-structural analysis. Representative images for cells with fewer than 8 ABs or cells with 8 or more ABs are shown. The percentages of cells classified into each group are indicated in the corresponding images. Total number of cells counted for each genotype: 271 (WT), 256 ($\Delta iml1$), 337 ($\Delta npr2$), 232 ($\Delta npr3$), 134 ($\Delta atg5$). V, vacuole. AB, autophagic body.

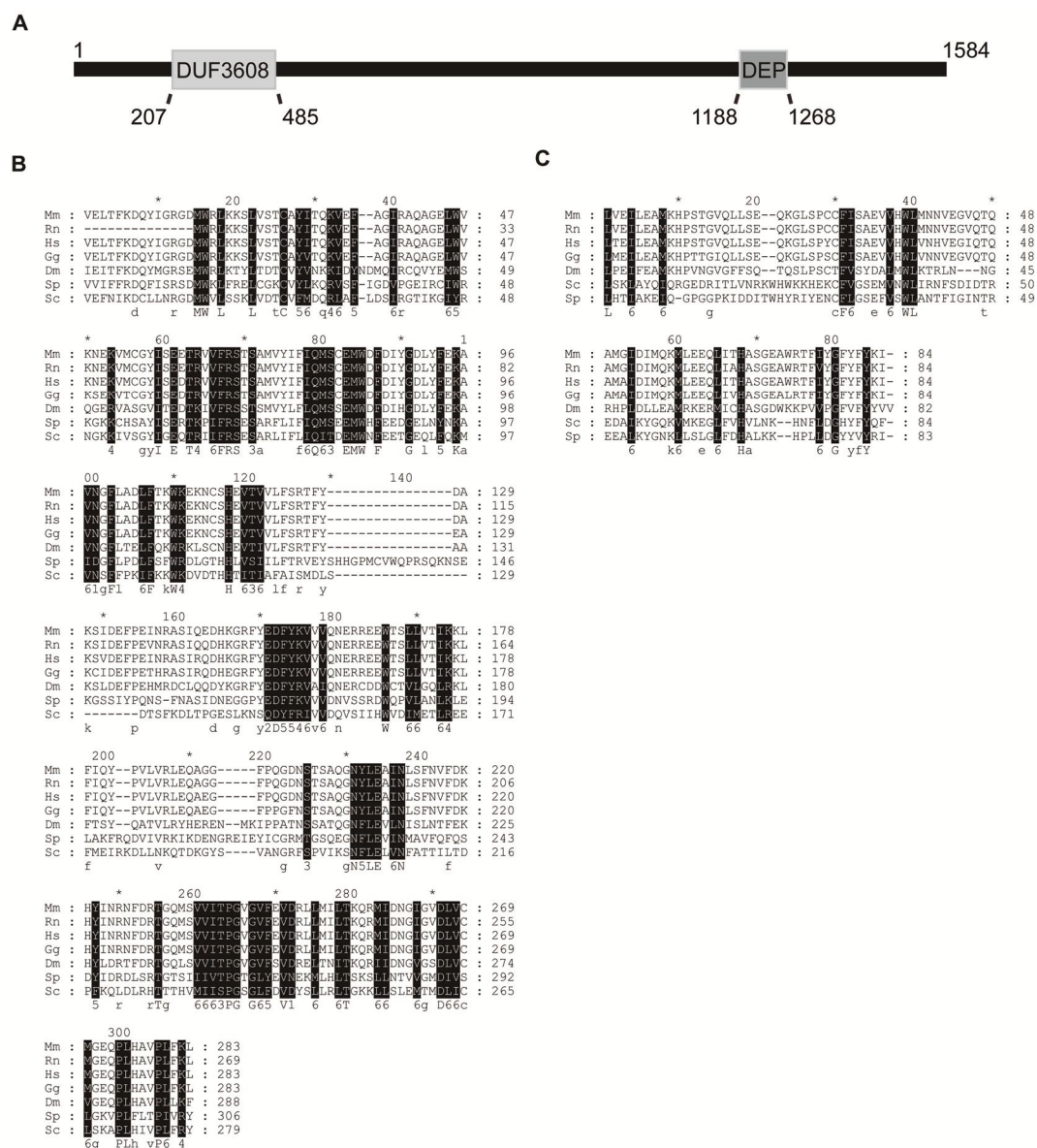


Figure i-16. Multiple Sequence Alignment of Iml1p and its Orthologs

Highly conserved residues are colored in black. Partially conserved residues are colored in gray. The DUF and DEP domains are highlighted by straight lines beneath the sequences. Mm, *Mus musculus*; Rn, *Rattus norvegicus*; Hs, *Homo sapiens*; Gg, *Gallus gallus*; Dm, *Drosophila melanogaster*; Sp, *Schizosaccharomyces pombe*; Sc, *Saccharomyces cerevisiae*.



Figure i-17. Multiple Sequence Alignment of Iml1p and its Orthologs

Highly conserved residues are colored in black. Partially conserved residues are colored in gray. The DUF and DEP domains are highlighted by straight lines beneath the sequences. Mm, *Mus musculus*; Rn, *Rattus norvegicus*; Hs, *Homo sapiens*; Gg, *Gallus gallus*; Dm, *Drosophila melanogaster*; Sp, *Schizosaccharomyces pombe*; Sc, *Saccharomyces cerevisiae*.

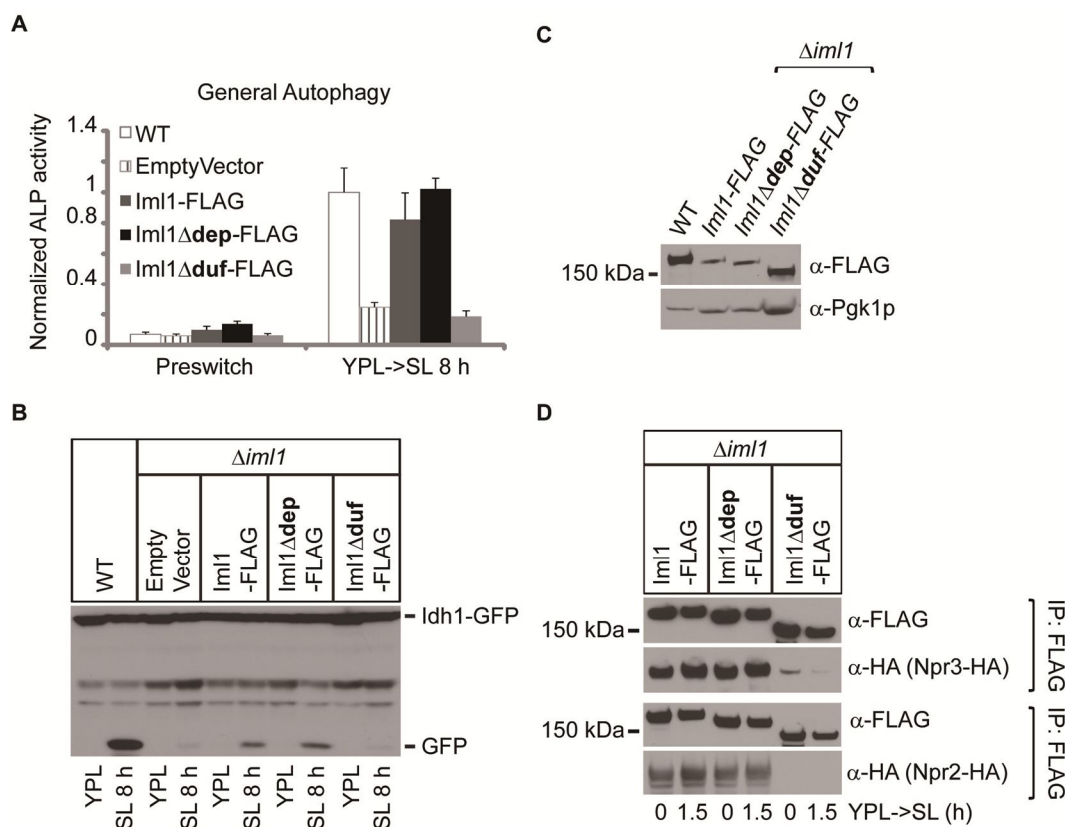


Figure i-18. Iml1p Contains an Evolutionarily Conserved Domain that Is Important for SL-Induced Autophagy and Formation of the Iml1p Complex

(A and B) The DUF domain of Iml1p is required for SL-induced autophagy as assessed by Western blot and ALP activity assay. The coding sequence for full length IML1-FLAG, iml1 Δ dep-FLAG or iml1 Δ duf-FLAG was cloned into a centromeric plasmid under the control of the *CYC1* promoter. Empty vector or plasmids expressing Iml1-FLAG, Iml1 Δ dep-FLAG or Iml1 Δ duf-FLAG were transformed into Δ iml1 cells to determine if they could rescue SL-induced autophagy. WT cells are shown for comparison. In (A), data represent averages of 3-5 samples with error bars for standard deviations.

(C) Ectopic expression of full-length and the domain-deleted versions of Iml1p. Cells were collected and analyzed as described in Figure 12D. Pgk1p was used as the loading control. WT cells expressing Iml1-FLAG from the endogenous chromosomal locus are shown for comparison.

(D) The DUF (RANS) domain of Iml1p is required for its interaction with Npr2p and Npr3p. Empty vector or plasmids expressing Iml1-FLAG, Iml1 Δ dep-FLAG or Iml1 Δ duf-FLAG were transformed into Δ iml1 cells and then used to pull down Npr2p or Npr3p.

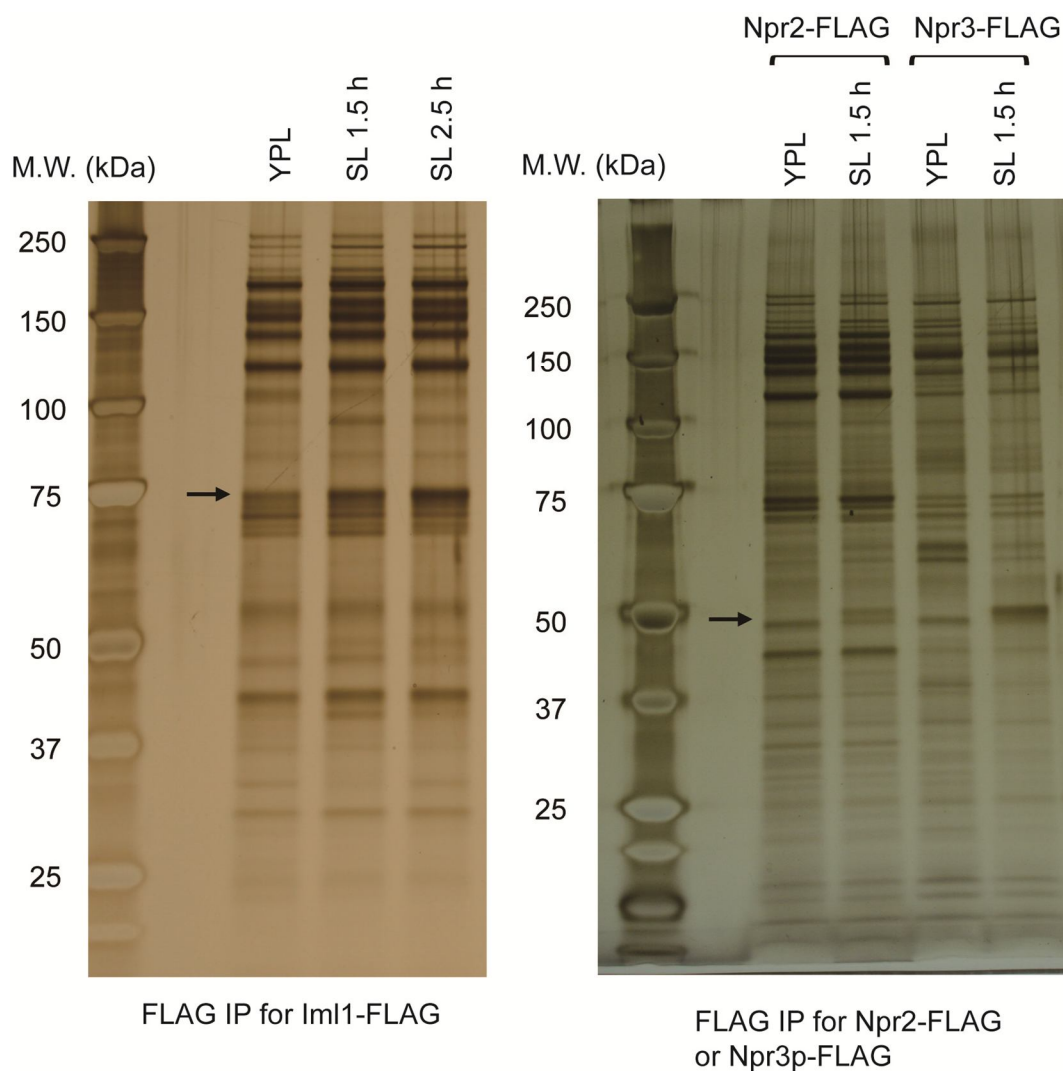


Figure i-19. Identification of Iml1p-, Npr2p- and Npr3p-Interacting Proteins by Immunoprecipitation

Cells were grown in YPL to log phase and then switched to SL medium. At the indicated time points, 80-150 OD cells of the specified FLAG-tagged strains were collected and subject to FLAG immunoprecipitation. The immunoprecipitates were then analyzed by SDS-PAGE and silver staining. Arrows indicate the bands that showed changes in intensity upon switch from YPL to SL medium and were later subject to protein identification by LC-MS/MS.

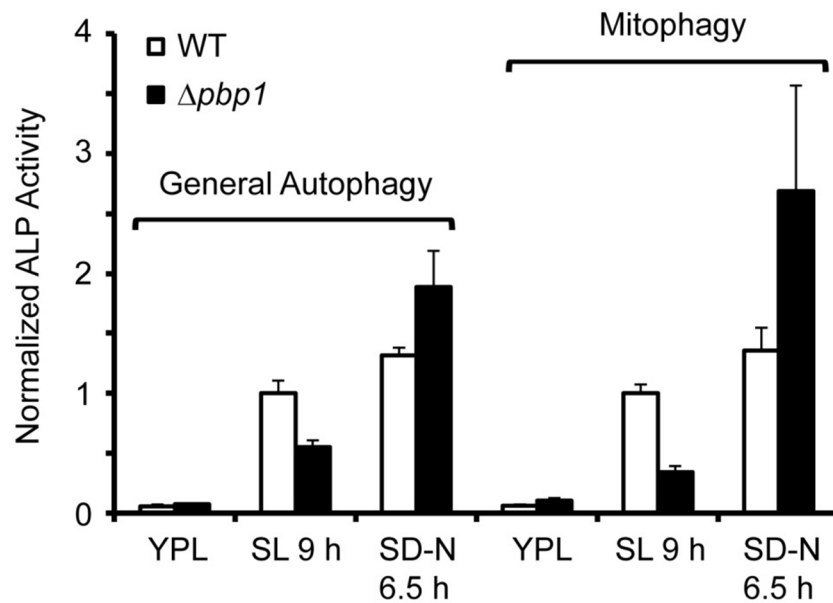


Figure ii-1. SL-Induced Autophagy Is Inhibited upon Deletion of *PBP1*

Cells were grown in YPL to log phase and then switched to nitrogen-starvation medium (SD-N) or SL medium. General autophagy and mitophagy were examined at the indicated time points by ALP activity assay. Data represent the averages of 3-5 samples with error bars for standard deviations.

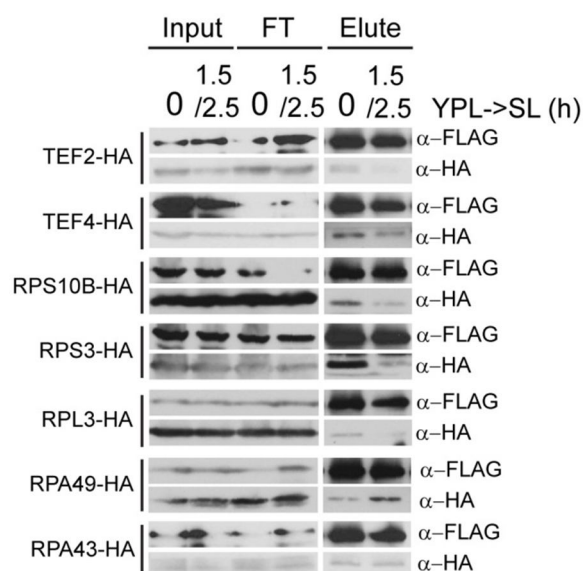


Figure ii-2. Pbp1p Interacts with Ribosome Proteins and Translation Elongation Factors

Cells were grown in YPL to log phase and then switched to SL medium. At the indicated time points, 80-150 OD cells of the specified double-tagged strains were collected and subject to FLAG immunoprecipitation for Pbp1-FLAG. Whole cell extracts (Input), flow through samples (FT) and Pbp1-FLAG immunoprecipitates (Elute) were analyzed by SDS-PAGE.

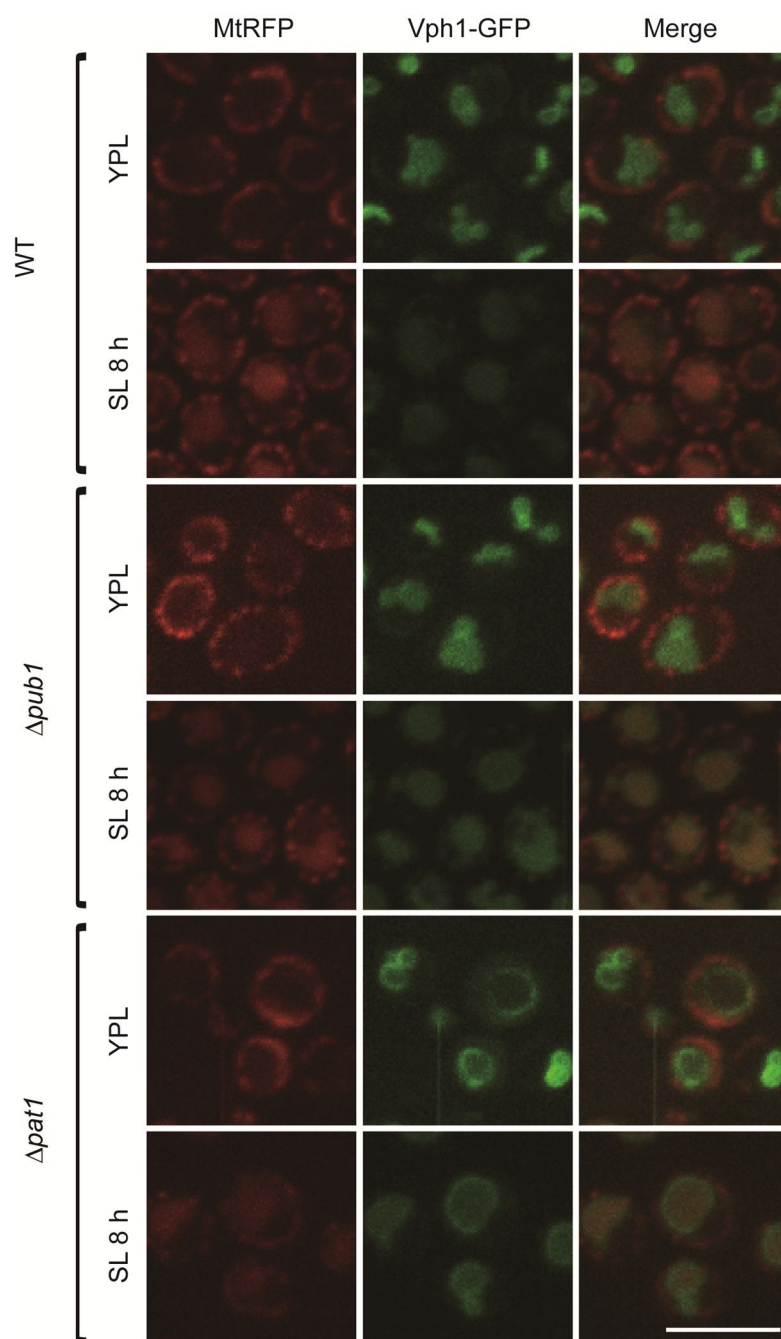


Figure ii-3. SL-Induced Mitophagy Was Not Affected in $\Delta pub1$ and $\Delta pat1$ Mutants

Cells were grown in YPL to log phase and then switched to SL medium. Mitophagy was assessed by imaging using MtRFP as the reporter. Scale bar, 10 μ m.

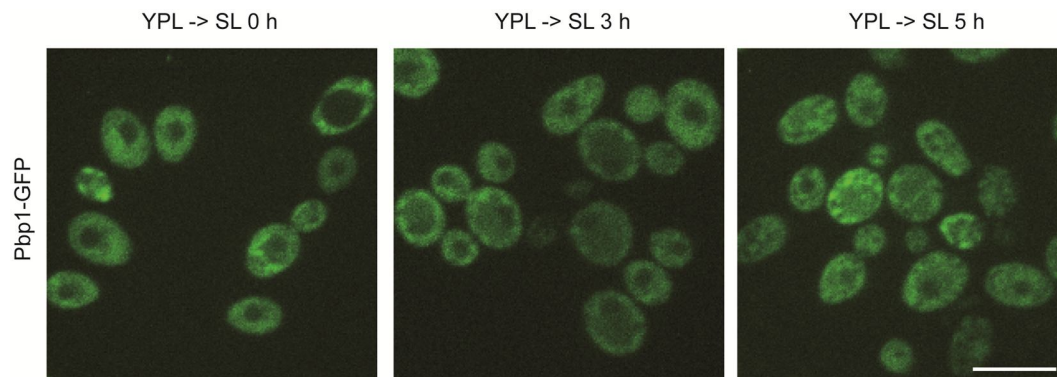


Figure ii-4. Localization of Pbp1-GFP in YPL and After Switch to SL Medium

Pbp1-GFP localization did not change after switch to SL medium. Cells were grown in YPL to log phase and then switched to SL medium. At the indicated time points, cells were collected for GFP imaging. Scale bar, 10 μ m.

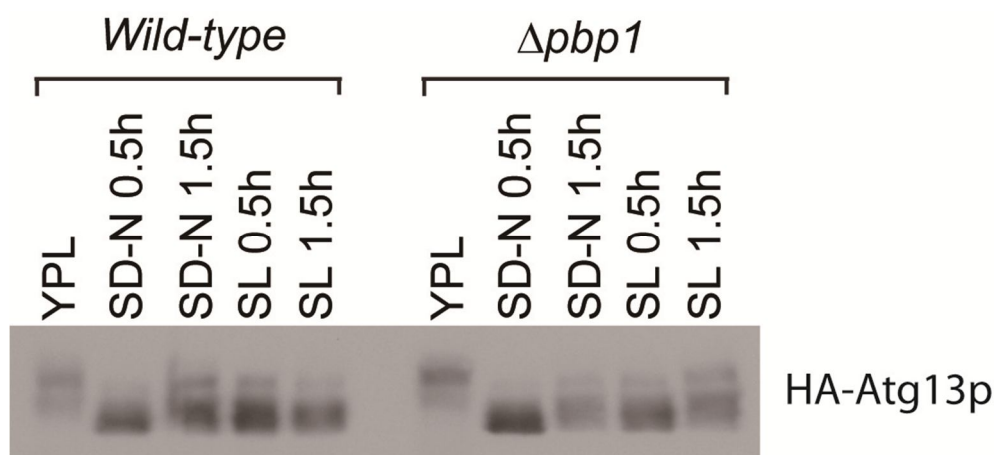
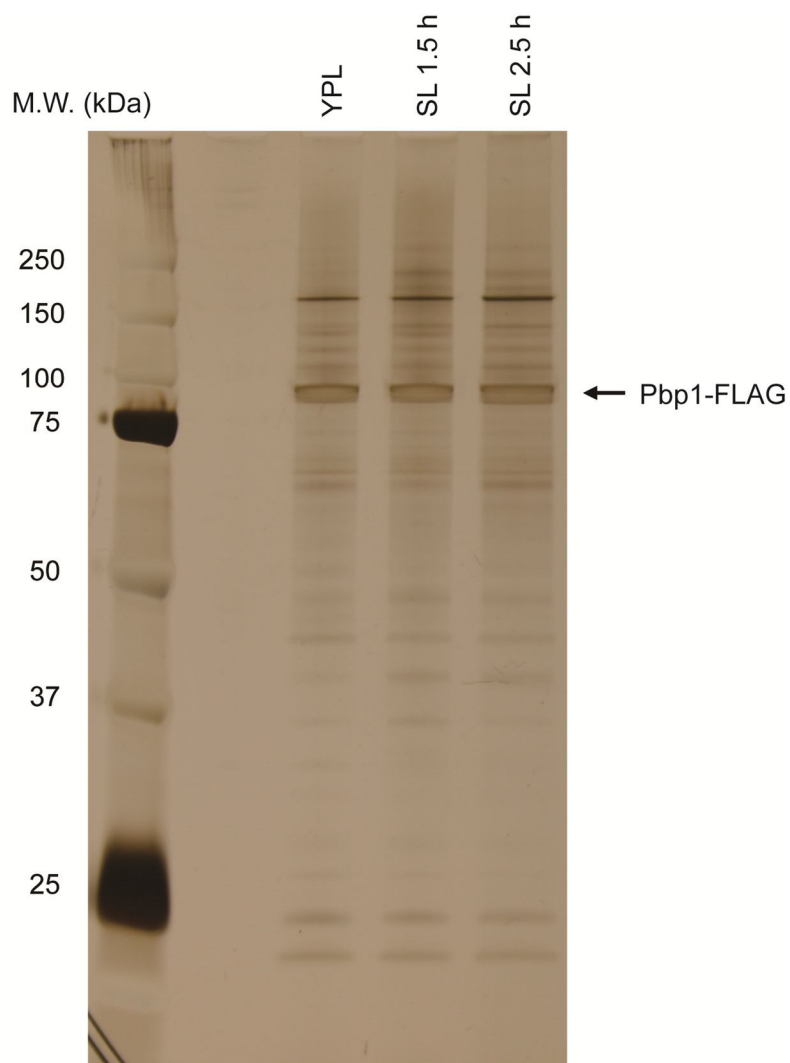


Figure ii-5. *PBPI* Does Not Regulate Atg13p Phosphorylations

Cells were grown in YPL to log phase before switch to nitrogen-starvation medium (SD-N) or SL medium. At the indicated time points, cells were collected and processed as described in Figure i-1E.



FLAG IP for Pbp1-FLAG

Figure ii-6. Identification of Pbp1p-Interacting Proteins by Immunoprecipitation

Cells were grown in YPL to log phase and then switched to SL medium. At the indicated time points, 80-150 OD cells of the specified FLAG-tagged strains were collected and subject to FLAG immunoprecipitation. The immunoprecipitates were then analyzed by SDS-PAGE and silver staining.

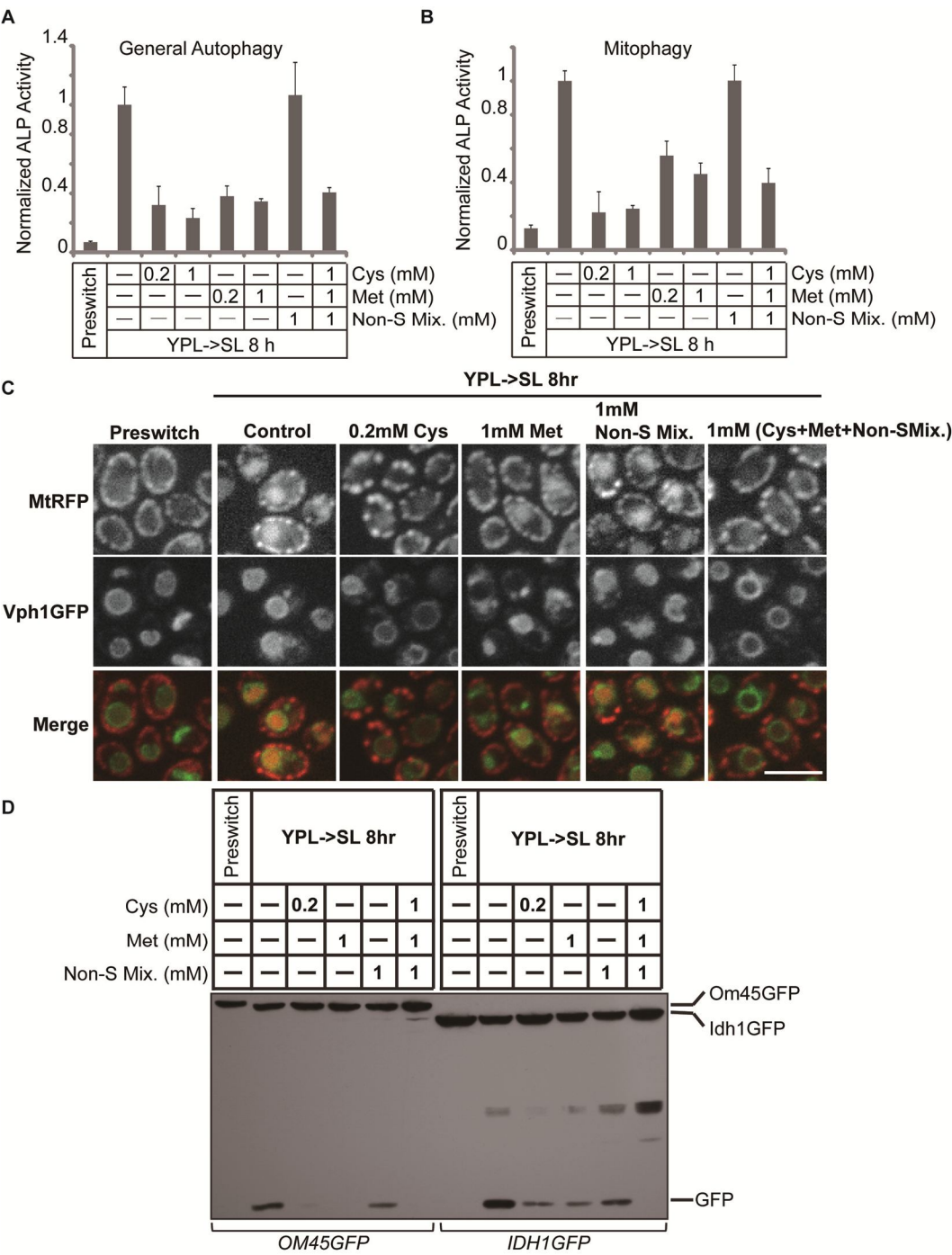


Figure iii-1. Selective Inhibition of SL-Induced Autophagy by Sulfur-Containing Amino Acids

Cells were grown in YPL to log phase and then switched to SL medium supplemented with or without amino acids. General autophagy and mitophagy were examined at the indicated time points.

(A) SL-induced general autophagy was strongly inhibited by cysteine and methionine, but not by a non-sulfur-containing amino acid mixture. Data represent the averages of 3-5 samples with error bars for standard deviations.

(B) SL-induced mitophagy was significantly inhibited by cysteine and methionine, but not by a non-sulfur-containing amino acid mixture. Methionine was less effective than cysteine at inhibiting SL-induced mitophagy. Data represent the averages of 3-5 samples with error bars for standard deviations.

(C) Translocation of MtRFP into the vacuole upon switch to SL medium was blocked by sulfur-containing amino acids, but not by non-sulfur containing amino acids. Scale bar, 10 μ m.

(D) Release of free GFP from Idh1-GFP or Om45-GFP upon switch to SL medium was inhibited by sulfur-containing amino acids, but not by non-sulfur containing amino acids.

Cysteine and methionine solutions were made fresh before all experiments. The non-sulfur-containing amino acid mixture (Non-S Mix.) contains all the non-sulfur-containing amino acids except for tyrosine (tyrosine exhibits very poor solubility, so was added separately (Figure iii-2)).

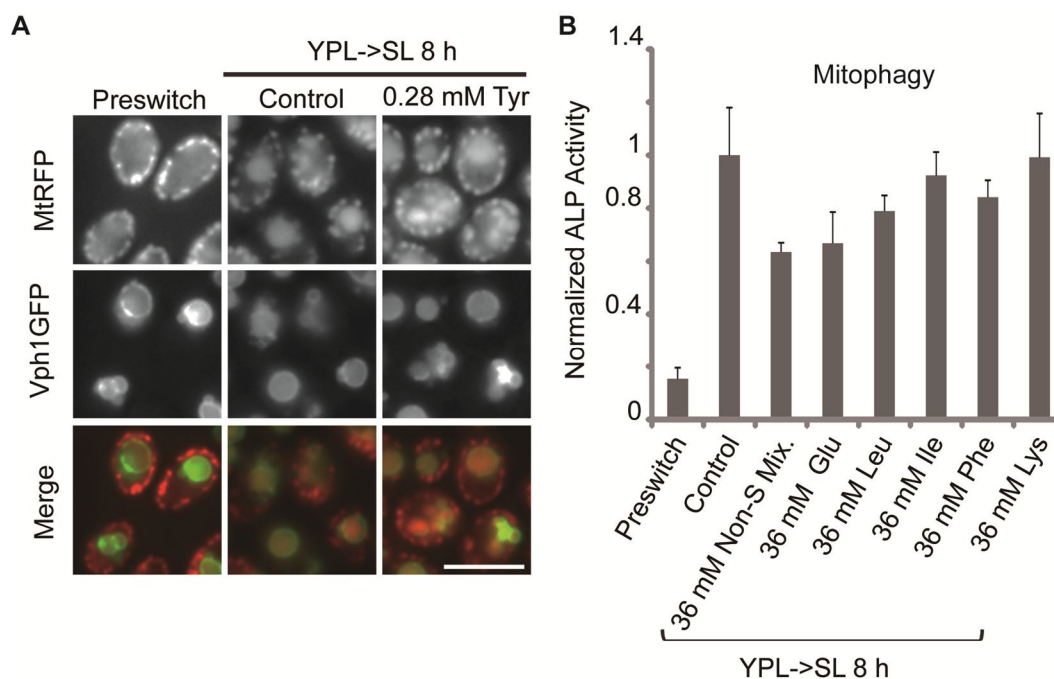


Figure iii-2. Non-Sulfur-Containing Amino Acids Have No or Minor Inhibitory Effect on SL-Induced Mitophagy

Cells were cultured as described in Figure iii-1.

(A) Tyrosine did not affect SL-induced mitophagy. Scale bar, 10 μ m.

(D) Non-sulfur-containing amino acids had minimal to no inhibitory effect on SL-induced mitophagy even when added at concentrations as high as 36 mM. The non-sulfur-containing amino acid mixture contained glutamate, arginine, aspartate, histidine, isoleucine, leucine, lysine, phenylalanine, threonine, tryptophan, serine and valine. Data represent the averages of 3-5 samples with error bars for standard deviations.

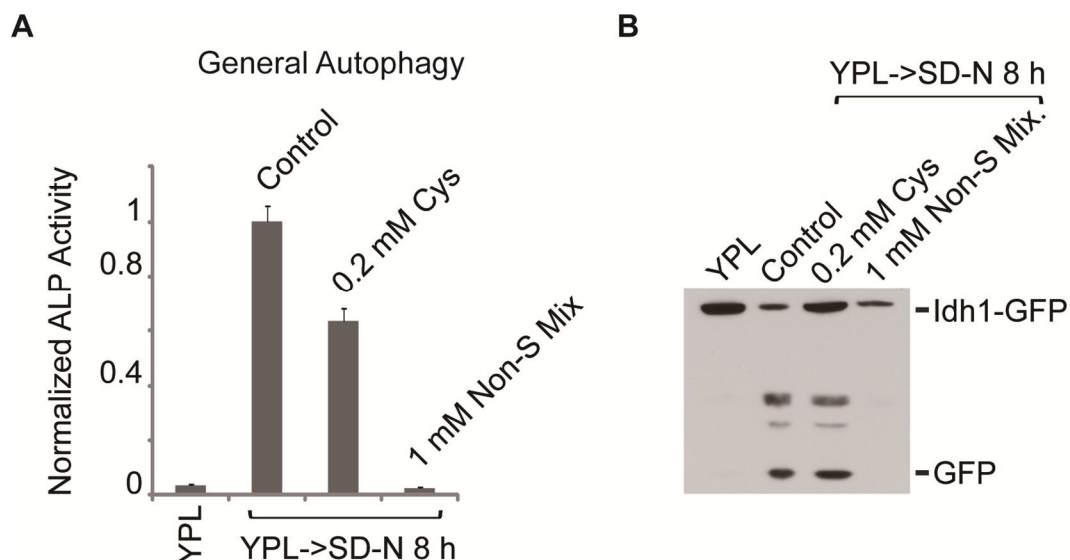


Figure iii-3. Effects of Amino Acids on Nitrogen-Starvation-Induced Autophagy

Cells were grown in YPL to log phase and then switched to nitrogen starvation medium (SD-N) supplemented with or without amino acids. General autophagy and mitophagy were measured at the indicated time points.

(A and B) Nitrogen-starvation-induced autophagy was completely inhibited by 1 mM non-sulfur-containing amino acid mixture. In contrast, 0.2 mM cysteine had only a minor effect on nitrogen-starvation-induced autophagy. In (A), data represent the averages of 3-5 samples with error bars for standard deviations. The non-sulfur-containing amino acid mixture (Non-S Mix.) contains all the non-sulfur-containing amino acids except for tyrosine.

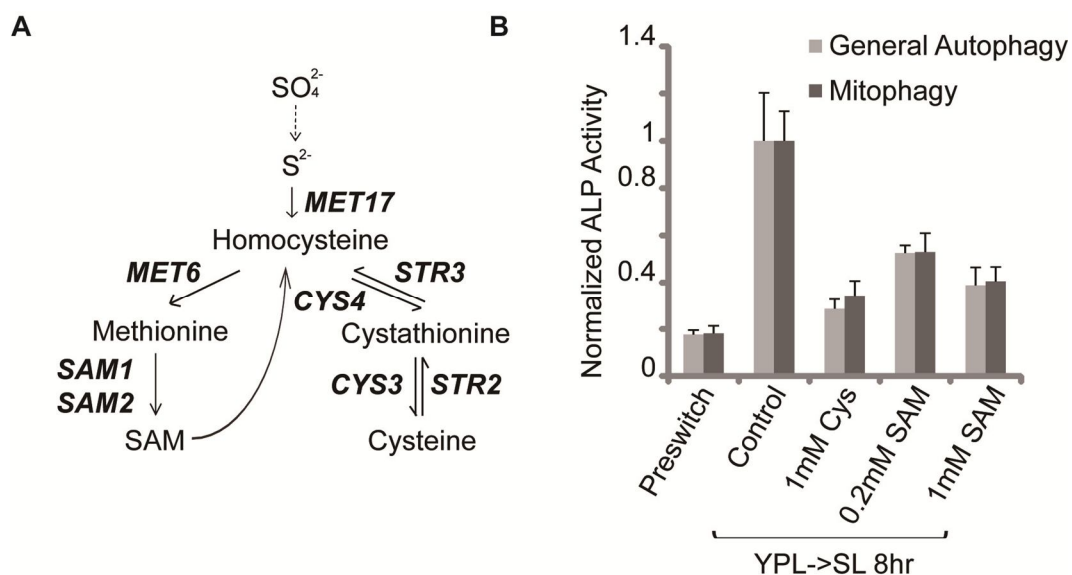


Figure iii-4. Inhibition of SL-Induced Autophagy by SAM

Cells were grown in YPL to log phase before switch to SL medium supplemented with or without the indicated metabolites.

(A) De novo biosynthesis pathway for sulfur-containing amino acids.

(B) Inclusion of SAM strongly inhibited SL-induced autophagy even at concentrations as low as 0.2 mM. Data represent the averages of 3-5 samples with error bars for standard deviations.

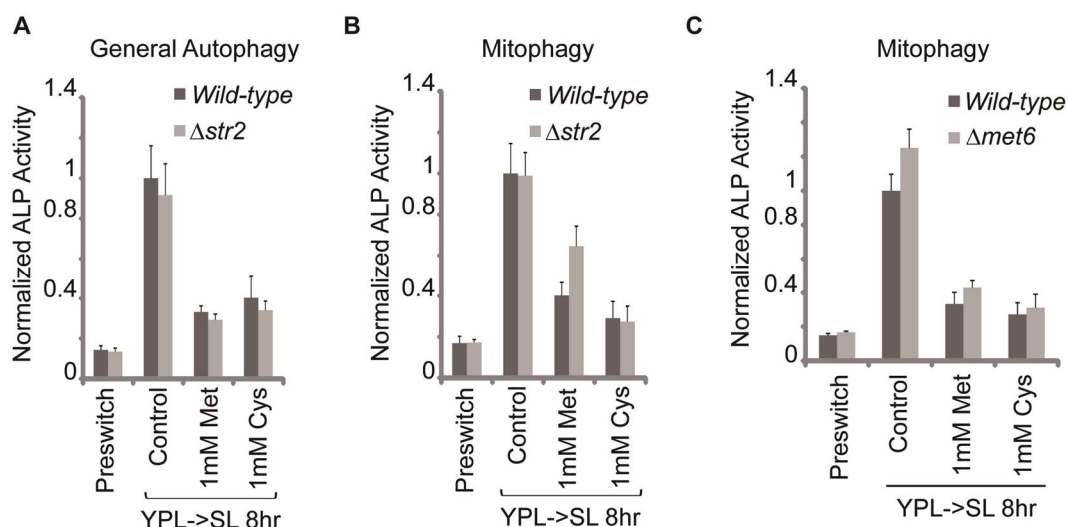


Figure iii-5. Metabolic Flux from Cysteine to Methionine Is Not Required for the Inhibitory Effect of Cysteine on SL-Induced Autophagy

Cells of the indicated genotypes were cultured as described in Figure iii-1. Data represent the averages of 3-5 samples with error bars for standard deviations.

(A and B) Cysteine still strongly inhibited SL-induced autophagy even when the metabolic flux from cysteine to methionine was blocked in the $\Delta str2$ mutants. Methionine was used as the positive control.

(C) Cysteine still strongly inhibited SL-induced mitophagy even when the metabolic flux from cysteine to methionine was blocked in the $\Delta met6$ mutants. Methionine was used as the positive control.

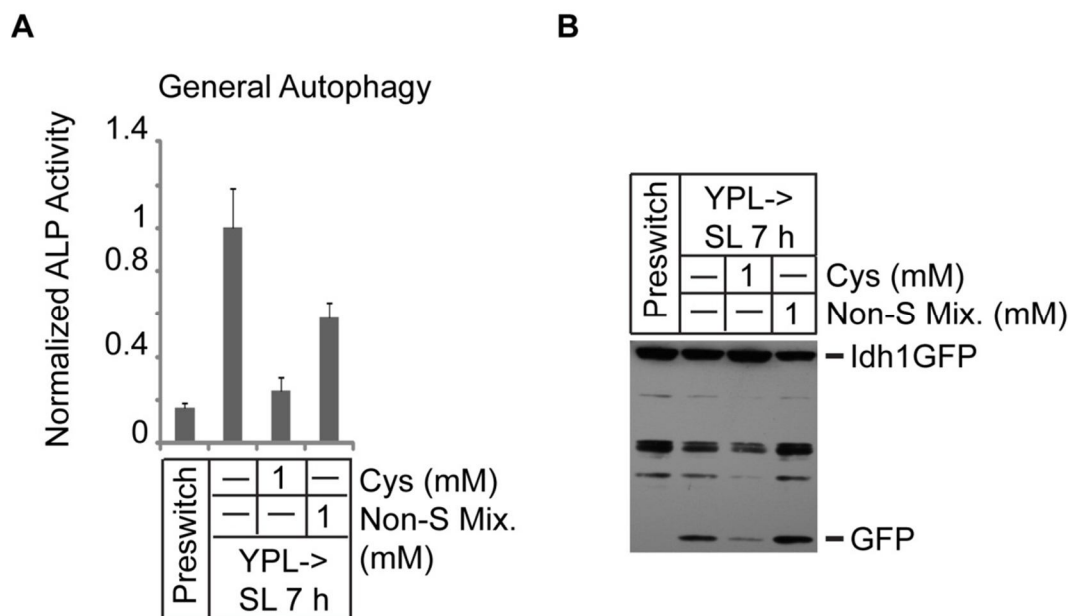


Figure iii-6. Effects of Amino Acids on SL-Induced Autophagy in the W303 Strain Background

Cells were cultured as described in Figure iii-1.

(A and B) SL-induced autophagy was strongly blocked by cysteine, while in striking contrast, only slightly inhibited by a non-sulfur-containing amino acid mixture. The non-sulfur-containing amino acid mixture (Non-S Mix.) contains all the non-sulfur-containing amino acids except for tyrosine. In (A), data represent the averages of 3-5 samples with error bars for standard deviations.

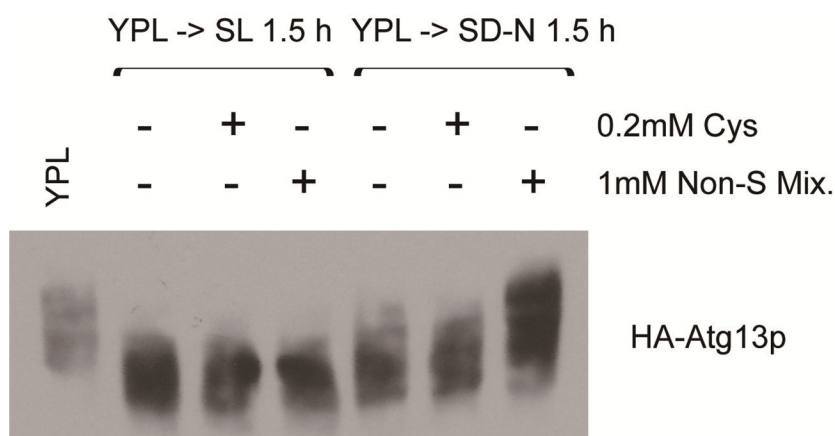


Figure iii-7. Inclusion of Cysteine Does Not Affect the Phosphorylation Level of Atg13p

Cells were grown in YPL to log phase and then switched to nitrogen-starvation medium (SD-N) or SL medium. At the indicated time points, Cells were collected and processed as described in Figure i-1E.

Atg13p was dephosphorylated upon switch from YPL medium to SD-N or SL medium. Dephosphorylation of Atg13p upon switch to SL medium was not affected by addition of either cysteine or a non-sulfur-containing amino acid mixture. Similarly, addition of cysteine into the SD-N medium did not affect the phosphorylation level of Atg13p. In contrast, dephosphorylation of Atg13p upon switched to SD-N medium was fully reversed by a non-sulfur-containing amino acid mixture, which is consistent with the effect of the mixture on nitrogen-starvation-induced autophagy. The non-sulfur-containing amino acid mixture (Non-S Mix.) contains all the non-sulfur-containing amino acids except for tyrosine.

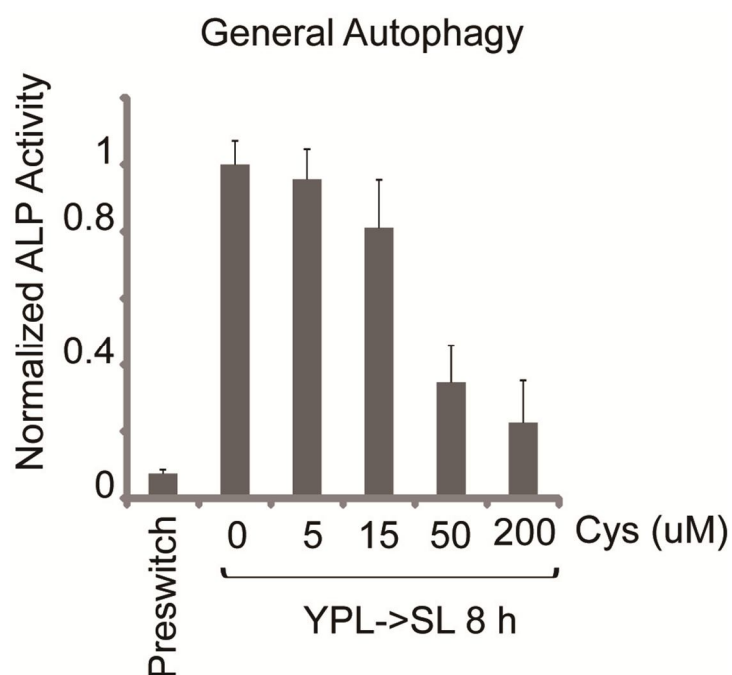


Figure iii-8. The Effect of Cysteine on SL-Induced Autophagy at Different Concentrations

Cells were grown in YPL to log phase and then switched to SL medium supplemented with or without a 3-5 fold serial dilution of cysteine. General autophagy was examined after 8 hours following medium switch. Cysteine exhibited inhibitory effect on SL-induced general autophagy at concentrations more than 15 μM . Data represent the averages of 3-5 samples with error bars for standard deviations.

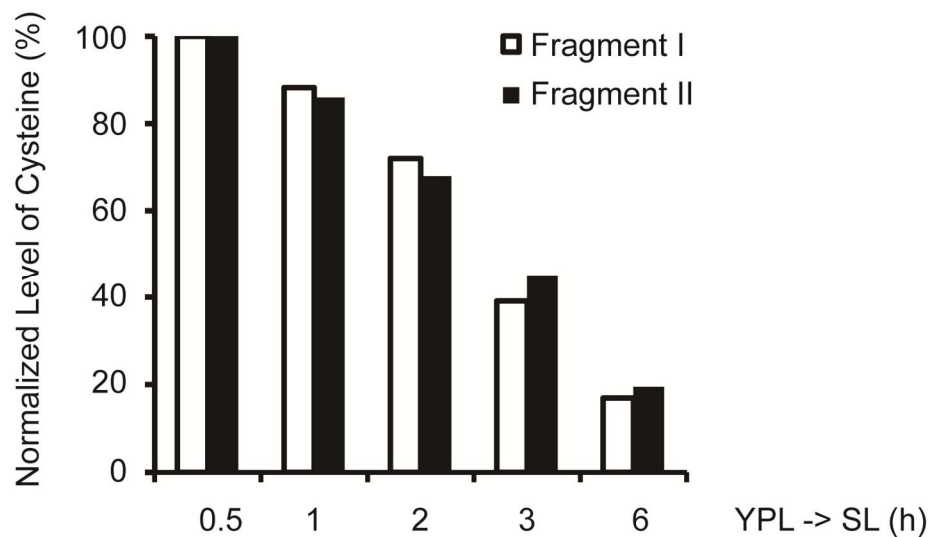


Figure iii-9. Intracellular Cysteine Is Quickly Consumed

Cells were grown in YPL to log phase (OD ~1) and then switched to SL medium supplemented with 1 mM cysteine. At the indicated time points, 5 mL of cells were collected and processed for metabolite analysis by LC-MS/MS. Data were normalized against the first time point.

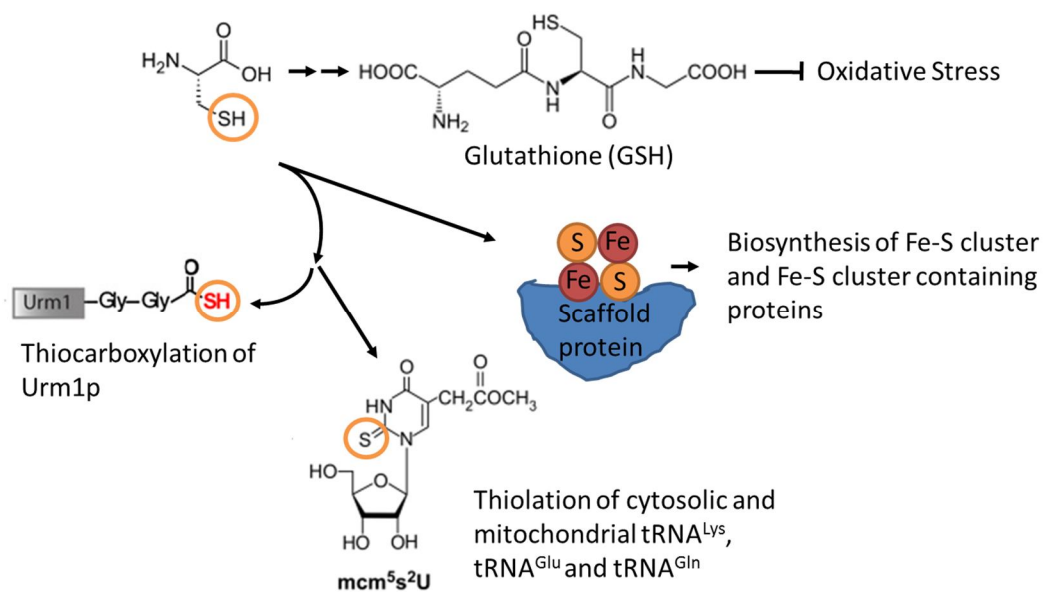


Figure iii-10. Cellular Pathways Related to Cysteine Metabolism

Please see the text for more details.

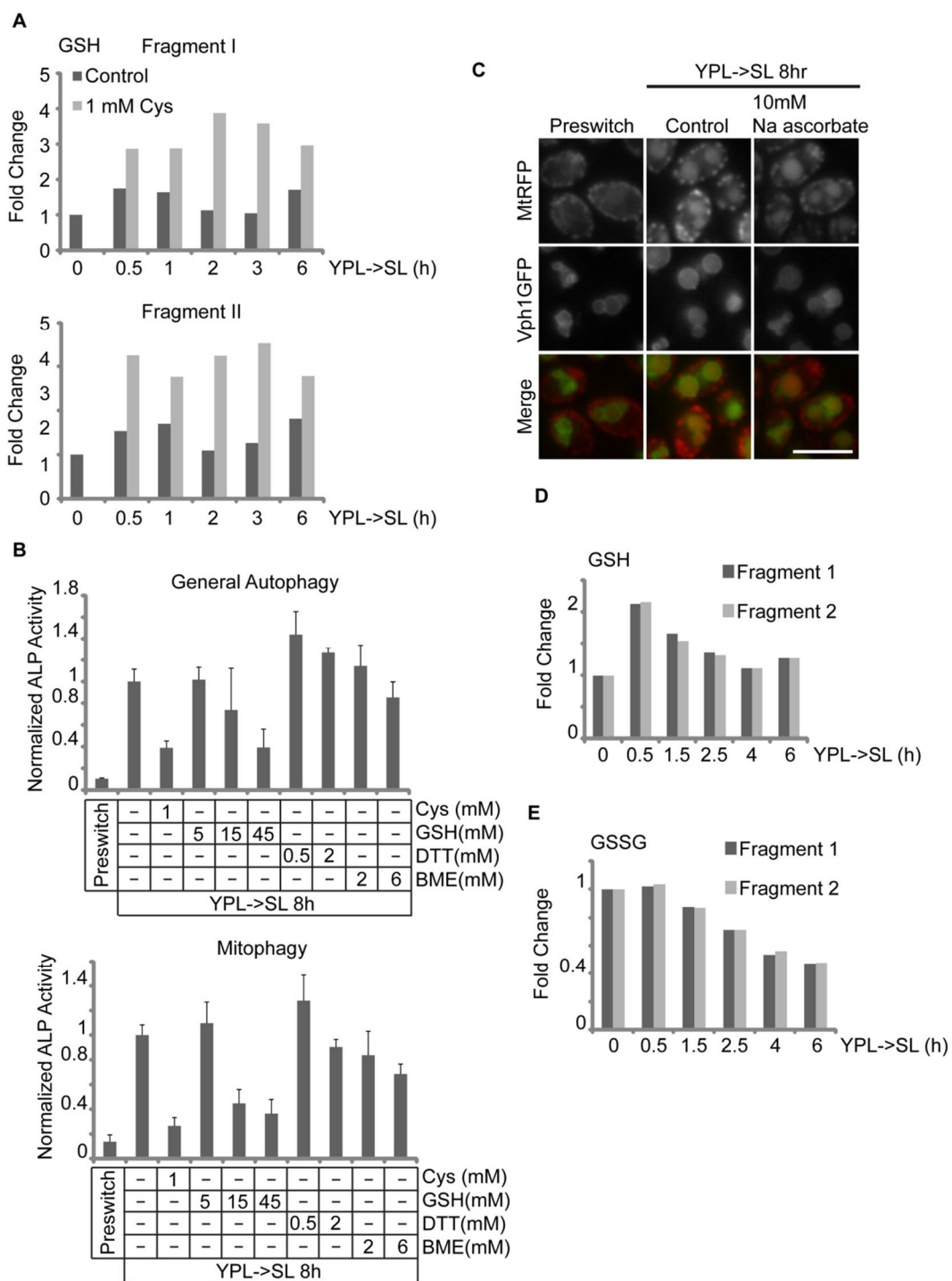


Figure iii-11. Cysteine Does Not Regulate SL-Induced Autophagy through Inhibiting Oxidative Stress

(A) Inclusion of cysteine in SL medium significantly increased the intracellular level of GSH. Cells were cultured and processed for metabolic analysis as described in Figure iii-9.

(B) Effects of glutathione (GSH) and another two antioxidants on SL-induced autophagy. 5 mM GSH had no effect on SL-induced autophagy. 15 mM GSH strongly inhibited SL-induced mitophagy but had minor effect on SL-induced general autophagy. 45 mM GSH effectively inhibited SL-induced autophagy. Another two antioxidants, DTT and BME, did not suppress SL-induced autophagy even when added at high concentrations.

Cells were grown in YPL and then switched to SL medium supplemented with or without the indicated metabolites or chemical compounds. DTT, dithiothreitol. BME, beta mercaptoethanol. Data represent the averages of 3-5 samples with error bars for standard deviations.

(C) Addition of antioxidant sodium ascorbate did not block SL-induced mitophagy. Scale bar, 10 μ m.

(D) Measurement of cellular GSH level before and after switch to SL medium.

(E) Measurement of cellular GSSG (oxidized GSH) level before and after switch to SL medium. In (D and E), cells were grown and processed as described in Figure iii-9.

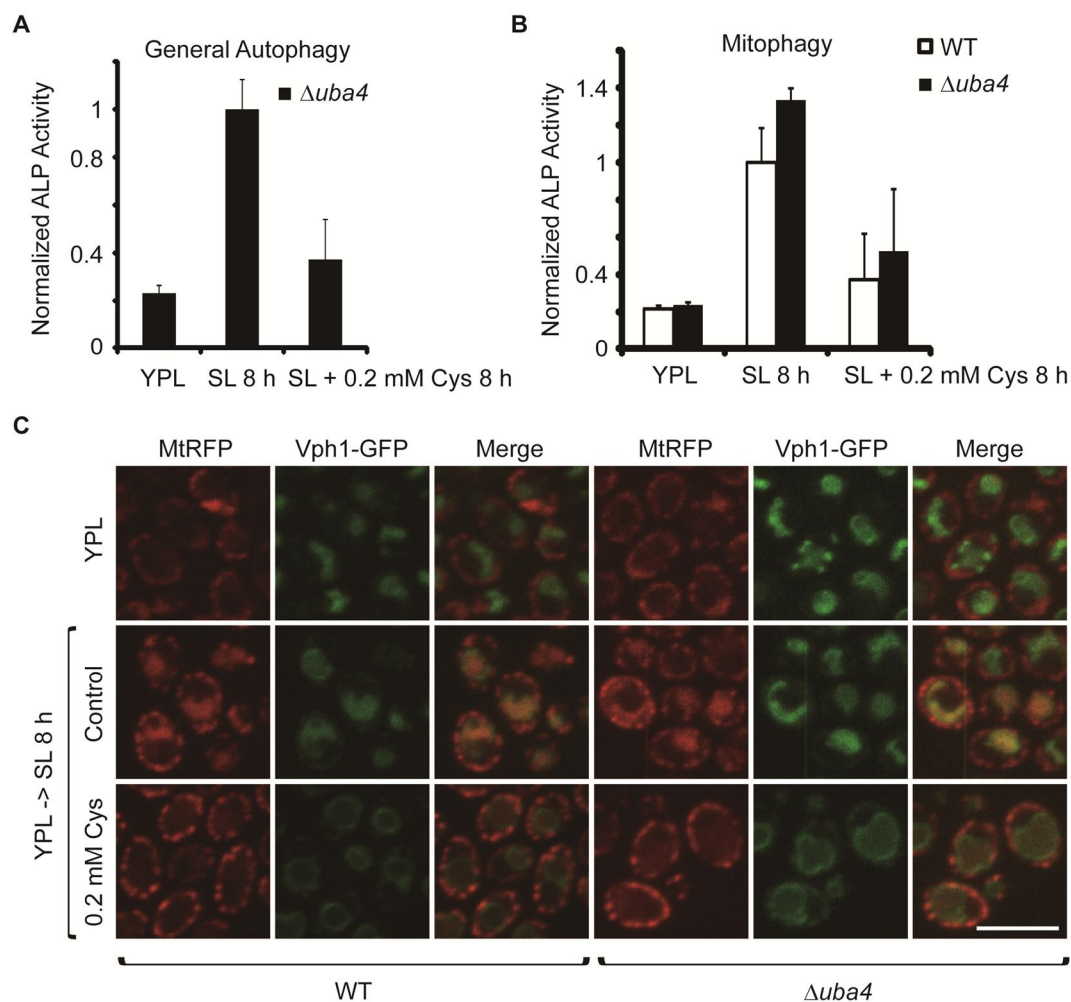


Figure iii-12. Cysteine Still Suppresses SL-Induced Autophagy in $\Delta uba4$ Mutants.

Cells were grown in YPL to log phase before switch to SL medium supplemented with or without cysteine. At the indicated time points, autophagic activity were examined by ALP activity assay or imaging.

(A and B) Deletion of *UBA4* did not affect the inhibitory effect of cysteine on SL-induced autophagy. Data represent the averages of 3-5 samples with error bars for standard deviations.

(C) Cysteine still inhibited SL-induced mitophagy in $\Delta uba4$ mutants as assessed by imaging. Scale bar, 10 μ m.

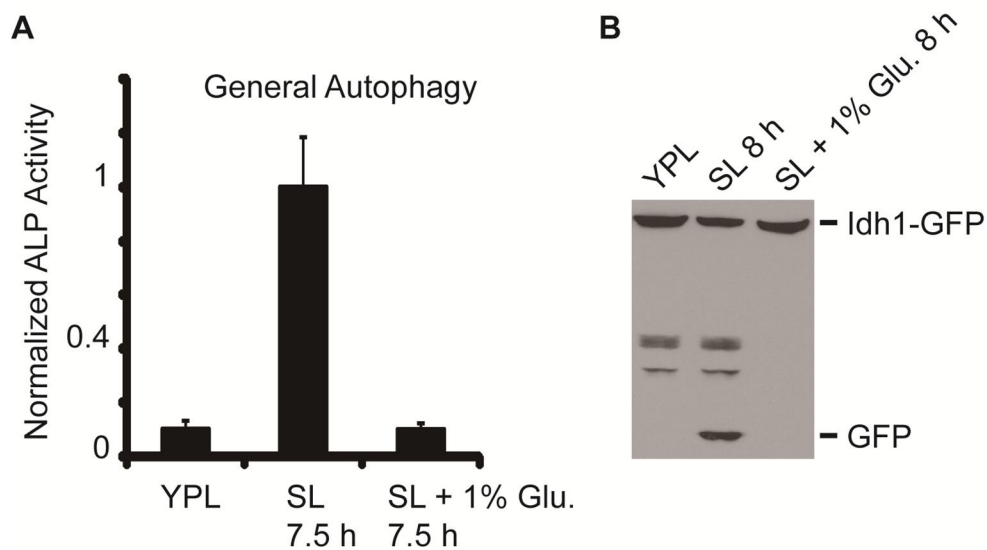


Figure iii-13. SL-Induced Autophagy Is Completely Blocked by Addition of Glucose

Cells were cultured in YPL to log phase and then switched to SL medium in the presence or absence of 1% glucose for about 8 hours. Glu., glucose.

(A) SL-induced general autophagy was totally blocked by addition of glucose. Data represent the averages of 3-5 samples with error bars for standard deviations.

(B) SL-induced mitophagy was totally blocked by addition of glucose.

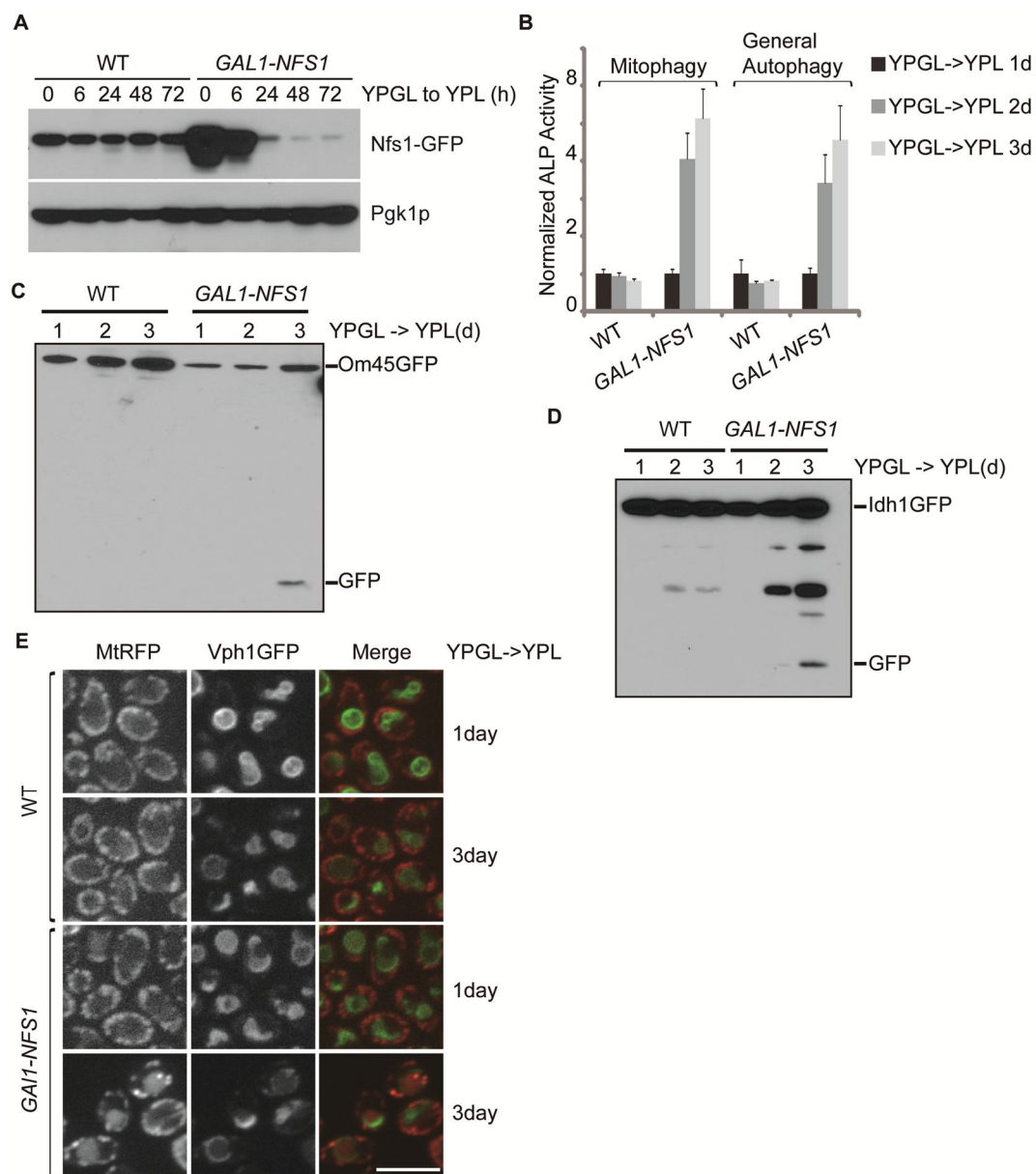


Figure iii-14. Autophagy Is Strongly Induced upon Depletion of Nfs1p

WT cells or mutant cells in which the transcription of *NFS1* is controlled by the *GAL1* promoter were grown in inducing medium (YPGL) to log phase and then switched to

non-inducing medium (YPL). Cells were collected for autophagic assays at the indicated time points after medium switch.

(A) Depletion of Nfs1p upon switch to the non-inducing medium (YPL) in the mutant cells, but not in the WT cells.

(B) Autophagy was strongly induced after two days following switch to the non-inducing medium (YPL) in the mutant cells, but not in the WT cells, as assessed by ALP activity assay for both general autophagy and mitophagy. Data represent the averages of 3-5 samples with error bars for standard deviations.

(C and D) Increase in the release of free GFP from Om45-GFP or Idh1-GFP were detected after 3 days following switch to the non-inducing medium (YPL) in the mutant cells, but not in the WT cells.

(E) Vacuolar mitochondrial signal was detected after 3 days following switch to the non-inducing medium (YPL) in the mutant cells, but not in the WT cells. Scale bar, 10 μ m.

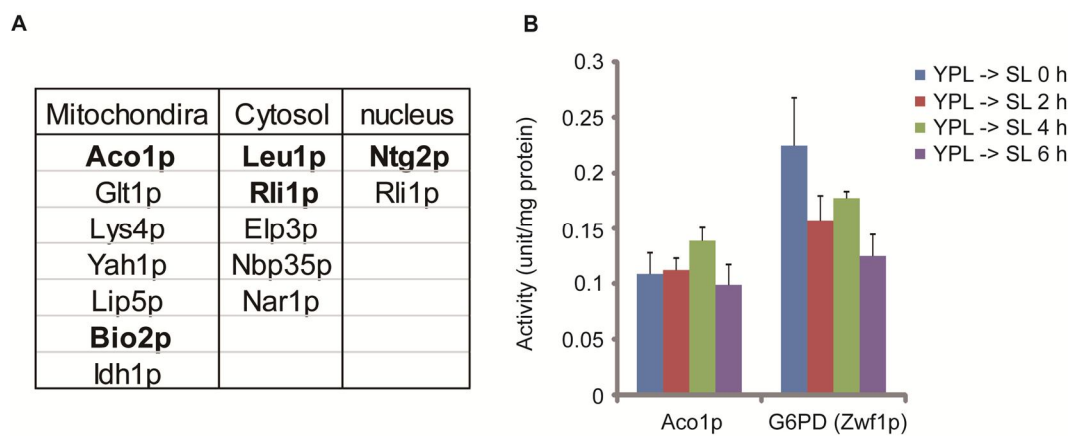


Figure iii-15. Measurement of Aco1p Activity in YPL and after switch to SL medium

(A) A list of most known Fe-S cluster containing proteins identified in yeast. The proteins were classified into three groups according to their subcellular localization.

(B) Activity measurements of Aco1p and Zwf1p in YPL and after switch to SL medium in WT cells. The activity of Aco1p did not change after switch to SL medium. The activity of Zwf1p or G6PD slightly decreased after switch to SL medium. One unit indicates 1 mM products generated in 1 min. G6PD, glucose-6-phosphate dehydrogenase.

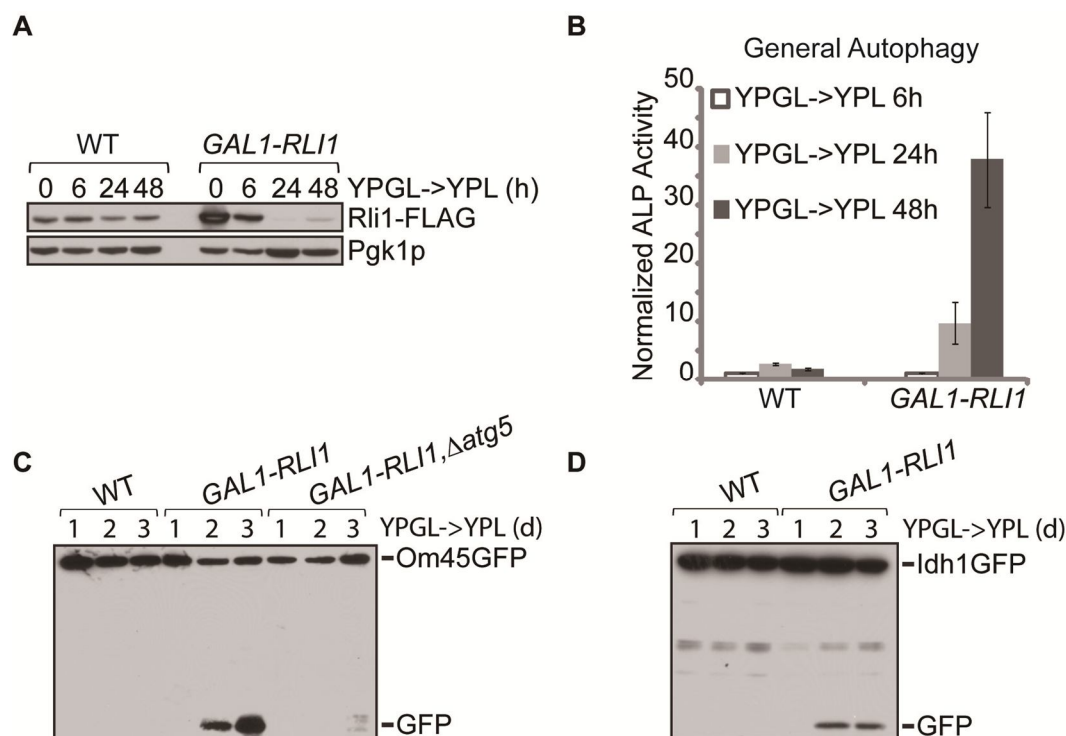


Figure iii-16. Autophagy Is Strongly Induced upon Depletion of a Fe-S Cluster Containing Protein, Rli1p

Cells of the indicated genotypes were cultured as described in Figure iii-14.

(A) Depletion of Rli1p upon switch to the non-inducing medium (YPL) in the mutant cells, but not in the WT cells.

(B) General autophagy was strongly induced after 1-2 days following switch to the non-inducing medium (YPL) in the mutant cells, but not in the WT cells, as assessed by ALP activity assay for both general autophagy and mitophagy. Data represent the averages of 3-5 samples with error bars for standard deviations.

(C and D) Increase in the release of free GFP from Om45-GFP or Idh1-GFP were detected after 2 days following switch to the non-inducing medium (YPL) in the mutant cells, but not in the WT cells. The release of free GFP from Om45-GFP induced by Rli1p depletion was blocked in $\Delta atg5$ cells.

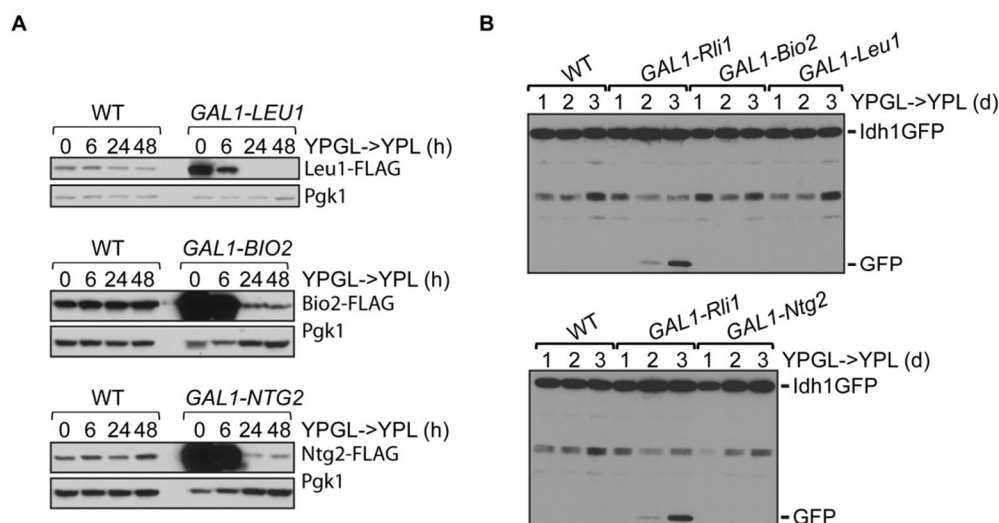


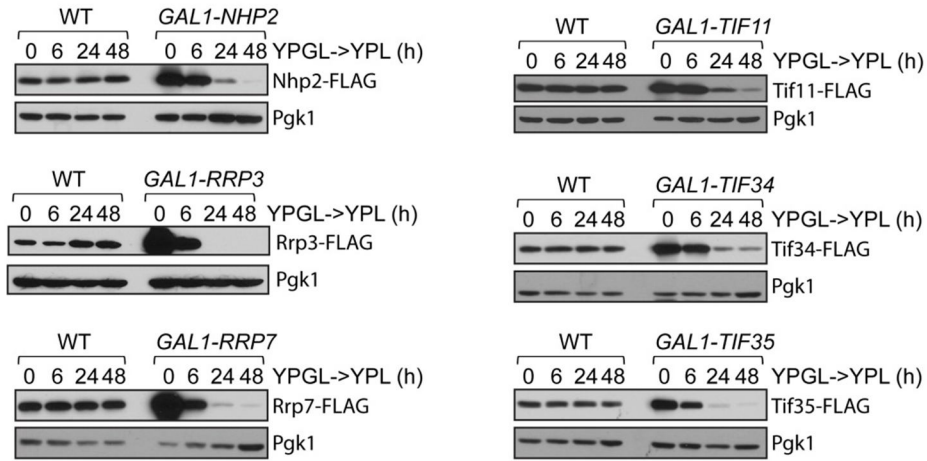
Figure iii-17. Autophagic Activity Is Not Affected upon Knocking-Down the Expression of other Fe-S Cluster Containing Proteins

Cells of the indicated genotypes were cultured as described in Figure iii-14.

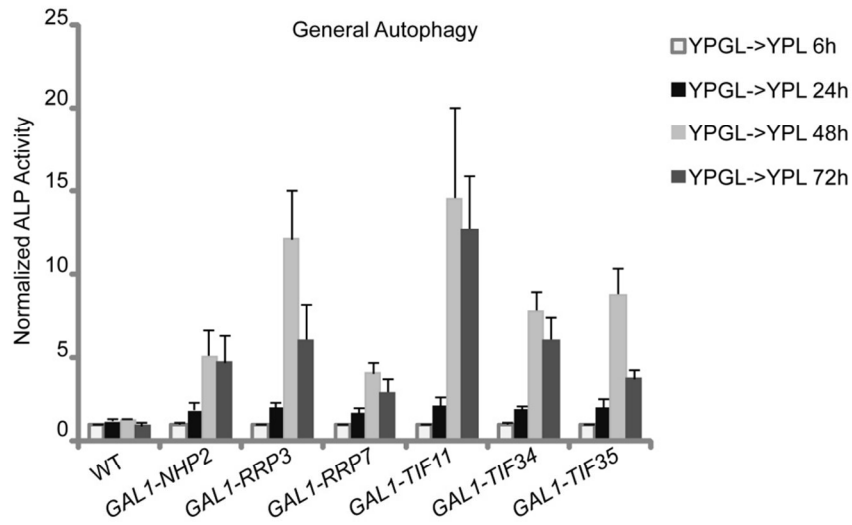
(A) Changes in the expression of Leu1p, Bio2p and Ntg2p upon switch to the non-inducing medium (YPL) both in WT cells and in the mutant cells.

(B) Mitophagy was not induced by decreasing the expression of Fe-S cluster containing proteins, Bio2p, Leu1p and Ntg2p. The mutant strain in which the transcription of *RLI1* is under the control of the *GAL1* promoter was used as the positive control.

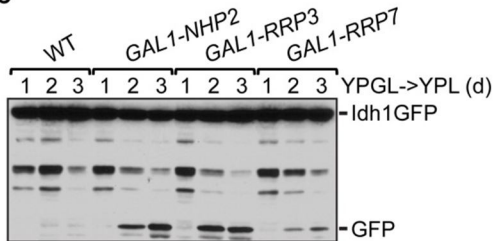
A



B



C



D

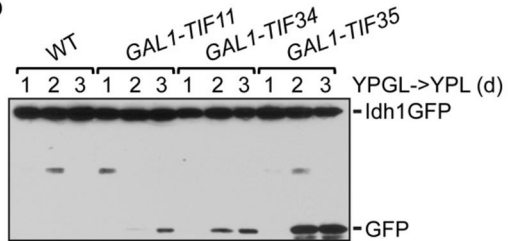


Figure iii-18. Induction of Autophagy upon Depletion of rRNA Processing Factors and Translation Initiation Factors

Cells of the indicated genotypes were cultured as described in Figure iii-14. *NHP2*, *RRP3* and *RRP7* encode proteins involved in rRNA processing. *TIF11*, *TIF34* and *TIF35* encode proteins involved in translation initiation (Baudin-Baillieu et al., 1997; Henras et al., 1998; O'Day et al., 1996; Phan et al., 1998; Verlhac et al., 1997; Wei et al., 1995)

(A) Depletion of rRNA processing factors and translation initiation factors upon switch to the non-inducing medium (YPL) in the mutant cells, but not in the WT cells.

(B) General autophagy was strongly induced after two days following switch to the non-inducing medium (YPL) in the mutant cells, but not in the WT cells, as assessed by ALP activity assay for both general autophagy and mitophagy. Data represent the averages of 3-5 samples with error bars for standard deviations.

(C and D) Increase in the release of free GFP from Idh1-GFP were detected after 2-3 days following switch to the non-inducing medium (YPL) in the mutant cells, but not in the WT cells.

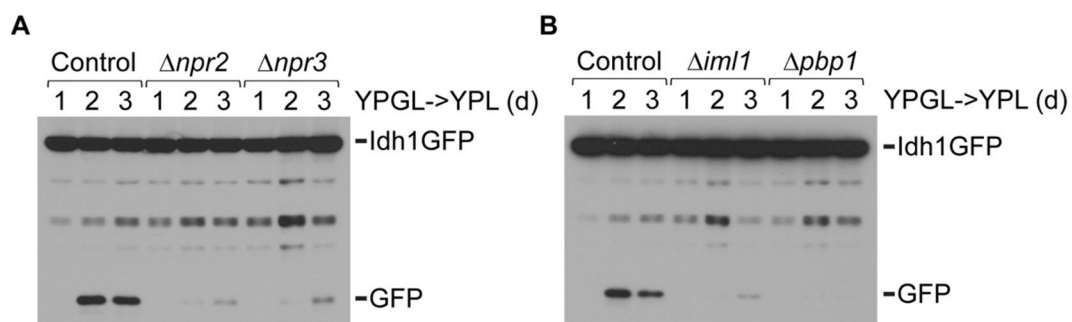


Figure iii-19. *IML1*, *NPR2*, *NPR3* and *PBP1* Are Required for Mitophagy Induced upon Depletion of Rli1p

Mitophagy induced by depletion of Rli1p was significantly inhibited in the $\Delta iml1$, $\Delta npr2$, $\Delta npr3$ and $\Delta pbp1$ cells.

The mutant strain in which the transcription of *RLI1* is under the control of the *GALI* promoter was used as the control strain here. Cells of the indicated genotypes were cultured as described in Figure iii-14. Mitophagy was assessed by Western blot using Idh1-GFP as the reporter. The experiments were performed by Benjamin Sutter. The figure was made by Xi Wu.

Table 1. Genes Identified Proximal to the Insertion Sites

| Genes identified proximal to the insertion sites | Validation of autophagy phenotype |
|--|--|
| <i>IML1</i> | Selectively inhibits SL-induced autophagy |
| <i>NPR2</i> | Selectively inhibits SL-induced autophagy |
| <i>NPR3</i> | Selectively inhibits SL-induced autophagy |
| <i>PBP1</i> | Selectively inhibits SL-induced autophagy |
| <i>ATG11</i> | Previously characterized; essential for mitophagy ¹ |
| <i>ATG32</i> | Previously characterized; essential for mitophagy ² |
| <i>IKS1</i> | No mitophagy phenotype |
| <i>MCK1</i> | No mitophagy phenotype |
| <i>COX18</i> | No mitophagy phenotype |
| <i>IRA1</i> | No mitophagy phenotype |
| <i>SSK2</i> | No mitophagy phenotype |
| <i>RIM15</i> | Not able to knock out this gene |
| <i>VPS5</i> | Not validated |
| <i>BEM2</i> | Not validated |
| <i>rRNA coding region</i> | Not able to validate |

¹(Kanki and Klionsky, 2008)

²(Kanki et al., 2009b; Okamoto et al., 2009)

Table 2. The Level of Cysteine and Cystine in the YP medium

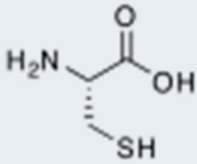
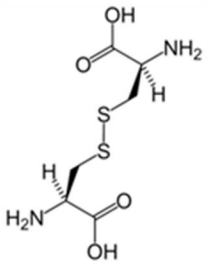
| [Cysteine] | [Cystine] | [Cysteine +2* Cystine] |
|---|---|---------------------------|
| 2.63±0.4 µM | 2.89±0.43 µM | ~8.5 µM |
|  |  | |

Table 3 Yeast Strains Used in the Study

| Name | Genotype | Strain Background |
|-------|--|---------------------|
| YXW1 | <i>MATa ho::ADH1^P-Mito-dsRed::kanMX4 vph1::VPH1-GFP::kanMX6</i> | prototrophic CEN.PK |
| YXW2 | <i>MATa om45::OM45-GFP::kanMX6 vph1::VPH1-mCherry::natNT2</i> | prototrophic CEN.PK |
| YXW3 | <i>MATa om45::OM45-GFP::kanMX6 vph1::VPH1-mCherry::natNT2 atg5::hphNT1</i> | prototrophic CEN.PK |
| YXW4 | <i>MATa om45::OM45-GFP::kanMX6 vph1::VPH1-mCherry::natNT2 atg11::hphNT1</i> | prototrophic CEN.PK |
| YXW5 | <i>MATa pho8::TEF1^P-OM-pho8Δ60::kanMX6 pho13::natNT2</i> | prototrophic CEN.PK |
| YXW6 | <i>MATa pho8::TEF1^P-OM-pho8Δ60::kanMX6 pho13::natNT2 atg5::hphNT1</i> | prototrophic CEN.PK |
| YXW7 | <i>MATa pho8::TEF1^P-OM-pho8Δ60::kanMX6 pho13::hphNT1 atg11::natNT2</i> | prototrophic CEN.PK |
| YXW8 | <i>MATa pho8::TEF1^P-OM-pho8Δ60::kanMX6 pho13::natNT2 atg32::hphNT1</i> | prototrophic CEN.PK |
| YXW9 | <i>MATa pho8::TEF1^P-OM-pho8Δ60::kanMX6 pho13::natNT2 iml1::hphNT1</i> | prototrophic CEN.PK |
| YXW10 | <i>MATa pho8::TEF1^P-OM-pho8Δ60::kanMX6 pho13::natNT2 npr2::hphNT1</i> | prototrophic CEN.PK |
| YXW11 | <i>MATa pho8::TEF1^P-OM-pho8Δ60::kanMX6 pho13::natNT2 npr3::hphNT1</i> | prototrophic CEN.PK |
| YXW12 | <i>MATa pho8::TEF1^P-OM-pho8Δ60::kanMX6 pho13::hphNT1 iml1::IML1-GFP::natNT2</i> | prototrophic CEN.PK |
| YXW13 | <i>MATa pho8::TEF1^P-OM-pho8Δ60::kanMX6 pho13::natNT2 npr2::NPR2-HA::hphNT1</i> | prototrophic CEN.PK |
| YXW14 | <i>MATa pho8::TEF1^P-OM-pho8Δ60::kanMX6 pho13::natNT2 npr3::NPR3-HA::hphNT1</i> | prototrophic CEN.PK |
| YXW15 | <i>MATa pho8::TEF1^P-pho8Δ60::kanMX6 pho13::natNT2</i> | prototrophic CEN.PK |
| YXW16 | <i>MATa pho8::TEF1^P-pho8Δ60::kanMX6 pho13::natNT2 atg5::hphNT1</i> | prototrophic CEN.PK |
| YXW17 | <i>MATa pho8::TEF1^P-pho8Δ60::kanMX6 pho13::hphNT1 atg11::natNT2</i> | prototrophic CEN.PK |
| YXW18 | <i>MATa pho8::TEF1^P-pho8Δ60::kanMX6 pho13::natNT2 iml1::hphNT1</i> | prototrophic CEN.PK |
| YXW19 | <i>MATa pho8::TEF1^P-pho8Δ60::kanMX6 pho13::natNT2 npr2::hphNT1</i> | prototrophic CEN.PK |
| YXW20 | <i>MATa pho8::TEF1^P-pho8Δ60::kanMX6 pho13::hphNT1 npr3::natNT2</i> | prototrophic CEN.PK |
| YXW21 | <i>MATa pho8::TEF1^P-pho8Δ60::kanMX6 pho13::hphNT1 iml1::IML1-GFP::natNT2</i> | prototrophic CEN.PK |
| YXW22 | <i>MATa pho8::TEF1^P-pho8Δ60::kanMX6 pho13::natNT2 npr2::NPR2-HA::hphNT1</i> | prototrophic CEN.PK |
| YXW23 | <i>MATa pho8::TEF1^P-pho8Δ60::kanMX6 pho13::natNT2 npr3::NPR3-HA::hphNT1</i> | prototrophic CEN.PK |
| YXW24 | <i>MATa idh1::IDH1-GFP::kanMX6</i> | prototrophic CEN.PK |
| YXW25 | <i>MATa iml1::IML1-FLAG::kanMX6 npr3::NPR3-HA::hphNT1</i> | prototrophic CEN.PK |
| YXW26 | <i>MATa iml1::IML1-FLAG::kanMX6 npr3::NPR3-HA::hphNT1 npr2::natNT2</i> | prototrophic CEN.PK |
| YXW27 | <i>MATa iml1::IML1-FLAG::natNT2 npr2::NPR2-HA::kanMX6</i> | prototrophic CEN.PK |

Table 3 Yeast Strains Used in the Study (Continued)

| Name | Genotype | Strain Background |
|-------|---|---------------------------------|
| YXW28 | MAT α <i>iml1::IML1-FLAG::natNT2 npr2::NPR2-HA::kanMX6 npr3::hphNT1</i> | prototrophic CEN.PK |
| YXW29 | MAT α <i>npr2::NPR2-FLAG::kanMX6 npr3::HA-NPR3::natNT2</i> | prototrophic CEN.PK |
| YXW30 | MAT α <i>npr2::NPR2-FLAG::kanMX6 npr3::HA-NPR3::natNT2 iml1::hphNT1</i> | prototrophic CEN.PK |
| YXW31 | MAT α <i>iml1::IML1-FLAG::kanMX6</i> | prototrophic CEN.PK |
| YXW32 | MAT α <i>npr2::NPR2-FLAG::kanMX6</i> | prototrophic CEN.PK |
| YXW33 | MAT α <i>npr3::NPR3-FLAG::kanMX6</i> | prototrophic CEN.PK |
| YXW34 | MAT α <i>iml1::IML1-GFP::kanMX6</i> | prototrophic CEN.PK |
| YXW35 | MAT α <i>iml1::IML1-GFP::kanMX6 vph1::VPH1-mCherry::natNT2</i> | prototrophic CEN.PK |
| YXW36 | MAT α <i>iml1::IML1-GFP::kanMX6 ape1::APE1-mRFP1::hphNT1</i> | prototrophic CEN.PK |
| YXW37 | MAT α <i>iml1::IML1-GFP::kanMX6 vph1::VPH1-mCherry::natNT2 npr2::hphNT1</i> | prototrophic CEN.PK |
| YXW38 | MAT α <i>iml1::IML1-GFP::kanMX6 vph1::VPH1-mCherry::natNT2 npr3::hphNT1</i> | prototrophic CEN.PK |
| YXW39 | MAT α <i>iml1::IML1-GFP::kanMX6 vph1::VPH1-mCherry::natNT2 atg8::hphNT1</i> | prototrophic CEN.PK |
| YXW40 | MAT α <i>ho::ADH1^P-Mito-dsRed::kanMX4 leu2::hphNT1</i> | prototrophic CEN.PK |
| YXW41 | MAT α <i>ho::ADH1^P-Mito-dsRed::kanMX4 leu2::hphNT1 [pRS41N-GFP-ATG8]</i> | prototrophic CEN.PK |
| YXW42 | MAT α <i>idh1::IDH1-GFP::kanMX6</i> | prototrophic W303 ¹ |
| YXW43 | MAT α <i>idh1::IDH1-GFP::kanMX6 atg5::hphNT1</i> | prototrophic W303 |
| YXW44 | MAT α <i>idh1::IDH1-GFP::kanMX6 iml1::hphNT1</i> | prototrophic W303 |
| YXW45 | MAT α <i>idh1::IDH1-GFP::kanMX6 npr2::hphNT1</i> | prototrophic W303 |
| YXW46 | MAT α <i>idh1::IDH1-GFP::kanMX6 npr3::hphNT1</i> | prototrophic W303 |
| YXW47 | MAT α <i>pho8::TEF1^P-pho8Δ60::kanMX6 pho13::natNT2</i> | prototrophic W303 |
| YXW48 | MAT α <i>idh1::IDH1-GFP::kanMX6</i> | prototrophic S288C ² |
| YXW49 | MAT α <i>pho8::TEF1^P-pho8Δ60::kanMX6 pho13::natNT2</i> | prototrophic S288C |
| YXW50 | MAT α <i>pho8::TEF1^P-pho8Δ60::kanMX6 pho13::natNT2 atg5::hphNT1</i> | prototrophic W303 |
| YXW51 | MAT α <i>pho8::TEF1^P-pho8Δ60::kanMX6 pho13::natNT2 iml1::hphNT1</i> | prototrophic W303 |
| YXW52 | MAT α <i>pho8::TEF1^P-pho8Δ60::kanMX6 pho13::natNT2 npr2::hphNT1</i> | prototrophic W303 |
| YXW53 | MAT α <i>pho8::TEF1^P-pho8Δ60::kanMX6 pho13::natNT2 npr3::hphNT1</i> | prototrophic W303 |
| YXW54 | MAT α <i>idh1::IDH1-GFP::natNT2 iml1::hphNT1 [p417-CYC1^P]</i> | prototrophic CEN.PK |

Table 3 Yeast Strains Used in the Study (Continued)

| Name | Genotype | Strain Background |
|-------|--|---------------------|
| YXW55 | <i>MATα</i> <i>idh1::IDH1-GFP::natNT2 iml1::hphNT1 [p417-CYC1^P-IML1-FLAG]</i> | prototrophic CEN.PK |
| YXW56 | <i>MATα</i> <i>idh1::IDH1-GFP::natNT2 iml1::hphNT1 [p417-CYC1^P-iml1Δdep-FLAG]</i> | prototrophic CEN.PK |
| YXW57 | <i>MATα</i> <i>idh1::IDH1-GFP::natNT2 iml1::hphNT1 [p417-CYC1^P-iml1Δduf-FLAG]</i> | prototrophic CEN.PK |
| YXW58 | <i>MATα</i> <i>pho8::TEF1^P-pho8Δ60::hphNT1 pho13::natNT2 iml1::hphNT1 [p417-CYC1^P]^J</i> | prototrophic CEN.PK |
| YXW59 | <i>MATα</i> <i>pho8::TEF1^P-pho8Δ60::hphNT1 pho13::natNT2 iml1::hphNT1 [p417-CYC1^P-IML1-FLAG]</i> | prototrophic CEN.PK |
| YXW60 | <i>MATα</i> <i>pho8::TEF1^P-pho8Δ60::hphNT1 pho13::natNT2 iml1::hphNT1 [p417-CYC1^P-iml1Δdep-FLAG]</i> | prototrophic CEN.PK |
| YXW61 | <i>MATα</i> <i>pho8::TEF1^P-pho8Δ60::hphNT1 pho13::natNT2 iml1::hphNT1 [p417-CYC1^P-iml1Δduf-FLAG]</i> | prototrophic CEN.PK |
| YXW62 | <i>MATα</i> <i>np2::NPR2-HA::natNT2 iml1::hphNT1 [p417-CYC1^P-IML1-FLAG]</i> | prototrophic CEN.PK |
| YXW63 | <i>MATα</i> <i>np2::NPR2-HA::natNT2 iml1::hphNT1 [p417-CYC1^P-iml1Δdep-FLAG]</i> | prototrophic CEN.PK |
| YXW64 | <i>MATα</i> <i>np2::NPR2-HA::natNT2 iml1::hphNT1 [p417-CYC1^P-iml1Δduf-FLAG]</i> | prototrophic CEN.PK |
| YXW65 | <i>MATα</i> <i>np3::NPR3-HA::natNT2 iml1::hphNT1 [p417-CYC1^P-IML1-FLAG]</i> | prototrophic CEN.PK |
| YXW66 | <i>MATα</i> <i>np3::NPR3-HA::natNT2 iml1::hphNT1 [p417-CYC1^P-iml1Δdep-FLAG]</i> | prototrophic CEN.PK |
| YXW67 | <i>MATα</i> <i>np3::NPR3-HA::natNT2 iml1::hphNT1 [p417-CYC1^P-iml1Δduf-FLAG]</i> | prototrophic CEN.PK |
| YXW68 | <i>MATα</i> <i>ho::ADH1^P-Mito-dsRed::kanMX4 vph1::VPH1-GFP::kanMX6 np3::HA-NPR3::natNT2</i> | prototrophic CEN.PK |
| YXW69 | <i>MATα</i> <i>ho::ADH1^P-Mito-dsRed::kanMX4 vph1::VPH1-GFP::kanMX6 atg1::hphNT1</i> | prototrophic CEN.PK |
| YXW70 | <i>MATα</i> <i>ho::ADH1^P-Mito-dsRed::kanMX4 vph1::VPH1-GFP::kanMX6 atg13::hphNT1</i> | prototrophic CEN.PK |
| YXW71 | <i>MATα</i> <i>ho::ADH1^P-Mito-dsRed::kanMX4 vph1::VPH1-GFP::kanMX6 atg8::hphNT1</i> | prototrophic CEN.PK |
| YXW72 | <i>MATα</i> <i>ho::ADH1^P-Mito-dsRed::kanMX4 vph1::VPH1-GFP::kanMX6 atg9::hphNT1</i> | prototrophic CEN.PK |
| YXW73 | <i>MATα</i> <i>atg13::HA-ATG13::natNT2</i> | prototrophic CEN.PK |
| YXW74 | <i>MATα</i> <i>atg13::HA-ATG13::natNT2 iml1::hphNT1</i> | prototrophic CEN.PK |
| YXW75 | <i>MATα</i> <i>atg13::HA-ATG13::natNT2 np2::hphNT1</i> | prototrophic CEN.PK |
| YXW76 | <i>MATα</i> <i>atg13::HA-ATG13::natNT2 np3::hphNT1</i> | prototrophic CEN.PK |
| YXW77 | <i>MATα</i> <i>atg1::hphNT1</i> | prototrophic CEN.PK |

Table 3 Yeast Strains Used in the Study (Continued)

| Name | Genotype | Strain Background |
|--------|--|---------------------|
| YXW78 | <i>MATα atg6::hphNT1</i> | prototrophic CEN.PK |
| YXW79 | <i>MATα atg7::hphNT1</i> | prototrophic CEN.PK |
| YXW80 | <i>MATα atg8::hphNT1</i> | prototrophic CEN.PK |
| YXW81 | <i>MATα atg9::hphNT1</i> | prototrophic CEN.PK |
| YXW82 | <i>MATα atg10::hphNT1</i> | prototrophic CEN.PK |
| YXW83 | <i>MATα atg13::hphNT1</i> | prototrophic CEN.PK |
| YXW84 | <i>MATα atg5::kanMX6</i> | prototrophic CEN.PK |
| YXW85 | <i>MATα iml1::hphNT1</i> | prototrophic CEN.PK |
| YXW86 | <i>MATα npr2::kanMX6</i> | prototrophic CEN.PK |
| YXW87 | <i>MATα npr3::kanMX6</i> | prototrophic CEN.PK |
| YXW88 | <i>MATα pep4::kanMX6 prb1::hphNT1</i> | prototrophic CEN.PK |
| YXW89 | <i>MATα pep4::natNT2 prb1::hphNT1 npr2::kanMX6</i> | prototrophic CEN.PK |
| YXW90 | <i>MATα pep4::natNT2 prb1::hphNT1 atg5::kanMX6</i> | prototrophic CEN.PK |
| YXW91 | <i>MATα pep4::natNT2 prb1::kanMX6 iml1::hphNT1</i> | prototrophic CEN.PK |
| YXW92 | <i>MATα pep4::kanMX6 prb1::hphNT1 npr3::natNT2</i> | prototrophic CEN.PK |
| YXW93 | <i>MATα pex14::PEX14-GFP::kanMX6</i> | prototrophic CEN.PK |
| YXW94 | <i>MATα [p417-GFP-ATG8]</i> | prototrophic CEN.PK |
| YXW95 | <i>MATα iml1::hphNT1 [p417-GFP-ATG8]</i> | prototrophic CEN.PK |
| YXW96 | <i>MATα npr2::kanMX6 [pRS41H-GFP-ATG8]</i> | prototrophic CEN.PK |
| YXW97 | <i>MATα npr3::kanMX6 [pRS41H-GFP-ATG8]</i> | prototrophic CEN.PK |
| YXW98 | <i>MATα atg32::kanMX6</i> | prototrophic CEN.PK |
| YXW99 | <i>MATα pho8::TEF1^P-OM-pho8Δ60::kanMX6 pho13::natNT2 str2::hphNT1</i> | prototrophic CEN.PK |
| YXW100 | <i>MATα pho8::TEF1^P-pho8Δ60::kanMX6 pho13::natNT2 str2::hphNT1</i> | prototrophic CEN.PK |
| YXW101 | <i>MATα pho8::TEF1^P-OM-pho8Δ60::kanMX6 pho13::natNT2 me6::hphNT1</i> | prototrophic CEN.PK |

¹The prototrophic version of W303 is a kind gift from Andrew Murray.

²The prototrophic version of S288C was purchased from ATCC (Catalog No. 204508).

VI. Bibliography

- Baba, M. (2008). Electron microscopy in yeast. *Methods Enzymol* 451, 133-149.
- Baudin-Baillieu, A., Tollervey, D., Cullin, C., and Lacroute, F. (1997). Functional analysis of Rrp7p, an essential yeast protein involved in pre-rRNA processing and ribosome assembly. *Mol Cell Biol* 17, 5023-5032.
- Buchan, J.R., Muhrad, D., and Parker, R. (2008). P bodies promote stress granule assembly in *Saccharomyces cerevisiae*. *J Cell Biol* 183, 441-455.
- Burns, N., Grimwade, B., Ross-Macdonald, P.B., Choi, E.Y., Finberg, K., Roeder, G.S., and Snyder, M. (1994). Large-scale analysis of gene expression, protein localization, and gene disruption in *Saccharomyces cerevisiae*. *Genes Dev* 8, 1087-1105.
- Dokudovskaya, S., Waharte, F., Schlessinger, A., Pieper, U., Devos, D.P., Cristea, I.M., Williams, R., Salamero, J., Chait, B.T., Sali, A., *et al.* (2011). A conserved coatomer-related complex containing Sec13 and Seh1 dynamically associates with the vacuole in *Saccharomyces cerevisiae*. *Mol Cell Proteomics*.
- Dong, J., Lai, R., Nielsen, K., Fekete, C.A., Qiu, H., and Hinnebusch, A.G. (2004). The essential ATP-binding cassette protein RLI1 functions in translation by promoting preinitiation complex assembly. *J Biol Chem* 279, 42157-42168.
- Furukawa, K., Mizushima, N., Noda, T., and Ohsumi, Y. (2000). A protein conjugation system in yeast with homology to biosynthetic enzyme reaction of prokaryotes. *J Biol Chem* 275, 7462-7465.
- Goehring, A.S., Rivers, D.M., and Sprague, G.F., Jr. (2003). Urmyleation: a ubiquitin-like pathway that functions during invasive growth and budding in yeast. *Mol Biol Cell* 14, 4329-4341.
- Graef, M., and Nunnari, J. (2011). Mitochondria regulate autophagy by conserved signalling pathways. *EMBO J* 30, 2101-2114.
- Harding, T.M., Morano, K.A., Scott, S.V., and Klionsky, D.J. (1995). Isolation and characterization of yeast mutants in the cytoplasm to vacuole protein targeting pathway. *J Cell Biol* 131, 591-602.
- Henras, A., Henry, Y., Bousquet-Antonelli, C., Noaillac-Depeyre, J., Gelugne, J.P., and Caizergues-Ferrer, M. (1998). Nhp2p and Nop10p are essential for the function of H/ACA snoRNPs. *EMBO J* 17, 7078-7090.
- Kamada, Y., Funakoshi, T., Shintani, T., Nagano, K., Ohsumi, M., and Ohsumi, Y. (2000). Tor-mediated induction of autophagy via an Apg1 protein kinase complex. *J Cell Biol* 150, 1507-1513.
- Kanki, T., Kang, D., and Klionsky, D.J. (2009a). Monitoring mitophagy in yeast: the Om45-GFP processing assay. *Autophagy* 5, 1186-1189.
- Kanki, T., and Klionsky, D.J. (2008). Mitophagy in yeast occurs through a selective mechanism. *J Biol Chem* 283, 32386-32393.
- Kanki, T., Wang, K., Cao, Y., Baba, M., and Klionsky, D.J. (2009b). Atg32 is a mitochondrial protein that confers selectivity during mitophagy. *Dev Cell* 17, 98-109.

- Keogh, M.C., Kim, J.A., Downey, M., Fillingham, J., Chowdhury, D., Harrison, J.C., Onishi, M., Datta, N., Galicia, S., Emili, A., *et al.* (2006). A phosphatase complex that dephosphorylates gammaH2AX regulates DNA damage checkpoint recovery. *Nature* 439, 497-501.
- Kirisako, T., Baba, M., Ishihara, N., Miyazawa, K., Ohsumi, M., Yoshimori, T., Noda, T., and Ohsumi, Y. (1999). Formation process of autophagosome is traced with Apg8/Aut7p in yeast. *J Cell Biol* 147, 435-446.
- Kispal, G., Csere, P., Prohl, C., and Lill, R. (1999). The mitochondrial proteins Atm1p and Nfs1p are essential for biogenesis of cytosolic Fe/S proteins. *EMBO J* 18, 3981-3989.
- Kispal, G., Sipos, K., Lange, H., Fekete, Z., Bedekovics, T., Janaky, T., Bassler, J., Aguilar Netz, D.J., Balk, J., Rotte, C., *et al.* (2005). Biogenesis of cytosolic ribosomes requires the essential iron-sulphur protein Rli1p and mitochondria. *EMBO J* 24, 589-598.
- Klionsky, D.J., Cregg, J.M., Dunn, W.A., Jr., Emr, S.D., Sakai, Y., Sandoval, I.V., Sibirny, A., Subramani, S., Thumm, M., Veenhuis, M., *et al.* (2003). A unified nomenclature for yeast autophagy-related genes. *Dev Cell* 5, 539-545.
- Klionsky, D.J., and Ohsumi, Y. (1999). Vacuolar import of proteins and organelles from the cytoplasm. *Annu Rev Cell Dev Biol* 15, 1-32.
- Leidel, S., Pedrioli, P.G., Bucher, T., Brost, R., Costanzo, M., Schmidt, A., Aebersold, R., Boone, C., Hofmann, K., and Peter, M. (2009). Ubiquitin-related modifier Urm1 acts as a sulphur carrier in thiolation of eukaryotic transfer RNA. *Nature* 458, 228-232.
- Levine, B., and Klionsky, D.J. (2004). Development by self-digestion: molecular mechanisms and biological functions of autophagy. *Dev Cell* 6, 463-477.
- Lill, R., and Muhlenhoff, U. (2008). Maturation of iron-sulfur proteins in eukaryotes: mechanisms, connected processes, and diseases. *Annu Rev Biochem* 77, 669-700.
- Lohr, D., Venkov, P., and Zlatanova, J. (1995). Transcriptional regulation in the yeast GAL gene family: a complex genetic network. *FASEB J* 9, 777-787.
- Longtine, M.S., McKenzie, A., 3rd, Demarini, D.J., Shah, N.G., Wach, A., Brachat, A., Philippsen, P., and Pringle, J.R. (1998). Additional modules for versatile and economical PCR-based gene deletion and modification in *Saccharomyces cerevisiae*. *Yeast* 14, 953-961.
- Mangus, D.A., Amrani, N., and Jacobson, A. (1998). Pbp1p, a factor interacting with *Saccharomyces cerevisiae* poly(A)-binding protein, regulates polyadenylation. *Mol Cell Biol* 18, 7383-7396.
- Mari, M., Griffith, J., Rieter, E., Krishnappa, L., Klionsky, D.J., and Reggiori, F. (2010). An Atg9-containing compartment that functions in the early steps of autophagosome biogenesis. *J Cell Biol* 190, 1005-1022.
- Mizushima, N., Levine, B., Cuervo, A.M., and Klionsky, D.J. (2008). Autophagy fights disease through cellular self-digestion. *Nature* 451, 1069-1075.
- Nakai, Y., Umeda, N., Suzuki, T., Nakai, M., Hayashi, H., Watanabe, K., and Kagamiyama, H. (2004). Yeast Nfs1p is involved in thio-modification of both mitochondrial and cytoplasmic tRNAs. *J Biol Chem* 279, 12363-12368.

- Nakatogawa, H., Suzuki, K., Kamada, Y., and Ohsumi, Y. (2009). Dynamics and diversity in autophagy mechanisms: lessons from yeast. *Nat Rev Mol Cell Biol* 10, 458-467.
- Neklesa, T.K., and Davis, R.W. (2009). A genome-wide screen for regulators of TORC1 in response to amino acid starvation reveals a conserved Npr2/3 complex. *PLoS Genet* 5, e1000515.
- Noda, T., Matsuura, A., Wada, Y., and Ohsumi, Y. (1995). Novel system for monitoring autophagy in the yeast *Saccharomyces cerevisiae*. *Biochem Biophys Res Commun* 210, 126-132.
- Noda, T., and Ohsumi, Y. (1998). Tor, a phosphatidylinositol kinase homologue, controls autophagy in yeast. *J Biol Chem* 273, 3963-3966.
- Noma, A., Sakaguchi, Y., and Suzuki, T. (2009). Mechanistic characterization of the sulfur-relay system for eukaryotic 2-thiouridine biogenesis at tRNA wobble positions. *Nucleic Acids Res* 37, 1335-1352.
- O'Day, C.L., Chavanikamannil, F., and Abelson, J. (1996). 18S rRNA processing requires the RNA helicase-like protein Rrp3. *Nucleic Acids Res* 24, 3201-3207.
- Ohsumi, Y. (2001). Molecular dissection of autophagy: two ubiquitin-like systems. *Nat Rev Mol Cell Biol* 2, 211-216.
- Ohtake, Y., and Yabuuchi, S. (1991). Molecular cloning of the gamma-glutamylcysteine synthetase gene of *Saccharomyces cerevisiae*. *Yeast* 7, 953-961.
- Okamoto, K., Kondo-Okamoto, N., and Ohsumi, Y. (2009). Mitochondria-anchored receptor Atg32 mediates degradation of mitochondria via selective autophagy. *Dev Cell* 17, 87-97.
- Phan, L., Zhang, X., Asano, K., Anderson, J., Vornlocher, H.P., Greenberg, J.R., Qin, J., and Hinnebusch, A.G. (1998). Identification of a translation initiation factor 3 (eIF3) core complex, conserved in yeast and mammals, that interacts with eIF5. *Mol Cell Biol* 18, 4935-4946.
- Pierik, A.J., Netz, D.J., and Lill, R. (2009). Analysis of iron-sulfur protein maturation in eukaryotes. *Nat Protoc* 4, 753-766.
- Pilkington, G.R., and Parker, R. (2008). Pat1 contains distinct functional domains that promote P-body assembly and activation of decapping. *Mol Cell Biol* 28, 1298-1312.
- Ralser, M., Albrecht, M., Nonhoff, U., Lengauer, T., Lehrach, H., and Krobitsch, S. (2005). An integrative approach to gain insights into the cellular function of human ataxin-2. *J Mol Biol* 346, 203-214.
- Reggiori, F., Tucker, K.A., Stromhaug, P.E., and Klionsky, D.J. (2004). The Atg1-Atg13 complex regulates Atg9 and Atg23 retrieval transport from the pre-autophagosomal structure. *Dev Cell* 6, 79-90.
- Riley, J., Butler, R., Ogilvie, D., Finniear, R., Jenner, D., Powell, S., Anand, R., Smith, J.C., and Markham, A.F. (1990). A novel, rapid method for the isolation of terminal sequences from yeast artificial chromosome (YAC) clones. *Nucleic Acids Res* 18, 2887-2890.
- Sherman, F. (2002). Getting started with yeast. *Methods Enzymol* 350, 3-41.

- Spielewoy, N., Guaderrama, M., Wohlschlegel, J.A., Ashe, M., Yates, J.R., 3rd, and Wittenberg, C. (2010). Npr2, yeast homolog of the human tumor suppressor NPRL2, is a target of Grr1 required for adaptation to growth on diverse nitrogen sources. *Eukaryot Cell* 9, 592-601.
- Suzuki, K., Kubota, Y., Sekito, T., and Ohsumi, Y. (2007). Hierarchy of Atg proteins in pre-autophagosomal structure organization. *Genes Cells* 12, 209-218.
- Suzuki, K., and Ohsumi, Y. (2010). Current knowledge of the pre-autophagosomal structure (PAS). *FEBS Lett* 584, 1280-1286.
- Tadauchi, T., Inada, T., Matsumoto, K., and Irie, K. (2004). Posttranscriptional regulation of HO expression by the Mkt1-Pbp1 complex. *Mol Cell Biol* 24, 3670-3681.
- Taxis, C., and Knop, M. (2006). System of centromeric, episomal, and integrative vectors based on drug resistance markers for *Saccharomyces cerevisiae*. *Biotechniques* 40, 73-78.
- Thomas, D., and Surdin-Kerjan, Y. (1997). Metabolism of sulfur amino acids in *Saccharomyces cerevisiae*. *Microbiol Mol Biol Rev* 61, 503-532.
- Thumm, M., Egner, R., Koch, B., Schlumpberger, M., Straub, M., Veenhuis, M., and Wolf, D.H. (1994). Isolation of autophagocytosis mutants of *Saccharomyces cerevisiae*. *FEBS Lett* 349, 275-280.
- Tsukada, M., and Ohsumi, Y. (1993). Isolation and characterization of autophagy-defective mutants of *Saccharomyces cerevisiae*. *FEBS Lett* 333, 169-174.
- Tu, B.P. (2010). Ultradian metabolic cycles in yeast. *Methods Enzymol* 470, 857-866.
- Tu, B.P., Kudlicki, A., Rowicka, M., and McKnight, S.L. (2005). Logic of the yeast metabolic cycle: temporal compartmentalization of cellular processes. *Science* 310, 1152-1158.
- Tu, B.P., Mohler, R.E., Liu, J.C., Dombek, K.M., Young, E.T., Synovec, R.E., and McKnight, S.L. (2007). Cyclic changes in metabolic state during the life of a yeast cell. *Proc Natl Acad Sci U S A* 104, 16886-16891.
- Van der Veen, A.G., Schorpp, K., Schlieker, C., Buti, L., Damon, J.R., Spooner, E., Ploegh, H.L., and Jentsch, S. (2011). Role of the ubiquitin-like protein Urm1 as a noncanonical lysine-directed protein modifier. *Proc Natl Acad Sci U S A* 108, 1763-1770.
- van Dijken, J.P., Bauer, J., Brambilla, L., Duboc, P., Francois, J.M., Gancedo, C., Giuseppin, M.L., Heijnen, J.J., Hoare, M., Lange, H.C., *et al.* (2000). An interlaboratory comparison of physiological and genetic properties of four *Saccharomyces cerevisiae* strains. *Enzyme Microb Technol* 26, 706-714.
- Verlhac, M.H., Chen, R.H., Hanachi, P., Hershey, J.W., and Derynck, R. (1997). Identification of partners of TIF34, a component of the yeast eIF3 complex, required for cell proliferation and translation initiation. *EMBO J* 16, 6812-6822.
- Voth, W.P., Richards, J.D., Shaw, J.M., and Stillman, D.J. (2001). Yeast vectors for integration at the HO locus. *Nucleic Acids Res* 29, E59-59.
- Wei, C.L., Kainuma, M., and Hershey, J.W. (1995). Characterization of yeast translation initiation factor 1A and cloning of its essential gene. *J Biol Chem* 270, 22788-22794.

Westermann, B., and Neupert, W. (2000). Mitochondria-targeted green fluorescent proteins: convenient tools for the study of organelle biogenesis in *Saccharomyces cerevisiae*. *Yeast* 16, 1421-1427.

Yarunin, A., Panse, V.G., Petfalski, E., Dez, C., Tollervey, D., and Hurt, E.C. (2005). Functional link between ribosome formation and biogenesis of iron-sulfur proteins. *EMBO J* 24, 580-588.